IOWA STATE UNIVERSITY
Digital Repository

Retrospective Theses and Dissertations

Iowa State University Capstones, Theses and Dissertations

1972

Langmuir vaporization technique for liquid phase vapor pressure and partial pressure measurements: lead and indium-lead systems

Kenneth Leo Walter
Iowa State University

Follow this and additional works at: https://lib.dr.iastate.edu/rtd

 Part of the Chemical Engineering Commons

Recommended Citation

Walter, Kenneth Leo, "Langmuir vaporization technique for liquid phase vapor pressure and partial pressure measurements: lead and indium-lead systems " (1972). *Retrospective Theses and Dissertations*. 5872.
https://lib.dr.iastate.edu/rtd/5872

This Dissertation is brought to you for free and open access by the Iowa State University Capstones, Theses and Dissertations at Iowa State University Digital Repository. It has been accepted for inclusion in Retrospective Theses and Dissertations by an authorized administrator of Iowa State University Digital Repository. For more information, please contact digirep@iastate.edu.

INFORMATION TO USERS

This dissertation was produced from a microfilm copy of the original document. While the most advanced technological means to photograph and reproduce this document have been used, the quality is heavily dependent upon the quality of the original submitted.

The following explanation of techniques is provided to help you understand markings or patterns which may appear on this reproduction.

1. The sign or "target" for pages apparently lacking from the document photographed is "Missing Page(s)". If it was possible to obtain the missing page(s) or section, they are spliced into the film along with adjacent pages. This may have necessitated cutting thru an image and duplicating adjacent pages to insure you complete continuity.

2. When an image on the film is obliterated with a large round black mark, it is an indication that the photographer suspected that the copy may have moved during exposure and thus cause a blurred image. You will find a good image of the page in the adjacent frame.

3. When a map, drawing or chart, etc., was part of the material being photographed the photographer followed a definite method in "sectioning" the material. It is customary to begin photoing at the upper left hand corner of a large sheet and to continue photoing from left to right in equal sections with a small overlap. If necessary, sectioning is continued again — beginning below the first row and continuing on until complete.

4. The majority of users indicate that the textual content is of greatest value, however, a somewhat higher quality reproduction could be made from "photographs" if essential to the understanding of the dissertation. Silver prints of "photographs" may be ordered at additional charge by writing the Order Department, giving the catalog number, title, author and specific pages you wish reproduced.

University Microfilms

300 North Zeeb Road
Ann Arbor, Michigan 48106

A Xerox Education Company

72-26,949

WALTER, Kenneth Leo, 1941-
LANGMUIR VAPORIZATION TECHNIQUE FOR LIQUID PHASE VAPOR PRESSURE AND PARTIAL PRESSURE MEASUREMENTS. LEAD AND INDIUM-LEAD SYSTEMS.

Iowa State University, Ph.D., 1972
Engineering, chemical

University Microfilms, A XEROX Company, Ann Arbor, Michigan

© 1972

KENNETH LEO WALTER

ALL RIGHTS RESERVED

THIS DISSERTATION HAS BEEN MICROFILMED EXACTLY AS RECEIVED.

Langmuir vaporization technique for liquid phase vapor pressure and partial pressure measurements. Lead and indium-lead systems

by

Kenneth Leo Walter

A Dissertation Submitted to the
Graduate Faculty in Partial Fulfillment of
The Requirements for the Degree of
DOCTOR OF PHILOSOPHY

Major: Chemical Engineering

Approved:

Signature was redacted for privacy.

In Charge of Major Work

Signature was redacted for privacy.

For the Major Department

Signature was redacted for privacy.

For the Graduate College

Iowa State University
Ames, Iowa

1972

Copyright © Kenneth Leo Walter, 1972. All rights reserved.

PLEASE NOTE:

Some pages may have

indistinct print.

Filmed as received.

University Microfilms, A Xerox Education Company

TABLE OF CONTENTS

LIST OF FIGURES

LIST OF TABLES

NOMENCLATURE

a	activity, thermodynamic
α	condensation coefficient
C_p	heat capacity at constant pressure
c	integration constant
Δ	denotes difference
D,d	diameter
δ	molecular diameter
e	base of natural logarithms
ε	emissivity
f	fugacity
F	radiation view factor
γ	activity coefficient
G	Gibb's free energy/mole
H	enthalpy/mole
K	Clausing factor
l	distance from top of crucible hole to equator of spherical meniscus
λ	mean free path
m	mass vaporized
M	molecular wt.
n	number of samples
n'	number of molecules/unit volume
ν	function defined by Equation 32
P	vapor pressure
p	partial pressure
R	gas law constant
r	radius of crucible hole
ρ	density
π	3.14159
σ	standard deviation
S	entropy/mole
s	surface area (effective)
T	temperature
t	time of run
v	volume/mole
w	weight fraction
W	surface flux ($g/sec\text{-}cm^2$)
x	mole fraction of condensed phase
y	mole fraction of gas phase

Subscripts

Pb, In	
v	vaporization
T	constant temperature
av	average

Superscripts

° standard state

- partial molar quantity

INTRODUCTION

Today's methods of measuring very low vapor pressures (10^{-2} mm Hg and below) are essentially the same as those devised at the turn of the century. Despite great improvements in preparing purer substances and in vacuum technology, recent measurements often show wide scatter and disagreement among different workers. It is possible that at least part of the problem lies in basic misunderstanding of some of the important variables.

Probably the simplest conceptual way of measuring a pressure is to measure the force exerted on a known area. Ingenious ways of doing this have been devised. However, once the pressure falls below about 10^{-2} mm Hg, these direct methods are not precise. The optical absorption method (18) is capable of measuring relative pressures accurately for some systems at equilibrium, but does not measure absolute pressures.

It is then necessary to turn to non-equilibrium methods. The most widely used of these is the Knudsen effusion method (57), which is an attempt to maintain a condensed phase and its vapor near equilibrium in a small chamber, completely sealed except for a small pinhole of the order of one millimeter diameter. It has been assumed that the kinetic theory of gases applies to this low pressure, near-equilibrium gas.

Therefore, the pressure inside the cell could be computed from the rate of escape through the orifice. While others have tried to remedy inconsistencies in this interpretation, Ward (120) has recent experimental evidence showing that this is not entirely possible.

Another, though often demeaned, technique is the Langmuir method (65) in which a condensed phase evaporates from a free surface with no attempt made to approximate equilibrium. While nearly the same equation applies as in computing Knudsen pressures, several different assumptions apply. The main problems in the Langmuir technique are experimental, since an uncontaminated surface must be maintained for long periods of time and its temperature accurately measured. In the work reported here, a modification of the Langmuir method is employed to measure the vapor pressures of lead and indium, and the partial pressure of lead over their alloys. New techniques have been developed to overcome the experimental problems.

Thermodynamic activities of the indium-lead system had been measured only once before this research was begun. Terpilowski and Gregorczyk (110) used the EMF method to measure the indium activity, and calculated the lead activity using the Gibbs-Duhem equation. While the EMF method usually gives more reliable entropy and enthalpy of mixing data than partial pressure measurements, the metals used should differ

significantly in electonegativity. Since indium and lead are similar in this respect (viz. In-1.7, Pb-1.8 (51)), a partial pressure determination of thermodynamic activities for this system was highly desirable. Shiu and Munir (103) have recently published thermodynamic data on the indium-lead system which shows larger deviations from ideality than Terpilowski and Gregorczyk's data. They measured the lead partial pressure by the torsion effusion method, a very useful modification of the Knudsen method.

The objectives of this research, then, were 1) development of a theoretically and experimentally sound method for measuring liquid metal vapor pressures in the low pressure region, and 2) application of this method to measure lead partial pressures over the indium-lead system, thus enabling calculation of thermodynamic activities and related mixing properties for the indium-lead system.

THEORY

Equilibrium and Non-Equilibrium Measurements

The Knudsen effusion method (57) is the oldest and most widely accepted way to measure low vapor pressures. A great deal of its appeal lies in the fact that it attempts to work with a near-equilibrium system. In the Knudsen method a condensed phase together with its gas phase is maintained at a constant temperature inside a cell (see Figure 1). The cell is tightly sealed except for the presence of a small orifice through which a negligibly small amount of the gas phase continuously escapes into a vacuum outside. If the validity of the kinetic theory of gases is assumed, the mass rate at which the gas molecules strike and escape the orifice is

$$W = P \sqrt{\frac{M}{2\pi RT}} \qquad (1)$$

where W is the mass flux of gas molecules,

P is the vapor pressure of the substance,

M is the molecular weight of the gas molecules,

R is the ideal gas law constant, and

T is the absolute temperature.

A variation of the Knudsen effusion method is the torsion effusion method (114) wherein the cell is suspended by a thin fiber. The orifices are located off the axis of rotation, so that the force of reaction to the escaping molecules creates

Figure 1. Schematic diagram of three vaporization methods for liquids at low pressures

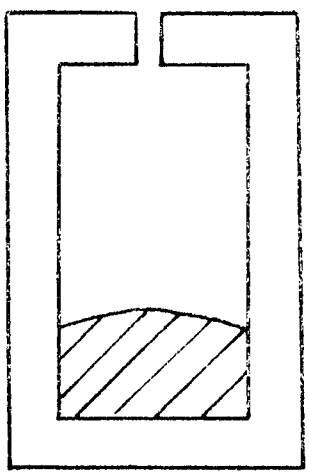

Knudsen

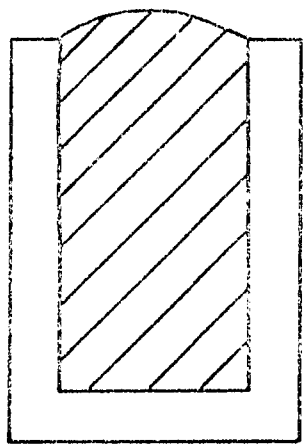

Langmuir

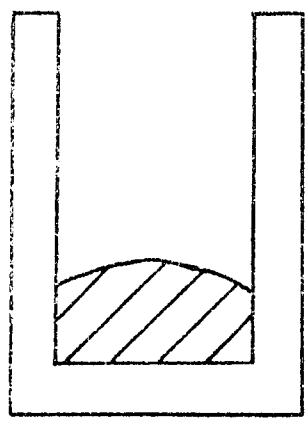

Modified
Langmuir

a measurable torque.

The only reason the effusion method is restricted to low pressures is the need to ensure that every molecule which strikes the orifice will escape. If no molecular collisions occur in or near the orifice opening, this need will be satisfied.

In the kinetic theory of gases, the mean free path is defined as the average length a molecule will travel before suffering a collision with another molecule. The mean free path is given by (54)

$$\lambda = \frac{1}{2\pi\delta^2 n'} \qquad (2)$$

where δ is the molecular diameter and n' is the number of molecules per unit volume.

It can be seen, then, that if the mean free path is significantly larger than the diameter of the Knudsen cell orifice, few collisions will occur in the opening and Equation 1 will predict the effusion rate. Knudsen said that the mean free path should be at least ten times the orifice diameter (57) while others suggested lower (15) or higher (35) factors were needed. The use of too large an orifice will result in a measured pressure which is too low because the gas phase would not be in equilibrium with the condensed phase. On the other hand, if too small an orifice is used, several authors (16, 123,124) have pointed out that surface diffusion of molecules

along the cell walls and out the orifice may result in too high a measured pressure. To be valid, Knudsen pressures should be independent of orifice size. Application of a Clausing factor to Equation 1 is usually necessary to account for the resistance to molecular flow caused by the finite thickness of the orifice. This will be discussed later.

In the foregoing the concept of an equilibrium gas inside a Knudsen cell was assumed valid. When the experimenter complies with Knudsen's criterion for the ratio of mean free path to orifice diameter and uses a small enough cell to be certain of maintaining its temperature constant, he finds that the inner dimensions of the cell may be comparable to, or less than, the mean free path. This means that most of the gas molecules suffer no collisions with each other before colliding with either the container walls, the condensed phase, or the orifice. In other words, the majority of molecules effusing from the Knudsen cell have come directly from the cell or sample surface rather than from an equilibrium gas inside the cell.

It then becomes necessary to consider 1) how an atom or molecule vaporizes from solid and liquid phases, and also 2) how the vapor reacts to collisions with container walls and to collisions with its own condensed phase. Unfortunately, both these questions are far from being answered. At higher pressures, the rate determining step is not the surface

rate of vaporization, but is either gas phase mass transfer or heat transfer. At the low pressures considered here, vaporization rate mechanisms are in the developmental stage (45).

Langmuir's (65) early solution to the problem remains the only practical one at this time. He first considered a dynamic equilibrium between a condensed phase and a vapor phase. Provided that the kinetic theory of gases applies, Equation 1 may be modified to obtain the mass rate of condensation of vapor molecules on the condensed phase:

$$W = \alpha P \sqrt{\frac{M}{2\pi RT}} \tag{3}$$

where α is the condensation coefficient.

$$\alpha = \frac{\text{number of molecules which condense}}{\text{number of molecules striking condensed phase}} \tag{4}$$

Naturally, at equilibrium, Equation 3 also gives the mass rate of vaporization, since it must equal the mass rate of condensation.

At this point Langmuir made an important assumption which limits his method to low pressures. He assumed that at equilibrium, at pressures less than about one millimeter of mercury, the vaporization mechanism is independent of the condensation rate since both rates are very low. Hence the mass vaporization flux is given by Equation 3 whether

or not any molecules are condensing. The net flux, of course, is given by the difference of vaporization and condensation fluxes. In the experimental use of this method, condensation of molecules on the vaporizing surface is prevented by immediately condensing vaporized molecules on a condenser. At a pressure of one millimeter of mercury, the vaporization rate based on Equation 3 with a condensation coefficient of unity is approximately 10^5 atomic layers per second. This apparently high rate is slow on an atomic scale compared to an atomic rate of "jumping" from one lattice site to another of about 10^8 jumps per second for solids and 10^{11} jumps per second for liquids as calculated from self diffusion theory.

Interaction of Molecules with Surfaces

Before discussing the condensation coefficient it is necessary to consider how vapor molecules interact with surfaces. Vapor molecules may condense; they may reflect specularly, with the angle of reflection equal to the angle of incidence; they may reflect diffusely according to the cosine law, with the flux in the direction of any angle of reflection proportional to the cosine of that angle and independent of the angle of incidence; or they may reflect in some other manner.

Because of the uncertainty of this mechanism, it is again helpful to consider the equilibrium condition. As a consequence of the completely random motion of molecules of an equilibrium gas, if the molecules do not condense upon striking a surface they must reflect diffusely in accordance with the cosine law, just as molecules must vaporize according to the cosine law (15). Under non-equilibrium conditions, molecules and atoms have been found to reflect diffusely (16, 58,66,109,121), specularly (27) and in other ways (15). The most common type of reflection is the diffuse or cosine reflection, which can be caused by an adsorption and re-emission process or simply because of surface roughness on a molecular scale (120).

In the case of vapor molecules striking a clean condensed phase of the same substance, in most cases all the vapor molecules will condense, i.e. the condensation coefficient is unity. Langmuir (66) hypothesized that this should be so, and others have confirmed his hypothesis by measurement (105). The only valid exceptions to unity condensation coefficients are those materials having one molecular structure in the vapor phase and another structure in the liquid phase. Examples are sodium carbonate (77) which decomposes to Na, CO_2 and O_2 in the vapor, and arsenic (11,95,97), which forms primarily As_4 molecules in the vapor and consists of As_2 molecules in the lattice. Antimony's behavior is similar to

arsenic (96,97). Hirth and Pound (45), studying the mechanics of the condensation process, show that the condensation coefficient for a liquid will nearly always be as high or higher than that for the corresponding solid, and will tend toward unity as the temperature rises. Many have shown this experimentally (13,14,95,115). Littlewood and Rideal (68) point out that many who have measured α's less than unity have been deceived because of a lack of surface thermal equilibrium, especially with substances of low thermal conductivity. Their conclusions are backed with experimental evidence on fatty acids.

Problems with Effusion Measurements

Having briefly considered the interrelated processes of vaporization, condensation and reflection, we are ready to return to a consideration of Knudsen cell pressure determinations. Speiser and Johnston (105), Whitman (122), Rossmann and Yarwood (98,99), Motzfeldt (77), Carlson (15), Balson (5) and Rosenblatt (93,94) are some of those who recognized that the gaseous molecules inside the cell were not at equilibrium. They recognized 1) that the sample area could have an effect on the cell weight loss; 2) that non-unit condensation coefficients could affect Knudsen as well as Langmuir vaporizations; 3) that dimensions of the cell other than orifice size and thickness may be important; 4) that surface conditions on

the condensed phase such as temperature, cleanliness and composition are important; 5) that the material, temperature, and cleanliness of the cell walls are critical.

In addition to these problems, which the equilibrium gas concept of Knudsen vaporizations does not treat, is the commonly used correction for the resistance to gas flow offered by a finitely thick orifice referred to earlier. Clausing (17) solved this problem analytically for cylindrical orifices by assuming that the gas entering the orifice had an equilibrium cosine distribution (i.e. completely random), that gas phase collisions were negligible and that wall collisions were diffuse. Later DeMarcus (21) improved Clausing's numerical accuracy in the calculated molecular transmission probabilities or Clausing factors. In the list of papers mentioned above, several authors have questioned the validity of the cosine distribution assumption at the orifice of a Knudsen cell because of the lack of equilibrium. Hence the use of Clausing factors to correct for the orifice resistance may not be correct.

Recently Ward (120) made an excellent experimental study of the angular distribution of atoms effusing from Knudsen cells with knife-edged orifices. The mean free paths were longer than any cell dimension. The angular distribution showed marked and reproducible deviations from a cosine distribution, which proved that the molecules coming from

inside the cell were not from an equilibrium gas. In addition Ward (121) used a Monte-Carlo computer technique to simulate the vaporization of about one million molecules per run from the liquid metal inside the cell. Assuming a unit condensation coefficient for the liquid gold and plutonium, and assuming cosine reflections from the cell walls, the computed results matched the experimental non-cosine distribution. Also demonstrated experimentally and with the computer were 1) changes in the angular distribution caused by changing the shape of the vaporization surface from flat to hemispherical, 2) changes caused by varying internal cell geometry, and 3) changes caused by failure of parts of the cell walls to re-emit all the incident vapor atoms. In one trial at higher temperature and pressure, such that the mean free path was about the same as the cell diameter and half its height, the distribution of the effusing atoms was cosine, indicating that gaseous collisions had become important.

One of Ward's (121) recommendations is that the effusate of the Knudsen cell be collimated such that only the molecules coming directly from the sample surface are collected. In this way uncertainties due to wall losses can usually be avoided. Even then, he points out, the thermodynamic equilibrium pressure is not being directly measured since the cosine law is not obeyed. Essentially what he is advocating is the use of a modification of the Langmuir method.

It should be noted in the case of the torsion effusion modification of the Knudsen method that the angular distribution of the effusing molecules is needed as well as the number which escape. Freeman and Searcy (30) have computed correction factors for finitely thick orifices assuming that the entering molecules have a cosine distribution. As Ward (120) has shown, this is not necessarily true, and a Monte-Carlo computation of the true angular distribution would be of use in torsion effusion work.

Problems with Langmuir Measurements

A number of early authors who were using the Knudsen technique criticized the Langmuir method for a number of reasons. Harteck (40) criticized the method because it was not an equilibrium method, as he supposed Knudsen's method was. As we have seen, in order to have a nearly equilibrium method, numerous gas phase collisions are necessary. For this condition to hold, the molecular mean free path must be small in comparison to container dimensions, and yet large in comparison to the orifice diameter. A factor which limits compliance with the latter requirement is that surface diffusion of atoms out of the orifice must be small in comparison to vapor atoms escaping (123,124). Hence the orifice cannot be satisfied by enlarging the effusion cell beyond a

size that can be maintained at a constant temperature. Effectively this limits the near-equilibrium use of the Knudsen cell to a narrow range of pressures which is often exceeded in practice.

Fajans (29) criticized the Langmuir method because it required a clean surface to give valid results, a condition often difficult to obtain. Nevertheless clean sample surfaces (as well as no-loss cell surfaces) are just as necessary to the Knudsen method when used outside the pressure range where gas phase collisions are frequent, and only slightly less important inside this range. Rauh and Thorn (91) found that the vapor pressure of liquid uranium was very dependent upon residual oxygen pressures as low as 10^{-7} mm Hg. Borg and Birchenall (9) and Kensok, Myers and Saxer (55) found that magnesium partial pressures over solid Mg-Cd alloys were affected by surface oxygen and nitrogen compounds. Greenbank and Argent (34) show that oxide inhibits the vaporization of magnesium, zinc and cadmium, with the apparent magnesium pressures being only about 50% of equilibrium values. All these workers used the Knudsen method.

Fajans (29) also criticized the Langmuir method because the surface temperature lowering due to the latent heat of vaporization was often not accounted for. This is a valid criticism which must be allowed for when the surface temperature is not measured directly. Usually in practice the

vaporization rates are sufficiently low that the latent heat loss is small in comparison to radiation heat loss, but care must be exercised in measuring true surface temperatures. The primary advantage of the Knudsen method is that the internal temperature of the cell can be more accurately measured than the Langmuir vaporization surface temperature. At high temperatures where optical pyrometers are used, the Knudsen cell forms a black body cavity, whereas the emissivity of the surface is required in the Langmuir method. At lower temperatures where thermocouples are most often used, it is easier to measure the temperature inside a volume than to measure the temperature at a surface.

Another problem evident in the Langmuir method is the determination of the area of the vaporizing surface. In the case of a solid of easily measured geometrical area, the question arises as to whether or not microscopic cracks or surface roughness increases the true vaporization area. Melville (75) showed for substances with unity condensation coefficient that the effective vaporization area was the gross geometrical surface area. When the condensation coefficient is less than unity, however, the effective surface area is increased by cracks or roughness. Some experimenters have used this effect to show for metals that the condensation coefficient is essentially unity. The difficult experimental

problem is to maintain the entire vaporizing surface at a uniform, constant temperature.

In the case of a liquid, the vaporization area may be difficult to determine experimentally. This has been a primary reason why the Langmuir method has been infrequently used with liquids. Nevertheless the Knudsen method also depends upon the shape and location of a vaporizing liquid. Ward (119) found that the apparent vapor pressures of liquid gold was 14% higher if the liquid was globular rather than flat on the cell bottom. If the sample shape is known or can be estimated, Sandry and Stevenson (101) and Ward, Mulford and Bivins (121) have devised Monte Carlo computer techniques for Langmuir and Knudsen vaporizations, respectively, which can be used to obtain molecular transmission probabilities. These probabilities together with rate of weight loss data can be translated into vapor pressures.

The Langmuir method has two obvious advantages over the Knudsen method other than the contrasts which have already been made. The first advantage is that pressures can be measured by the Langmuir method which are a factor of 10^3 to 10^4 (105) lower than the Knudsen method, since the entire sample area is available for vaporization rather than just the orifice area. The highest boiling elements have all had their vapor pressures measured almost exclusively by the Langmuir method. The inherent accuracy of the torsion effusion method

naturally decreases with the pressure to be measured (87). The second advantage is that for solids, no crucible is necessary; hence the extra possibility of contamination of the sample is avoided. This advantage is important for reactive substances and high temperatures.

Multicomponent Measurements

The partial pressure of a multicomponent solid or liquid may be measured in the same way as a pure component by either the Knudsen or Langmuir techniques. For example, applying Equation 3, corrected for molecular flow resistance by a Clausing factor K, to the first component:

$$W_1 = K\alpha_1 p_1 \sqrt{\frac{M_1}{2\pi RT}} \tag{5}$$

Here p_1 is the partial pressure of the first component, and α_1 is the condensation coefficient for molecules of the first component condensing on the condensed phase in question. Of course p_1 and α_1 will, in general, depend on the composition of the condensed phase, and it is possible that M_1 may also.

It is important in working with multicomponent systems to realize that it is the surface composition which determines the vaporization rate. Often, especially with solids and dilute liquids, a surface depletion effect may set in. This happens when the vaporizing surface becomes depleted of a volatile component with respect to the bulk composition

because the volatile component's rate of evaporation is greater than its rate of diffusion to the surface. Only recently has this effect been studied. For example, Roy and Hultgren (100) using torsion effusion detected significant surface depletion of manganese from solid iron manganese alloys. This depletion was most important at higher vaporization temperatures and low manganese concentrations. Surface depletion in liquids is less of a problem because liquid phase diffusion coefficients are about a thousand times greater than those for the solid phase, and because convection effects are usually operative.

Nevertheless, Ohno and Ishida (84), studying the Langmuir vaporization of dilute (< 3 wt.%) liquid iron alloys at high rates, attributed their lower than expected separation rates to surface depletion. They calculated surface depletion ratios (surface concentration to bulk concentration) of 9 to 92%. Uyeha and Hagihara (112) utilized film theory in order to predict the resistance to evaporation caused by surface depletion. Walsh and Burnet (118) also reported surface depletion in high-rate Langmuir vaporizations of liquid alloys by directly measuring surface concentrations with an X-ray fluorescence spectrometer. They found surface depletion ratios as low as 37% with moderate concentration (24 to 53 atom % volatile component) alloys, but also reported that a slight amount of turbulence caused by gentle vibration eliminated the surface depletion.

On the other hand, even using forced convection Bradley and Webster (10) could reduce but not eliminate surface depletion when distilling very dilute (50 ppm) solutions of polonium, zinc and cadmium in bismuth. Forced convection consisted of a perforated tantalum disk oscillating vertically in the top half inch of liquid at about two cycles per second. Penetration theory was successfully used to estimate forced convection and natural convection mass transfer coefficients.

It may be concluded that the Knudsen method is superior to the Langmuir method in reducing surface depletion since each element of surface in the Knudsen cell has a net vaporization far less than the maximum Langmuir rate. Von Lange and Lindsheid (116) have recently investigated the effect of surface depletion in Knudsen effusion cells. With solids, surface depletion is a very important effect, whereas with liquids surface depletion can be eliminated even with the Langmuir method. It should be kept in mind that in the Knudsen method, the surface area directly under the orifice is making a higher contribution to the effusion rate than the area near the wall.

In summary, it is suggested that the near-equilibrium concept of Knudsen vaporization is not valid at pressures where gas phase collisions in the cell are negligible. In this range of pressures the choice of Langmuir or Knudsen vaporization methods depends on the substance to be studied,

with full realization that surface conditions are of high importance in either method.

Use of the Langmuir Method with In-Pb Alloy

A modified Langmuir method was chosen in this work in order to see whether or not surface temperature, surface cleanliness and surface area measurement could be controlled well enough to approach experimentally the theoretical maximum Langmuir vaporization rate. Many experimenters have been unable to do this. All three of these variables are relatively easy to control in Knudsen measurements, but conditions in the Langmuir technique are similar to those existing in industrially important molecular distillation equipment. A better understanding of Langmuir evaporation will contribute to a better understanding of how to design this equipment. The indium-lead system was chosen in this study for two reasons. First, thermodynamic data on the In-Pb system was needed. Second, since indium has a vapor pressure about 350 times smaller than lead, its weight loss is almost negligible in measuring lead weight losses during Langmuir vaporizations. Yet it has an isotope with a convenient 50-day half-life should independent measurements of its vaporization rate be desired.

Figure 2 shows the mean free paths of lead and indium divided by the vaporization tube diameter to be used in this work. If Knudsen's criterion is valid for molecular flow of a

Figure 2. Mean free paths for lead and indium based on equilibrium vapor pressures

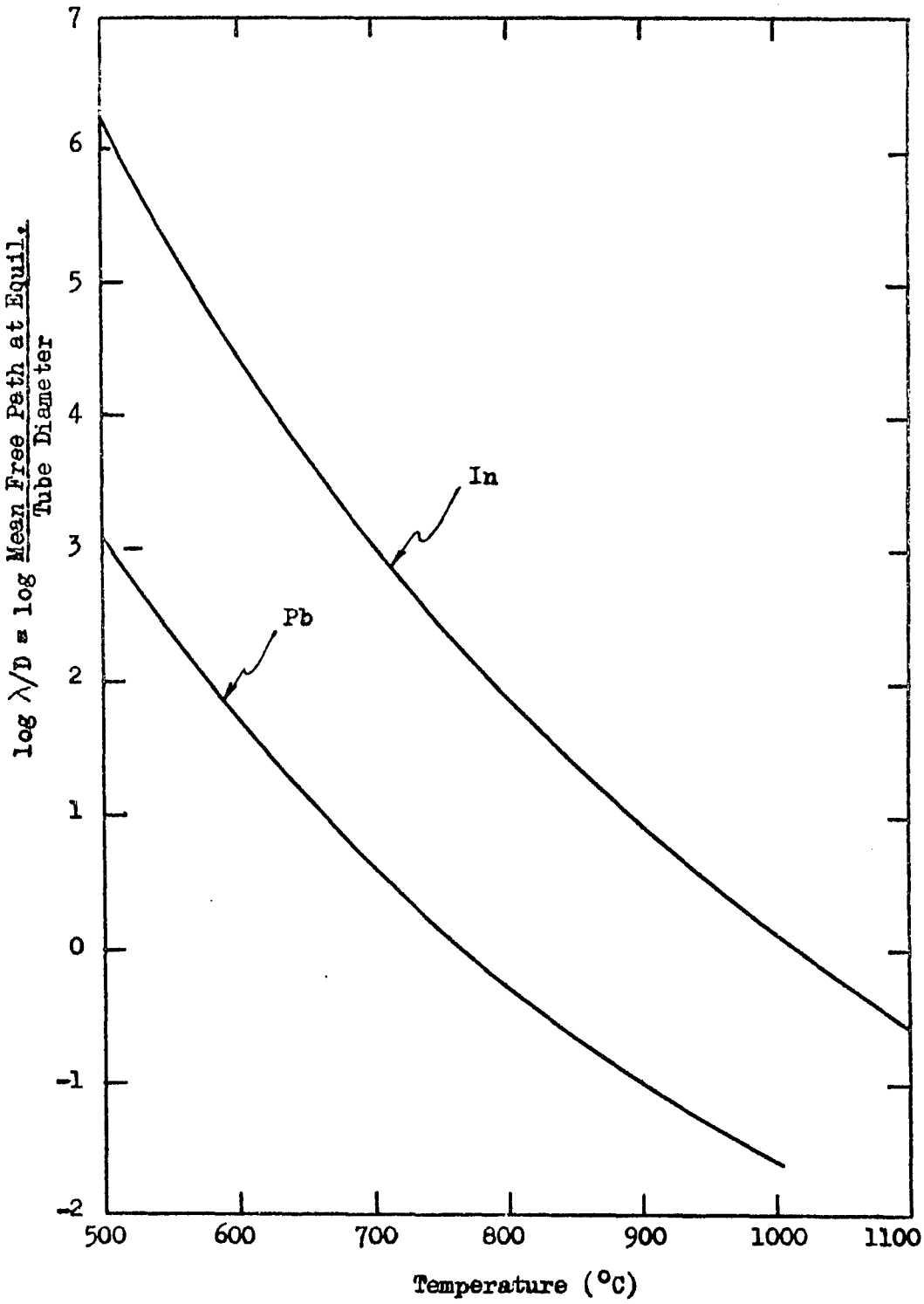
7
6
5
4
3
2
1
0
-1
-2
500
600
700
800
900
1000
1100
In
Pb
log λ/D = log Mean Free Path at Equil. / Tube Diameter
Temperature (°C)

mean free path to tube diameter ratio of 10 or more, then deviations from linearity of the Clauius-Clapeyron equation should be noted at the higher temperature for lead near 680°C and for indium near about 900°C. The mean free paths were computed from Equation 2 using molecular diameters of 3.5 angstroms for lead and 3.32 angstroms for indium (54).

Therefore, we see that the modified Langmuir technique can determine lead and indium vapor pressures, and also the partial pressures of each component over an alloy. Thermodynamic analysis of such data taken over temperature and composition ranges can lead to further information. This information will also give clues as to whether or not the original data is valid.

Thermodynamics of One Component System

The most common way to present vapor pressure data is the log P versus 1/T plot. Its basis is the Clausius-Clapeyron equation:

$$d \ln P = -\Delta H_v \, d(1/RT), \tag{6}$$

where ΔH_v is the latent heat of vaporization at temperature T. In its integrated form with a constant of integration c, where P is in atmospheres,

$$\log P = \frac{-\Delta H_v}{2.303 RT} + c \tag{7}$$

are implicit the valid assumptions that the specific volume of the condensed phase is much less than that of the gas phase, and that the ideal gas law applies. How the value of c can be related to the standard entropy of vaporization ΔS°_v will be discussed shortly. Also ΔH_v is assumed constant over the temperature range of interest. This latter assumption is verified by Hultgren et al. (49,50), since ΔH_v varies by only about 1% and 0.5% for lead and indium, respectively, over the temperature range studied here. Determining ΔH_v from the slope of Equation 7 is known as the second law method, because its basis is the second law of thermodynamics.

The third law of thermodynamics is the basis for another method of determining a heat of vaporization. The third law is used to tabulate a free energy function $\frac{G^\circ_T - H^\circ_{298}}{T}$ for vapor and condensed phases from specific heat or spectrographic data for each pure component. The free energy function for each phase of a substance is a function only of T. The superscript ° represents standard state conditions, which will be discussed shortly. A value of $\Delta H^\circ_{v,298}$ can be computed for each experimental vapor pressure from

$$\Delta H^\circ_{v,298} = -T\Delta\left(\frac{G^\circ_T - H^\circ_{298}}{T}\right) - RT \ln P \qquad (8)$$

where P is in atmospheres, using the tabulated gaseous and liquid free energy functions of Hultgren et al. (49,50).

Cubicciotti (20) has developed a method which uses the increment above 298°K (or any reference temperature desired) of the value of the free energy function to determine $\Delta H^\circ_{V,298}$ directly from a slope. He shows that

$$\Sigma' = -R \ln P - \Delta fef\ incr = \frac{\Delta H^\circ_{V,298}}{T} - \Delta S^\circ_{V,298} \qquad (9)$$

where the free energy function increment for each phase is

$$fef\ incr = \frac{G^\circ_T - H^\circ_{298}}{T} - \frac{G^\circ_{298} - H^\circ_{298}}{298} \qquad (10)$$

If Σ' is plotted versus 1/T, the value of the slope is $\Delta H^\circ_{V,298}$ and the intercept is $-\Delta S^\circ_{V,298}$. The same values may be obtained by a least squares analysis. If Equation 9 is compared with Equation 8, it may be seen that

$$\Delta S^\circ_{V,298} = -\Delta fef + \Delta fef\ incr = -\Delta fef + \Delta fef - \Delta(fef)_{298}$$

$$\Delta S^\circ_{V,298} = -\Delta(fef)_{298} = -\Delta\left[\frac{G^\circ_{298} - H^\circ_{298}}{298}\right] \qquad (11)$$

Hultgren *et al.* (50) report lead's value as 41.888 - 15.55 = 26.34 cal/g-mole-°K. For indium (49) it is 41.507 - 13.82 = 27.69 cal/g-mole-°K. Therefore, we should expect to find these values for $\Delta S^\circ_{V,298}$. Any differences will be related to how much second law and third law values of $\Delta H^\circ_{V,298}$ differ.

It is not correct to call Cubicciotti's Σ' method a third law method for obtaining $\Delta H^\circ_{V,298}$, since it does not depend

upon the free energy function, but only its increment. It is perhaps slightly more accurate than the second law method, because it is not necessary to assign an average value of T for the range of the experimental data, as will be discussed shortly for the second law method. The Σ' method is in actuality a slightly improved second law method.

The standard state conditions chosen for the liquid metals of this study are pure components at the system temperature and one atmosphere pressure. The conversion of liquid thermodynamic quantities from one atmosphere pressure to the pure component vapor pressure causes no appreciable change, so the pressure specification for the liquids in this case is not significant. The standard state conditions for the vapors are the ideal gas state at one atmosphere pressure and system temperature. Since lead and indium vapors are nearly ideal gases at one atmosphere and below, the enthalpy change in converting the real gas at its vapor pressure to the ideal gas at one atmosphere is zero. Hence the actual heat of vaporization from Equation 7, $\Delta H_v = \Delta H_v^\circ$. Also, tables for the liquid and vapor phase values of $H_T^\circ - H_{298}^\circ$ of Hultgren *et al.* (49,50) can be used to convert ΔH_v to 298°K:

$$\Delta H_v - \Delta(H_T^\circ - H_{298}^\circ) + \Delta H_{v,298}^\circ \qquad (12)$$

The value of T used is the midpoint of the temperature range of the experimental data.

Therefore the second law $\Delta H^\circ_{v,298}$ obtained from Equations 7 and 12 may be compared to the average of the third law values obtained from Equation 8. The agreement of these values is a check on the validity of the vapor pressures determined. In addition, the third law values should not show a trend with temperature, as such a trend indicates either faulty free energy function values or temperature dependent errors in the vapor pressure measurements.

Because of the fact that in this instance $\Delta H_v = \Delta H^\circ_v$, and since $\Delta G^\circ_v = -RT \ln P = \Delta H^\circ_v - T\Delta S^\circ_v$, it is apparent that the constant c in Equation 7 must be

$$c = \Delta S^\circ_v/2.303R. \tag{13}$$

The tables of $S^\circ_T - S^\circ_{298}$ referred to can be used to calculate $\Delta S^\circ_{v,298}$ from ΔS°_v obtained from Equation 13 as was done in calculating $\Delta H^\circ_{v,298}$ using Equation 12.

$$\Delta S^\circ_{v,298} = \Delta S^\circ_v - \Delta(S^\circ_T - S^\circ_{298}) \tag{14}$$

The value of T used is again the midpoint of the temperature range of experimental data.

Thermodynamics of Binary Component System

Since the standard state for the liquid metals is chosen as the pure component in this work,

$$\frac{a}{x} = 1$$

when x = 1, or

$$\frac{f/f^\circ}{x} = 1$$

when x = 1,

where a is the thermodynamic activity of a liquid component,

x is the liquid mole fraction of that component,

f is the liquid fugacity of that component, and

f° is the standard state fugacity of that component.

Now since the gas phase is ideal, the gas phase fugacity must equal its pressure. Also at equilibrium, the gas and liquid phase fugacities must be equal. Hence,

$$f^\circ = (f)_{x=1} = P \tag{15}$$

and

$$a = \gamma x = f/f^\circ = p/P \tag{16}$$

where γ is the activity coefficient of a liquid phase component,

p is the partial pressure of that component, and

P is the vapor pressure of that component.

Equation 16 indicates that we can experimentally determine activities and activity coefficients for each component by measuring the ratio of its partial pressure to its vapor pressure. If radioactive tracer indium is used to enable independent determination of each component's vaporization rates - hence also partial pressures and activity coefficients - the Gibbs-Duhem equation could be used to test the thermodynamic

consistency of these results.

The Gibbs-Duhem equation may be written (47) as follows for a binary In-Pb system:

$$x_{Pb}\ d\ \ln\ \gamma_{Pb} + x_{In}\ d\ \ln\ \gamma_{In} - \frac{\Delta v}{RT}\ dP_{TOTAL}$$

$$+ \frac{\Delta H}{RT^2}\ dT = 0 \qquad (17)$$

where P_{TOTAL} is the total pressure

$\Delta v = v - x_{Pb}v^{\circ}_{Pb} - x_{IN}v^{\circ}_{In}$ = volume change on mixing,

$\Delta H = H - x_{Pb}H^{\circ}_{Pb} - x_{In}H^{\circ}_{In}$ = enthalpy change on mixing.

Because the activity coefficients will be measured at several constant temperatures, the fourth term in Equation 17 vanishes. Because the volume change on mixing for the indium-lead system is less than 4.5% deviant from an ideal solution at 500°C according to Pokrovskii et al. (86) and less than 2% deviant according to Predel and Emam (88), and because pressure changes are so minute, the third term can be neglected. With experimental values of γ_{Pb} and γ_{In} across the alloy composition range, a slope consistency test can be made at any value of x_{Pb} or an integral test made across the entire range or any part thereof. Stevenson and Sater (107) point out that a number of integral tests on smoothed data made at 0.1 mole

fraction intervals along x_{Pb} may be effective in testing for Gibbs-Duhem consistency.

If the activity coefficient data are not too badly scattered (however, see Appendix A), temperature coefficients of activities can lead to partial molar and integral entropies, enthalpies and free energies of mixing, viz.:

$$\Delta\bar{G}_{Pb} = \bar{G}_{Pb} - G^{\circ}_{Pb} = RT \ln a_{Pb} \tag{18}$$

From the Gibbs-Helmholtz equation,

$$\left\{\frac{(\partial\bar{G}_{Pb})}{\partial T}\right\}_{p} = -\Delta\bar{S}_{Pb} \tag{19}$$

and

$$\Delta\bar{H}_{Pb} = \Delta\bar{G}_{Pb} + T\Delta\bar{S}_{Pb} \tag{20}$$

where the superscript bars represent partial molar quantities. Similar equations are naturally valid for indium.

The integral quantities are found from the partial molar quantities in the following manner:

$$\Delta G = x_{Pb}\Delta\bar{G}_{Pb} + x_{In}\Delta\bar{G}_{In}, \tag{21}$$

$$\Delta H = x_{Pb}\Delta\bar{H}_{Pb} + x_{In}\Delta\bar{H}_{In}, \tag{22}$$

and

$$\Delta S = x_{Pb}\Delta\bar{S}_{Pb} + x_{In}\Delta\bar{S}_{In}. \tag{23}$$

Hultgren (48) points out that integral heats of mixing and entropies determined in this manner are inferior to calorimetric measurements because of the large errors involved in measuring temperature coefficients of activities.

Hougen et al. (47) outlines two semi-empirical types of equations which may be used to fit activity coefficient data as a function of composition for binary systems. Both have only two constants to be determined. The modified van Laar method uses

$$\log \gamma_1 = \frac{Ax_2^2}{(\frac{A}{B} x_1+x_2)^2}, \quad \log \gamma_2 = \frac{Bx_1^2}{(x_1+\frac{B}{A} x_2)^2} \tag{24}$$

with the specification that

$$1 \leq \frac{A}{B} \leq 2. \tag{25}$$

The Redlich-Kister type 3 method fits the smoothed In-Pb data of Hultgren et al. (49) better:

$$\ln \gamma_1 = -4C\, x_2^3 + (3C+B)x_2^2, \ \ln \gamma_2 = 4C\, x_1^3 + (B-3C)x_1^2. \tag{26}$$

PREVIOUS WORK

In this section, three basic categories of previous work will be considered. The first of these is the determination of physical or chemical properties of the lead, indium and alloy, and also properties of thermocouples and crucibles used. The second category is a study of some of the previous Langmuir vaporization work with an emphasis on liquid metal vaporizations. Finally the third category is a review of others' work on lead and indium vapor pressures and on the alloy system.

Properties of Materials

McGonigal *et al.* (73) and Strauss *et al.* (108) have measured the densities of pure indium and lead, respectively, with the following results:

$$\rho_{In}(g/cc) = 7.129 - 6.798 \times 10^{-4}\ T(°C),\quad 156 \leq T \leq 2013°C \qquad (27)$$

$$\rho_{Pb}(g/cc) = 11.148 - 1.466 \times 10^{-3}\ T(°C) + 1.920 \times 10^{-7} T^2,$$

$$335 \leq T \leq 807°C. \qquad (28)$$

Pokrovskii *et al.* (86) was previously mentioned to have measured indium-lead alloy densities up to 500°C, showing a maximum deviation of 4.5% from ideal solution specific volumes. Predel and Emam (88) found that the maximum deviation is less than 2%. In calculation of Clausing factors, the solution

density is required, and it was found satisfactory to assume negligible volume change on mixing.

Honig (46) has shown with mass spectrometer work that lead vaporizes as a monomer in the temperature range of interest here. He found that at 800°K, $Pb_2/Pb=3 \times 10^{-5}$. DeMaria et al. (22) on similar work with indium likewise found $In_2/In \leq 3 \times 10^{-5}$ between 125° and 1351°K. Other species were negligible.

Figure 3 summarizes the work of Alcock and Belford (1) on the solubility of oxygen in liquid lead, and also the summary of Hansen and Anderko (39) of the solubilities of both carbon and oxygen. It is very important to note the rapid increase in solubility of oxygen in lead in the 600 to 700°C range. Bandyopadhyay and Ray (6) state that several hours are required to reach saturated conditions with liquid lead. Unfortunately, the carbon data is not given at low enough temperatures to be of much use, and no similar data for indium could be found.

Figure 4 shows Glassner's (31) summary of the standard free energy of formation of some oxides. The important point to notice here is that CO_2 or CO is more stable above room temperature than Pb, which indicates that reduction of lead oxides by graphite is favorable. However, In_2O_3 is more stable than gaseous carbon oxides below about 1050°. As Kubaschewski and Hopkins (64) point out, the free energies of oxides in surface films may vary considerably from those in the bulk.

Figure 3. Carbon and oxygen solubilities in liquid lead from Alcock and Belford (1) and Hansen and Anderko (39)

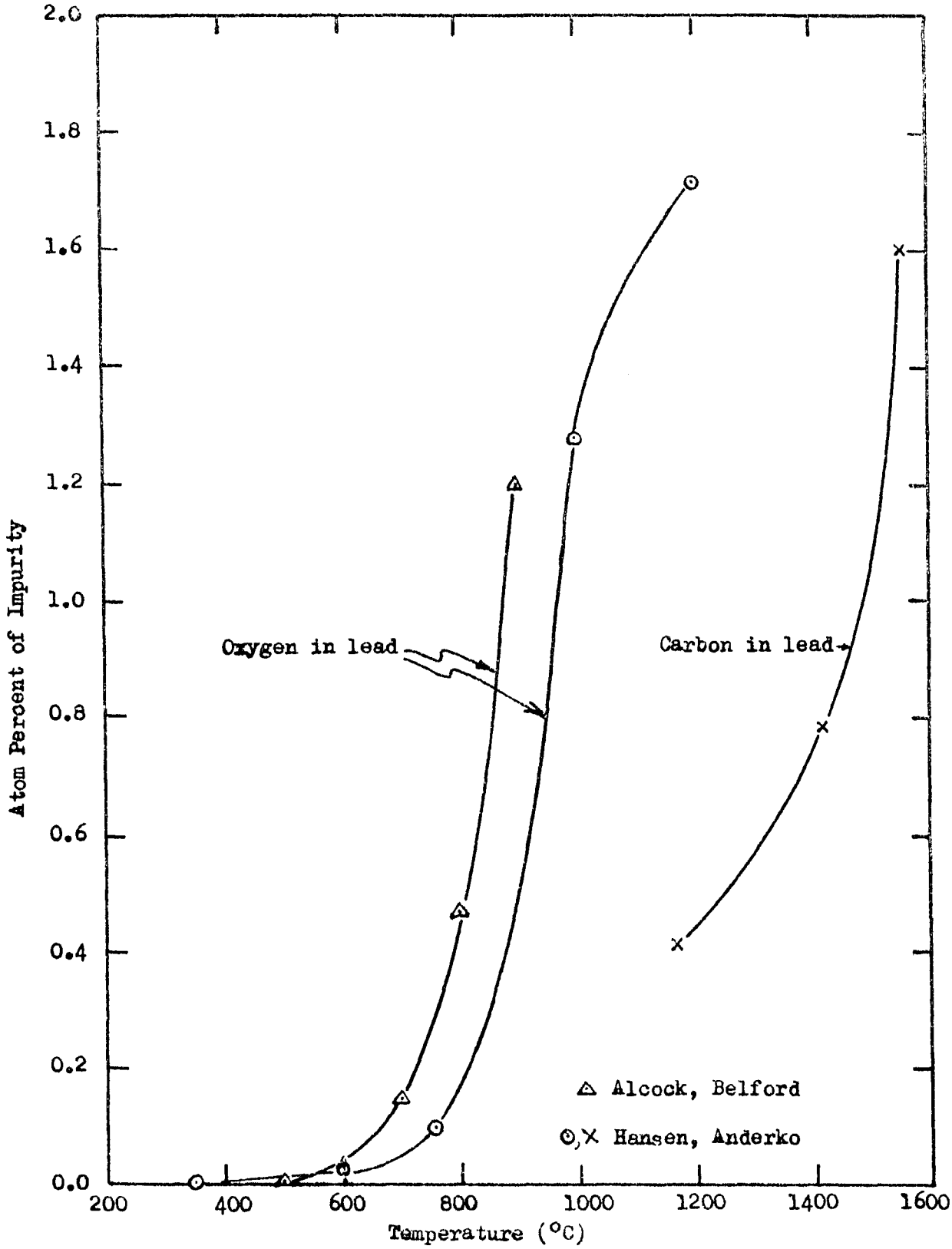
2.0
1.8
1.6
1.4
1.2
1.0
0.8
0.6
0.4
0.2
0.0
Atom Percent of Impurity
Oxygen in lead
Carbon in lead
Alcock, Belford
Hansen, Anderko
200
400
600
800
1000
1200
1400
1600
Temperature (°C)

Figure 4. Standard free energy of formation of some oxides according to Glassner (31)

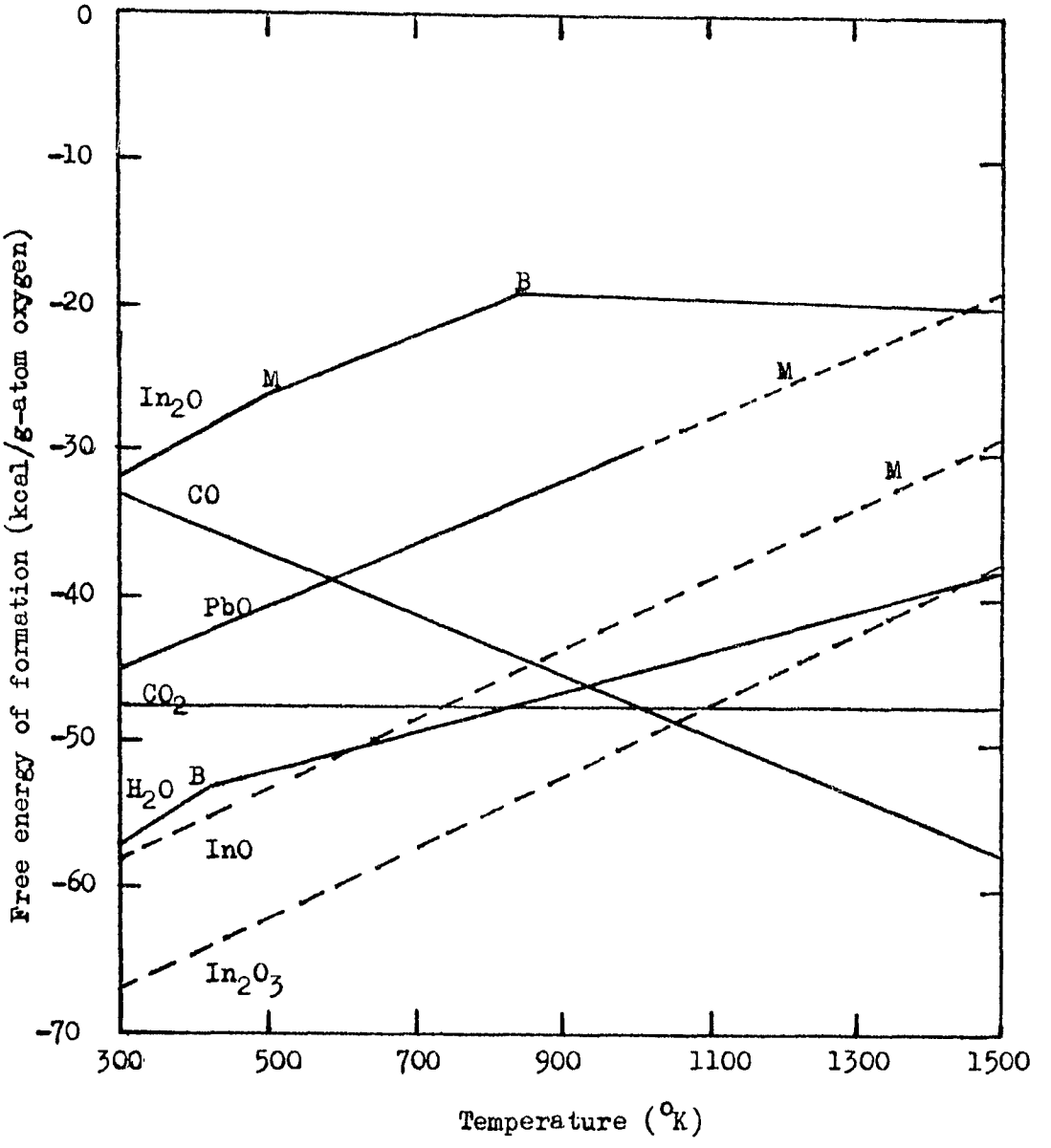
0
-10
-20
-30
-40
-50
-60
-70
Free energy of formation (kcal/g-atom oxygen)
300
500
700
900
1100
1300
1500
Temperature (°K)
B
M
In_2O
CO
PbO
CO_2
H_2O
B
InO
In_2O_3
M
M

Hence either this consideration or a lack of favorable kinetic rates may prevent actual surface oxide reduction.

Green and Hunt (33) have shown that chromel-alumel thermocouples are subject to drifts of 5°C in calibration up to a temperature of only 1000°F (538°C). Their calibrations show a hysteresis effect, also found later in this work. Hendricks and McElroy (42) also showed that Pt-Rh thermocouples under high vacuum service for up to 1000 hr. at 1200-1450°C held a constant calibration only within $\pm$ 10°C. From these results, it appears that chromel-alumel thermocouple calibration may not be especially helpful in view of the hysteresis effect. Also, platinum-rhodium thermocouples might require recalibration after long periods of use.

The National Carbon Co. (81) gives a method for finding the temperature coefficient of thermal expansion for any grade of graphite provided that this value is known at room temperature. Room temperature values for AGSX grade (81) and UF-4S grade (111) used in this work are listed. See Appendicies B and C properties. Since graphite is anisotropic, values are given for "with the grain" and "across the grain." The "with the grain" direction is the direction of extrusion, which is axial rather than radial in the crucibles used in this work.

Blakely and Overholser (7) studied the outgassing of reactor grade graphite, similar to UF-4S grade. The rate of outgassing at constant temperature varied inversely with time.

At 1000°C, which was the outgassing temperature in this work, the total outgassed volume (at standard conditions) was 15% of the graphite volume. At 700°C, the predominant constituents of the gas were fairly evenly divided between (in order, highest first) CO, hydrocarbons, H_2, CO_2, H_2O and N_2. This indicates that the water initially present is largely but, not completely, reduced.

Langmuir Vaporizations

Paule and Margrave (85) list a large number of the published works done using the Langmuir method up to 1966. An extensive literature search on Langmuir vaporization has also been done by this author, however space and time precludes mentioning each of them. Paule and Margrave (85) list about 56 Langmuir vaporization studies on metallic elements, and another 41 on non-metals and compounds, but list no alloys. This author has discovered seven additional published works on alloys not mentioned by Paule and Margrave, and other pure component Langmuir vaporizations they missed.

Gulbransen and Andrew (38) have made the only Langmuir study of the vaporization of solid alloys. They vaporized the alloys Fe-Al, Fe-Cr, Fe-Cr-Al at very low rates (pure component vapor pressures were less than 10^{-5} mm Hg) to insure surface depletion effects would not be present. In this study and others with pure Be (36) and Cr (37), they made careful

studies of the effects varying amounts of oxide and nitride surface layers had on the vaporization rate. Oxides caused reductions in the vapor pressures of from 7% to factors of 60. For Be, they found that the amount of vapor pressure lowering was proportional to the square root of the oxide layer (36).

Johnston and Marshall (52) measured the vapor pressure of solid nickel vaporizing through oxide layers from 2.1 to 9.2 x 10^5 angstroms thick, and found the vapor pressure reduced from 0 to 65% of the "clean" sample pressures. Blocher and Campbell (8) stated that oxide and nitride films on titanium diffused rapidly into solid solution and caused no vaporization rate slowdowns, but Edwards et al. (25) found results to the contrary in the same temperature range.

About 20% of the Langmuir metallic vaporizations have been done with liquids, and about half of these have been with alloys. Pure liquid metal vapor pressures have been measured by Marshall et al. (72), who vaporized copper from a groove in an inductively heated ring; Koch and coworkers, who vaporized titanium and iron (61), molybdenum and zirconium (59), and columbium and hafnium (60) using buttons of metal heated by electron beams; Krupkowski and Golonka (63), who vaporized copper and silver from an inductively heated one inch diameter crucible; Rossmann and Yarwood (99), whose Hg, Ag, Au and Al samples in tiny graphite crucibles were contaminated with carbon dust; and Endebrock and Engle (28), who achieved a

maximum rate only 45% of theoretical with bismuth because of oxide contamination.

Liquid alloy vaporizations or distillations conducted by the Langmuir method include those by Ohno and Ishida (84), who obtained surface depletion with several dilute (< 3 wt. % solute) iron alloys; Walsh and Burnet (118), who measured surface concentrations of three stagnant, moderate solute concentration alloys to detect surface depletion; Bradley and Webster (10), who could not eliminate surface depletion in very dilute (50 ppm) dismuth alloys even by forced convection; McKenzie (74), who used the radioactivity of Pu to detect removal of Pu from dilute (< 0.24 wt. % Pu) uranium alloys, and had surface oxidation problems; Voronin and Evseev (117), who vaporized Sb from moderate concentration Sb-Cu and Sb-Sn alloys at high rates and detected surface depletion; and Murphy et al. (80), who distilled impurities (especially Cr, Mn) from thorium and found lower than expected removal rates because of intermetallic compound formation or surface depletion.

It was also of interest to investigate published and unpublished previous Ames Laboratory Chemical Engineering Department work in this area. Kappraff (53) vaporized Sb-Bi, Pb-Bi, and Sb-Pb liquid alloys and obtained from 1 to 28% of theoretical rates. In attempting Knudsen vaporizations with different orifice sizes, the rates depended greatly on orifice size, and reached > 1000% of theoretical for small sizes.

Temperature measurements were inaccurate.

Stachura (106) used a Langmuir vaporization and was able to attain theoretical vaporization rates with pure, clean thallium, but his pure lead and alloy samples oxidized, causing these rates to drop to about 60% of theoretical. Activities computed from these rates agreed well with EMF activities, however. His temperature measurements are subject to error.

Lenz (67) obtained reasonable thallium activities in lead alloys, with modified Langmuir techniques, but vaporization rates given are three to seven times too high. However, he states temperatures measured checked pure component melting points within 5°C. Walsh and Burnet (118) had 1.3 to 53% of theoretical vaporization rates with In-Zn alloys based on their surface concentration measurements, and the results correlated well with visual oxide conditions. The maximum rates were 16% and 53% of theoretical for the only two runs with no visible surface oxide. Rates for Bi-Cd and Sn-Zn were from 0.3 to 7% of theoretical, independent of oxide conditions.

Lead and Indium Vapor Pressures

Table 1 summarizes all work determining lead vapor pressures below 0.1 mm Hg. The errors shown are standard deviations. The column labeled σ_p gives the standard deviation of the pressure in percent from the least squares line

Table 1. Lead vapor pressure summary

Authors	Year	Temp. range (°K)	Data points	$\Delta H^{\circ}_{v, 298}$ (kcal/mole) 3rd law	2nd law	$\log_{10} P$ (mm) = A-B/T A	B
Shiu, Munir (103)	'71	950-1112	46	46.64 ±0.15	46.8 ±0.3	7.758	9,670
Hawkins, Hultgren (41)	'67	950-1125	103	46.63 ±0.14	46.69 ±0.24	7.736	9,651
Kim, Cosgarea (56)	'66	877-975	13	46.59 ±0.04	47.1 ±0.2	7.853	9.750
Aldred, Pratt (3)	'61	880-1050	34	46.81 ±0.52	51.65	8.888	10,804
Goldfinger, Jeunehomme (32)	'63	913-1032	6	46.77 ±0.11 (K=1)	47.3 ±1.1	7.882	9,824
				46.48 ±0.12 (K=.86)	47.3 ±1.1	7.948	9,824
Egerton (26)	'23	800-1045	23	47.21 ±0.22	47.6 ±0.7	7.908	9.923

σ_P (%)	$\Delta S^\circ_{v,\,298}$ $\left(\frac{cal}{mole\text{-}K^\circ}\right)$	Method	Crucible	Thermocouple temperature measurement	Surface preparation	Residual pressure (mm Hg)
2.6	26.6 ±0.2	Torsion effusion; 2.0, 1.5 mm D	ZT101 graphite	Chromel-alumel; cal. in situ	Dil. HCl etch	$\sim 5\times10^{-6}$
4.9	26.4 ±0.2	Torsion effusion; 1.0, 1.5 mm D	Non-porous, high purity graphite	Chromel-alumel, calibrated		$<2\times10^{-5}$
1.5	26.8 ±0.2	Knudsen, torsion effusion; 0.8, 1.1 mm D	Graphite, with plugs	Chromel-alumel in well 1/2" from cell; calibrated		$\sim 5\times10^{-6}$
	31.6	Torsion effusion	Graphite	Pt-Pt 13%Rh in silica sheath 5mm from cell; cal. vs. another in cell		$\sim 5\times10^{-6}$
5.7	27.0 ±1.1	Knudsen; 1.4mm D	Quartz in stainless steel oven	Pt-Pt10%Rh, 0.1-0.05"D with tiny quartz insulators; cal. in situ		$<10^{-5}$
5.7	27.3 ±1.1					
11.4	28.1 ±0.7	Knudsen; 2mm D; start by H_2 evacuation	Nickel, or clear silica inside steel or nickel ovens	Fe-constantan cal. after each run vs. Pt-Rh (±0.1°C) and vs. m.p. (±1°C)	Filter in vacuum before run	$\sim 10^{-5}$

Table 1. (Continued)

Authors	Year	Temp. range (°K)	Data points	$\Delta H^{\circ}_{v,\ 298}$ (kcal/mole) 3rd law	2nd law	$\log_{10} P\ (mm) = \frac{A-B}{T}$ A	B
Present work, preliminary	'69	784-1030	42	46.99 ±0.24	47.7 ±0.4	7.968	9,940
Present work, final	'71	786-1019	27	46.59 ±0.13	47.1 ±0.2	7.906	9.795

σ_P (%)	$\Delta S^\circ_{v,\,298}$ $\left(\frac{cal}{mole\text{-}K^\circ}\right)$	Method	Crucible	Thermocouple temperature measurement	Surface preparation	Residual pressure (mm Hg)
11.1	27.3 ±0.4	Modified Langmuir; 6.37 mm D	AGSX graphite	Chromel-alumel in crucible; calibrated later vs. probe	Scraped with blade; melt and flow technique	$<1.5\times10^{-5}$ $\sim2\times10^{-6}$
4.7	27.0 ±0.2	Modified Langmuir; 6.32 mm D	UF-4S high purity graphite	Chromel-alumel surface probe 0.013" D; cal. vs. m.p.	50% HNO_3 etch after vac. melt; melt and flow technique	$<1.0\times10^{-5}$ $\sim2\times10^{-6}$

having the constants shown in the preceding columns for the respective authors. Some of the data given were calculated by this author from the original authors' data.

The values obtained in this work are shown for completeness, but will be discussed later. Hawkins and Hultgren (41), Aldred and Pratt (3) and Shiu and Munir (103) all used the torsion effusion method. Kim and Cosgarea (56) used concurrent Knudsen and torsion effusion methods, while Goldfinger and Jeunehomme (32) and Egerton (26), in his early determinations, used Knudsen effusion. Each of these authors used some type of resistance heating. Hawkins and Hultgren (41), Kim and Cosgarea (56) and Shiu and Munir (103) varied the size of their effusion orifices without affecting their results, and their third-law $\Delta H^{\circ}_{v,298}$ values were independent of temperature.

Egerton (26) and Shiu and Munir (103) are the only authors who mentioned any special sample preparation. Egerton filtered his samples under vacuum in an attempt to remove oxides, but mentioned that samples were often oxidized anyway and gave lower pressures. He attempted to include only results from apparently clean samples. Shiu and Munir used a dilute hydrochloric acid etch to remove surface oxides before use.

It is clear that Aldred and Pratt's (3) work is not reliable despite the proximity of their third law heat of vaporization value to the others' values. Their second and third law values disagree greatly, and $\Delta S^{\circ}_{v,298}$ is far from the

value of 26.34 cal/g-mole-°K expected from referenced (50) free energy function data, as mentioned in the Theory section. On the other hand, the work of Hawkins and Hultgren (41) and Shiu and Munir (103) are the most reliable for these same reasons. Egerton's (26) third law heat of vaporization is slightly high, which corresponds to lower vapor pressures than the others measured. This was undoubtedly due to his oxide problems. Kim and Cosgarea (56) showed excellent precision in their work as reflected in σ_p of only 1.5%, whereas most others were about 5%. Goldfinger and Jeunehomme (32) were not certain what value to use for the Clausing factor (K) of their thin orifices, but estimated that the minimum value was 0.86. They also said that this correction might not be appropriate, and that the correct values probably were between those given for K = 1 and K = 0.86.

Since every experimental value of the second law heat of vaporization is higher than the corresponding third law value, it is possible that Hultgren's (50) free energy function values are slightly in error.

Figure 5 shows the least square lines of the data in Table 1. Also shown are the vapor pressures determined for the lead oxide monomer by Drowart et al. (23) who used the Knudsen effusion technique coupled with a mass spectrograph, and the total pressure over lead oxide by Nesmeyanov et al. (82,83) who used the Knudsen, Langmuir and transpiration techniques.

Figure 5. Lead vapor pressures, total pressure over lead oxide and PbO monomer pressure by several workers

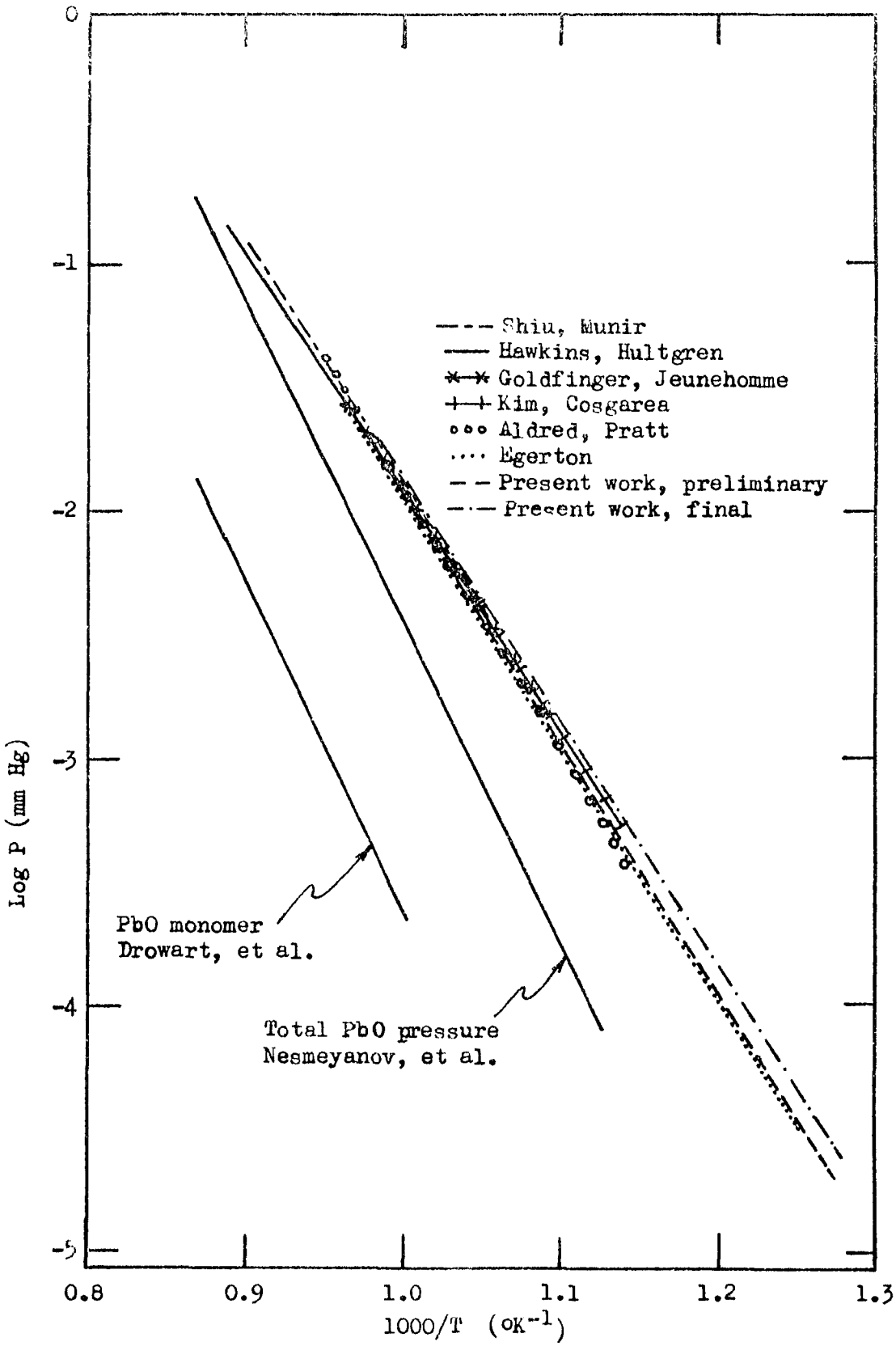
0
-1
-2
-3
-4
-5
Log P (mm Hg)
0.8
0.9
1.0
1.1
1.2
1.3
1000/T (°K-1)
Shiu, Munir
Hawkins, Hultgren
Goldfinger, Jeunehomme
Kim, Cosgarea
Aldred, Pratt
Egerton
Present work, preliminary
Present work, final
PbO monomer
Drowart, et al.
Total PbO pressure
Nesmeyanov, et al.

The transpiration (also called flow or transport) technique passes an inert gas over a substance at a rate so that it becomes saturated with the substance's vapors. The amount of gas used and weight of substance picked up determine the partial pressure of the substance in the gas, provided the ideal gas law holds. The proper flow rate to use is determined by experiment, and must be neither too high nor too low.

For both lead and indium, Brewer and Rosenblatt (12) show that vaporization will tend to result in a decrease of oxygen in the bulk metal since the ratio of oxygen to metal in the vapor is higher than the same ratio in the bulk. The fact that the oxide pressures are low ($P_{Pb} > 2.8\ P_{PbO,TOTAL}$) means that if oxide is present on the surface which blocks pure metal vaporization, the observed weight losses will be too low. Vaporization of oxide from the bulk contributes negligibly to the weight loss because its mole fraction is extremely low, but vaporization of oxide from a second surface phase which does not hinder vaporization of the metal below could cause an addition to the observed metal vaporization rate.

Table 2 summarizes indium vapor pressures determined below 0.1 mm Hg. The errors shown are standard deviations. The column headed σ_P gives the standard deviation of the pressures in percent from the least squares line having the constants shown in the preceding columns. Some of the data given were calculated by this author from the original authors'

Table 2. Indium vapor pressure summary

Authors	Year	Temp. range (°K)	Data points	$\Delta H^\circ_{v, 298}$ (kcal/mole) 3rd law	2nd law	$\log_{10} P$ (mm) = A-B/T A	B
Herrick (43)	'64	1102-1422	88	58.09 ±0.92	58.8 ±1.6	8.408	12,640
Anderson (4)	'43	1000-1348	8	58.18 ±0.24	57.5 ±0.9	8.003	12,180
Macur, Edwards, Wahlbeck (71)	'66	1197-1473	53	56.58 ±0.32	59.6 ±0.5	8.665	12,638
Priselkov, et al. (90)	'60	est. 1150-1320	9	56.79	53.0	7.453	11,221
Lyubimov, Lyubitov (70)	'57	646-1065	10	57.95 ±0.60	55.74		
Alcock, Cornish, Grieveson (2)	'66	1180-1301	7	57.24 ±0.23			
		----------	----------	----------	61.8 ±1.5	8.96	13,120
		1228-1346	3	57.08 ±0.23			
Present work, preliminary	'69	1208-1211	5	56.86 ±0.27			

σ_P (%)	$\Delta S^\circ_{v,\,298}$ $\left(\frac{cal}{mole-°K}\right)$	Method	Crucible	Thermocouple temperature measurement	Surface preparation	Residual pressure (mm Hg)
37.4	28.88 ±0.93	Torsion effusion	Stackpole graphite; 1.13-1.58 mm D; Ag calibrated	Pt-Pt10%Rh near cell	Arc melt to 1/4" rod in inert gas; benzene wash; 700°K outgas, 1 hour	$<2\times10^{-5}$
10.5	27.00 ±0.56	Knudsen; 1.42, 1.98 mm D	Silica liner in steel	Chromel-alumel, calibrated; in direct contact with steel		10^{-4}
9.5	30.09 ±0.32	Multiple Knudsen effusion; 0.8-1.5 mm D	Alumina AP 35; Hg calibrated	Pt-Pt10%Rh in center of Mo block; calibrated at 3 m.p. before, after	Wash with benzene; outgas 15 hr. at 200°C, 4 hr. at 600°C	10^{-4} to 10^{-5}
	24.47	Knudsen	Porcelain			
		Mass Spectrograph	Quartz			
		Knudsen; 0.55 mm D	Beryllia; Ta lid			$<10^{-5}$
6.6	31.42 ±0.87	----------	----------	Thermocouple		
		H_2 flow	Beryllia			
10.1		Modified Langmuir; 6.37 mm D	AGSX graphite	Chromel-alumel in crucible; calibrated later vs. probe	Scraped with blade prior to run; melt and flow technique	$<1.4\times10^{-5}$

data.

Alcock et al. (2) used both the Knudsen method (top) and transpiration method (bottom) and averaged the results except for third law enthalpy of vaporization values. Lyubimov and Lyubitov (70) used the mass spectrograph, Herrick (43) used torsion effusion, and the rest all used Knudsen effusion. Macur et al. (71) ran about seven Knudsen cells mounted in a large molybdenum block in the hope of promoting temperature uniformity. They succeeded in this, since the standard deviation of the pressures at constant temperature was only about 3%, compared to the σ_p (deviation from the least squares line) of 9.9%. This indicates that their temperature measurement technique was poor, however. In addition, their third law heats of vaporization show a slight decreasing trend with increasing temperature. Priselkov et al. (90) used induction heating, while all others used resistance heating.

Only Herrick's (43) and Anderson's (4) second law and third law heats of vaporization are in agreement with each other, and no author's entropy of vaporization is within one standard deviation of the value of 27.69 cal/g-mole-°K computed from referenced (49) free energy functions. Part of this may be due to uncertainties in the latter, since only estimates for the heat capacity and free energy functions in indium are used above 900°K. From these free energy functions, it appears that Anderson's early work is the most reliable. He and Macur

et al. (71) both varied the orifice size without effect on the vapor pressures. Herrick has large uncertainties in his pressures due to a lack of zero reproducibility in his torsion effusion measurements.

Figure 6 represents the larger uncertainty in indium vapor pressures compared to lead. The total pressures over indium oxide were obtained by Burns et al. (14) using the Knudsen method with a mass spectrograph and by Burns (13) combining Knudsen, Langmuir and mass spectrograph measurements. The oxide pressure is more than two orders of magnitude below the indium vapor pressure.

Indium-Lead Alloy Thermodynamic Data

The activity coefficients of indium in indium-lead melts were determined by an EMF method by Terpilowski and Gregorczyk (110), and the activity coefficients of lead were computed using Equation 17, the Gibbs-Duhem equation. The smoothed values at 400°C shown in Figure 7 are taken from the summary of Hultgren et al. (49). It is useful to note that the alpha function, $\log \gamma_1/x_2^2$ is useful for this system in extrapolating the activity coefficients to zero concentration. Moser (76) states that the indium-lead system is semi-regular. This means that the partial molar enthalpies and entropies are temperature independent. He also says that half Terpilowski and Gregorczyk's experimental data showed marked scatter, and hence used only the

Figure 6. Indium vapor pressures and total pressures over indium oxide by several workers

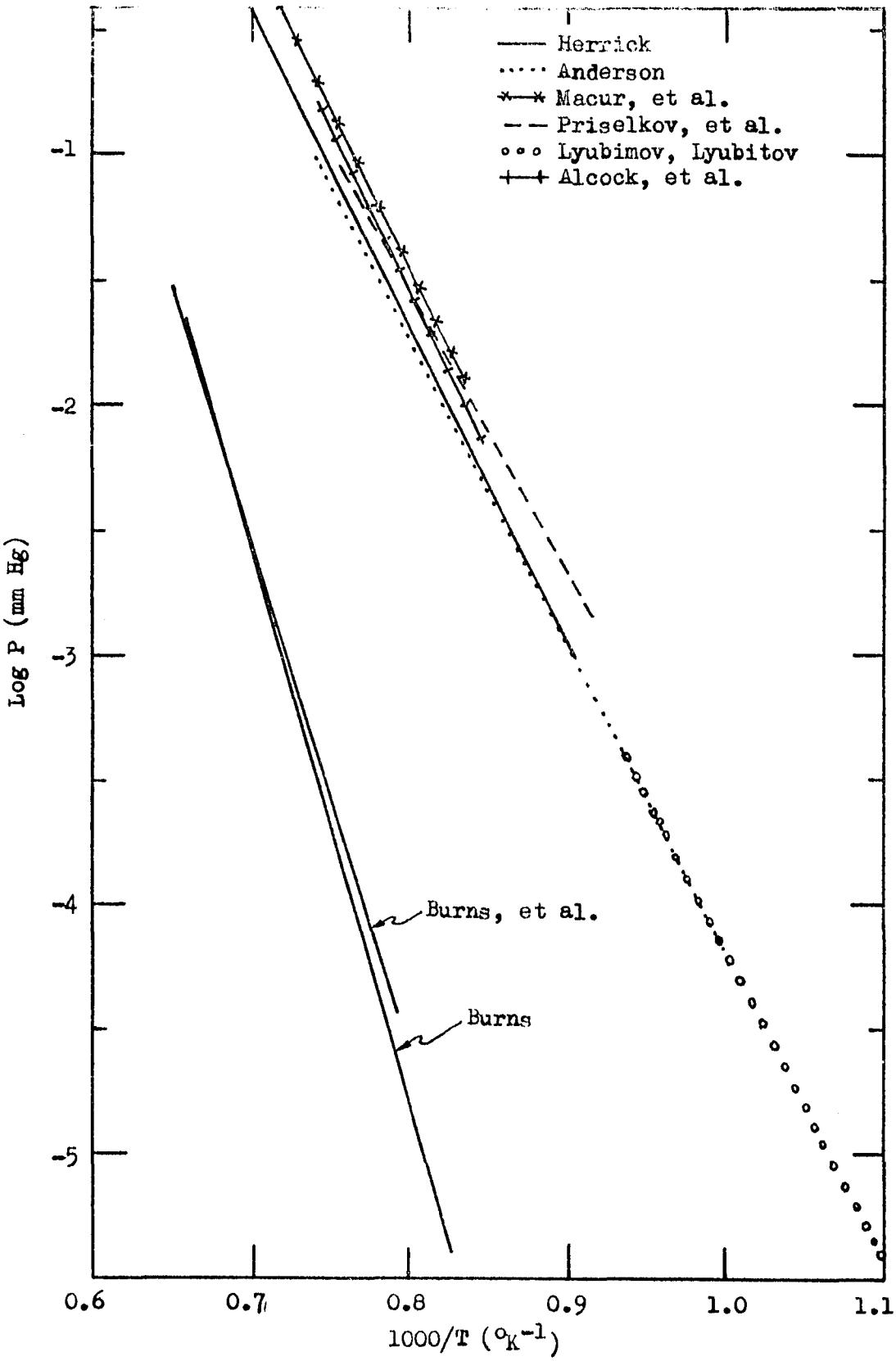
Herrick
Anderson
Macur, et al.
Priselkov, et al.
Lyubimov, Lyubitov
Alcock, et al.
Burns, et al.
Burns
Log P (mm Hg)
-1
-2
-3
-4
-5
0.6
0.7
0.8
0.9
1.0
1.1
1000/T (°K-1)

Figure 7. Smoothed indium-lead activity coefficient data at 400°C from Hultgren et al. (49)

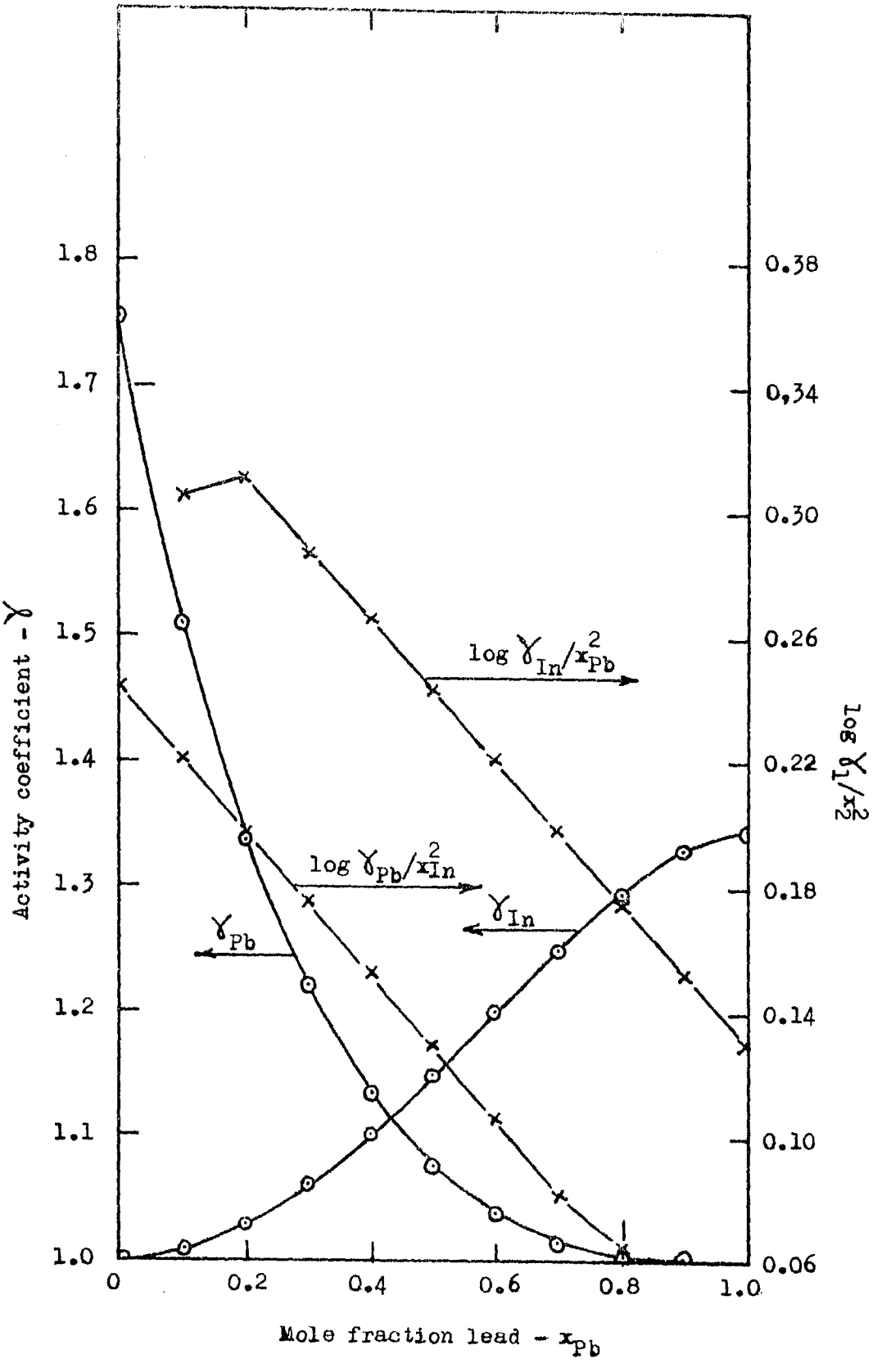
1.8
1.7
1.6
1.5
1.4
1.3
1.2
1.1
1.0
0.38
0,34
0.30
0.26
0.22
0.18
0.14
0.10
0.06
0
0.2
0.4
0.6
0.8
1.0
Activity coefficient - γ
log γ1/x2
Mole fraction lead - xPb
log γIn/x²Pb
log γPb/x²In
γIn
γPb

other half in fitting the equations

$$\ln\gamma_{In} = (576/T - 0.390)(1 - x_{In})^{1.9} \qquad (29)$$

$$\ln\gamma_{Pb} = (576/T - 0.390)[(1 - x_{In})^{1.9} - 2.111(1 - x_{In})^{0.9} + 1.111] \qquad (30)$$

where T is in °K. These equations are compared to others' data in the Results section (see Figure 29).

Recently Shiu and Munir (104) used the torsion effusion method to measure the partial pressure of lead over indium-lead melts in a temperature range of about 985 - 1155°K. Using their previous lead vapor pressure data (103), they then calculated lead activity coefficients. A maximum temperature error of 1°C is claimed for both the lead (103) and alloy (104) vaporizations using in situ calibration of chromel-alumel thermocouples. In earlier torsion effusion work (78,79) where a Pt - Pb 10% Rh thermocouple was calibrated in a dummy cell, a poorer 5°C maximum error was claimed. They computed the indium activity coefficients from the Gibbs-Duhem equation, Equation 17. Using the Gibbs-Helmholtz relation, Equation 19, along with Equations 16 and 18, and surprisingly only three or four data points to determine slopes, they also computed partial molar entropies, free energies and enthalpies for each component at 1070°K. These were then used to calculate the corresponding integral quantities using Equations 21, 22 and

23. Shiu and Munir (104) state that the indium-lead solution at 1070°K approximates the behavior of an ideal solution, or at least a regular solution. In a regular solution, the excess entropies are zero, and in an ideal solution, all activity coefficients are unity and all excess properties are zero. Their activity coefficient data will be given in the Results section (see Figure 29).

Calorimetric measurements of the heat of mixing of the indium-lead system have been made by Wittig and Scheidt (125) and Scheil and Lukas (102). Hultgren et al. (49) state that the heats of mixing computed from Terpilowski and Gregorczyk's (110) data agree with those of Wittig and Scheidt, which reach a maximum of 230 $\pm$ 50 cal/g-atom at 400°C when $x_{Pb} = 0.5$. Scheil and Lukas' corresponding heat is 220 cal/g-atom at 340°C, and Shiu and Munir's (104) derived heat at $x_{Pb} = 0.5$ is 320 $\pm$ 150 cal/g-atom at 797°C. Scheil and Lukas state that a small increase of the heat of mixing with temperatures was found. Within the relatively large scatter involved, all these heats of mixing agree.

Several authors have done recent work on both solid and liquid indium-lead alloys indicating positive deviations from ideality ($\gamma > 1.0$) and endothermic heats of mixing ($\Delta H > 0$). Heumann and Predel (44) calorimetrically found a maximum heat of mixing for solid alloys of 400 cal/g-atom based on measurement of heats of solidification of various composition alloys

and others' liquid phase heats of mixing. They also carried out phase diagram studies which indicated a solid state miscibility gap and a eutectoid reaction at -15°C. Koike and Sivertsen (62), in measuring diffuse X-ray scattering in room temperature solid alloys, observed positive local order parameters which indicate clustering of like atoms. From these local order parameters, they estimated a maximum solid phase heat of mixing of 340 cal/g-atom.

Liquid phase resistivity measurements by Dutchak and Korsunskii (24) and by Predel and Sandig (89) found anomalous increases in resistivity in the neighborhood of 20 atom percent lead. These are associated with changed bonding relations which lead to formation of an intermetallic phase in the solid state. Romanova and Mel'nik (92) studied the structure of pure lead and indium liquids using a high resolution X-ray technique to reveal microregions of short-range order.

EQUIPMENT AND EXPERIMENTAL PROCEDURE

A cutaway drawing of the graphite crucible used to obtain lead and indium[1] vapor pressures and partial pressures by the modified Langmuir method is shown in Figure 8. This crucible is an evolutionary product of many designs and has several advantages: 1) The most important is that the crucible forms a fresh, visually oxide-free liquid surface under vacuum. 2) The operator can visually inspect the liquid surface during the initial stages of vaporization. 3) The large vaporization area available permits obtaining lower pressures than attainable by the Knudsen method. 4) The importance of the meniscus location and curvature is minimized since the effective Clausing factor is not sensitive to 1/r at the experimental values of 1/r equal to about eight. 5) The screw in caps are vapor tight. 6) Five samples may be run at one time. The other hole is required for temperature measurement, as will be explained.

The crucible operates as follows for each of the six pairs of melting and vaporizing chambers. A sample of metal is weighed on an analytical balance and dropped into the

---

[1]Appendix B gives analyses of the nominal 9.999% purity lead and indium used, and also of the graphite. Appendix C gives a more detailed description of items of equipment used than is given in the text.

Figure 8. Graphite crucible used in the melt-and-flow method of obtaining clean vaporization surfaces

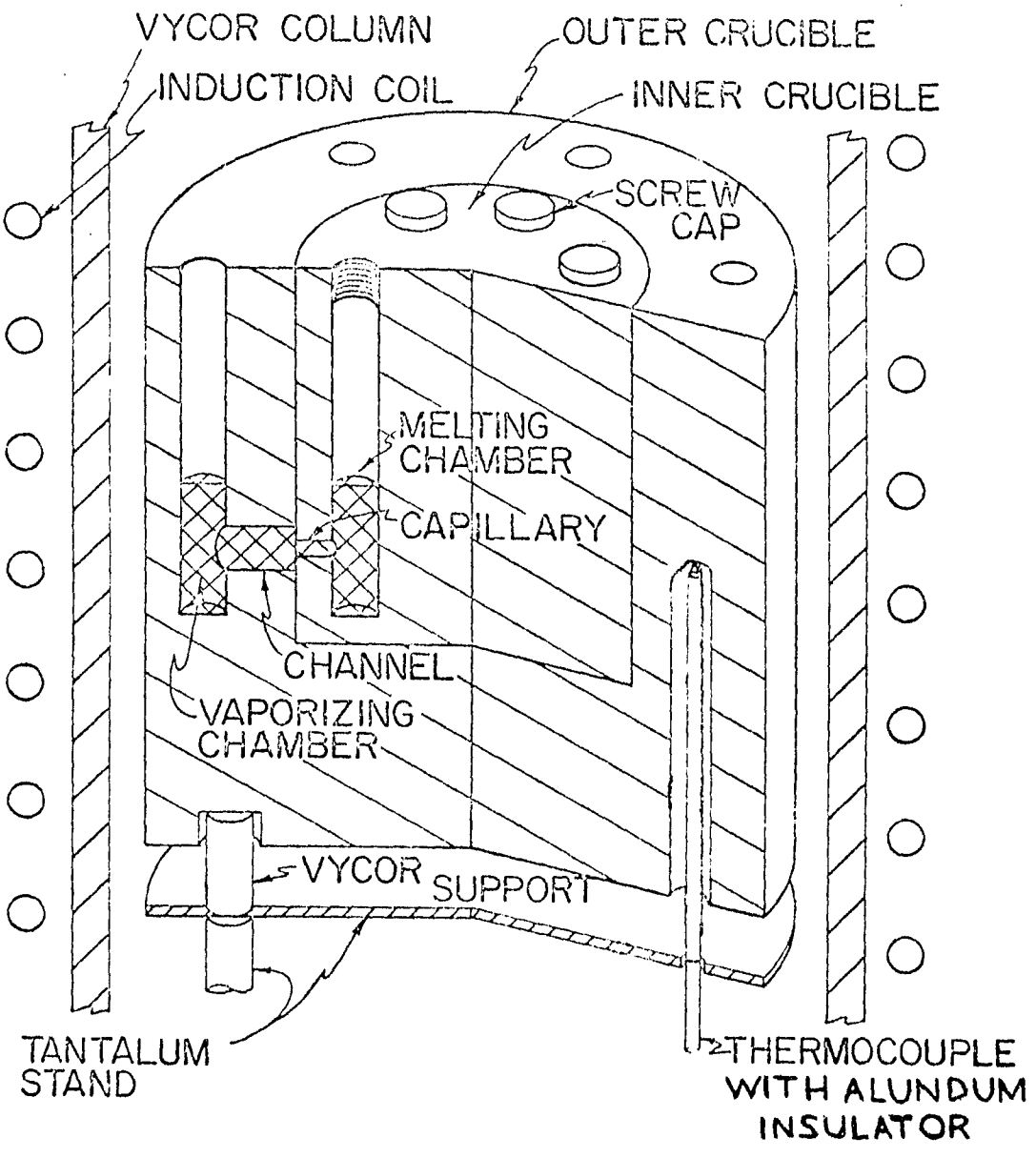
VYCOR COLUMN
INDUCTION COIL
OUTER CRUCIBLE
INNER CRUCIBLE
SCREW CAP
MELTING CHAMBER
CAPILLARY
CHANNEL
VAPORIZING CHAMBER
VYCOR SUPPORT
TANTALUM STAND
THERMOCOUPLE WITH ALUNDUM INSULATOR

melting chamber. The vapor-tight cap, also previously weighed, is screwed down. The system is outgassed by waiting for the pressure to reach at least 2×10^{-6} mm Hg, and then the temperature raised.

As the metal melts quickly, any oxides present float to the top of the liquid surface in the melting chamber, and the capillary admits clean liquid metal into the vaporizing chamber through the channel. The capillary diameter was 0.051 inch for all lead runs and the preliminary indium run in the AGSX crucible. It had to be enlarged to 3/32 inch for the final indium and alloy runs so as to allow completely free flow into the outer chamber. No level differences were ever obtained during a successful run. The vaporizing chamber is 1-1/2 inches deep with a diameter of 1/4 inch. The operator can visually check the surface cleanliness of the samples. In nearly every case, the surfaces are bright and shiny. The crucible is then heated rapidly to the vaporization temperature, which is monitored by two thermocouples. One of these thermocouples is shown in the right hand section of Figure 8, as well as in Figure 9.

Figure 9 shows the probe thermocouple used in measuring the liquid metal surface temperature, and one of two thermocouples in the crucible. One of these two crucible thermocouples is used in controlling the crucible temperature, and the other one monitors the crucible temperature.

Figure 9. Chromel-alumel thermocouple probe and crucible thermocouple used to measure liquid metal temperatures

TEMPERATURE MEASURING SYSTEM

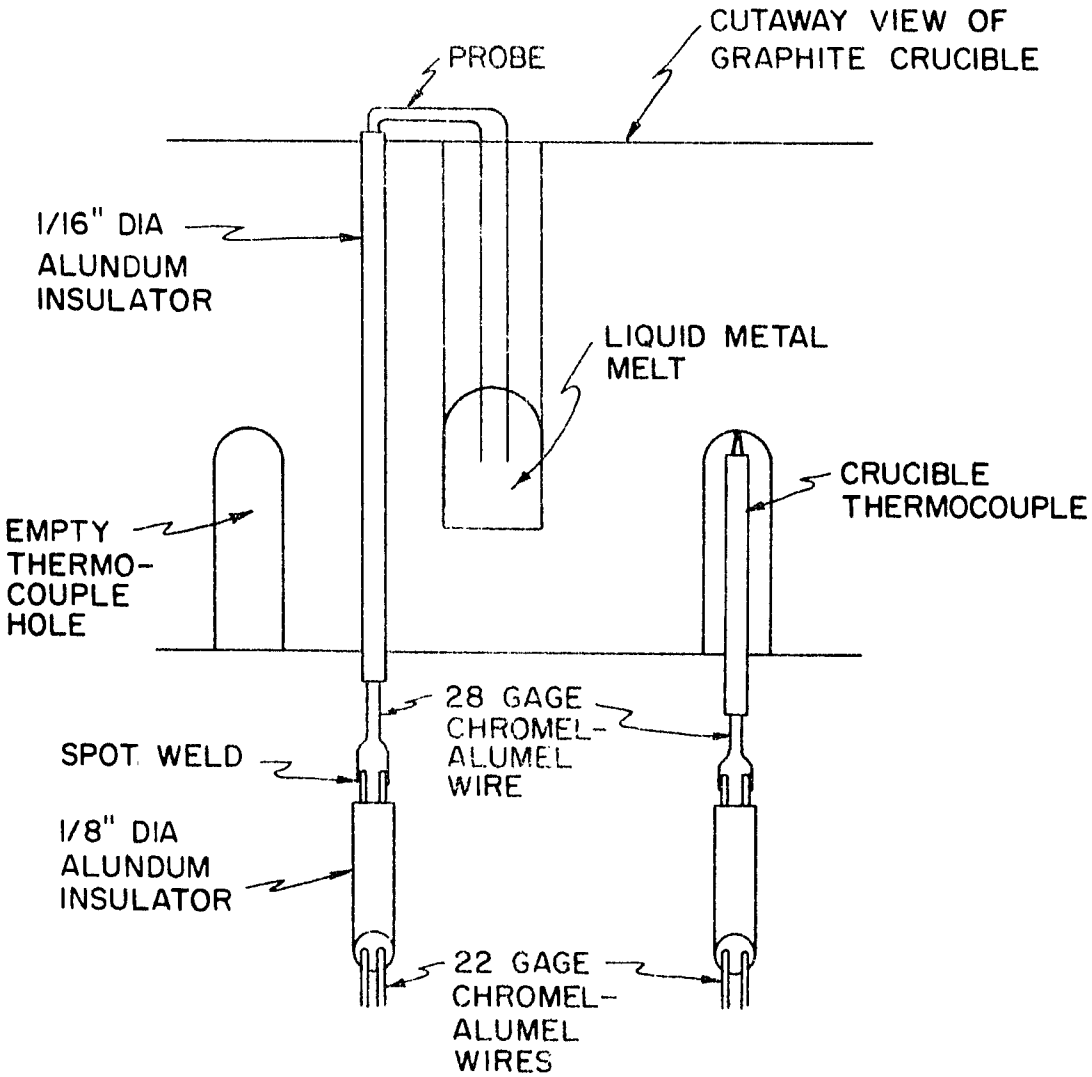

The probe is present in vaporization hole #2 during an experimental run. Chromel (90% nickel and 10% chromium by weight) and alumel (95% nickel, 3% manganese, 2% aluminum and 1% silicon) wires are soluble in lead and indium, but the dissolution takes place slowly, as is indicated in Figure 10 for a typical run. As soon as the temperature stabilizes (about 10 to 20 minutes after melting, and 3 to 4 minutes after reaching the run temperature), it is easy to measure the difference between the probe and crucible thermocouples. This difference is always less than 2°C, and is used to obtain the temperature of the metal in hole #2 from the measured crucible temperature as the run progresses. The other five sample temperatures are previously calibrated versus the temperature of the metal in hole #2 for a fixed geometrical alignment of the crucible and induction coil. Hence, readings of the crucible thermocouple can be translated into any sample temperature.

The probe is naturally replaced after every run by spot welding a new one into position. The probe wire is #28 gauge corresponding to a diameter of 0.0126 inch. The small size is used to minimize conduction losses through the wire. In addition, the probe wire is preheated by passing it through the crucible to further eliminate conduction losses. As will be explained later, the small wire size also helps to minimize the error in determining the surface temperature from the

Figure 10. Example calibration of crucible thermocouple against probe thermocouple at start of a run

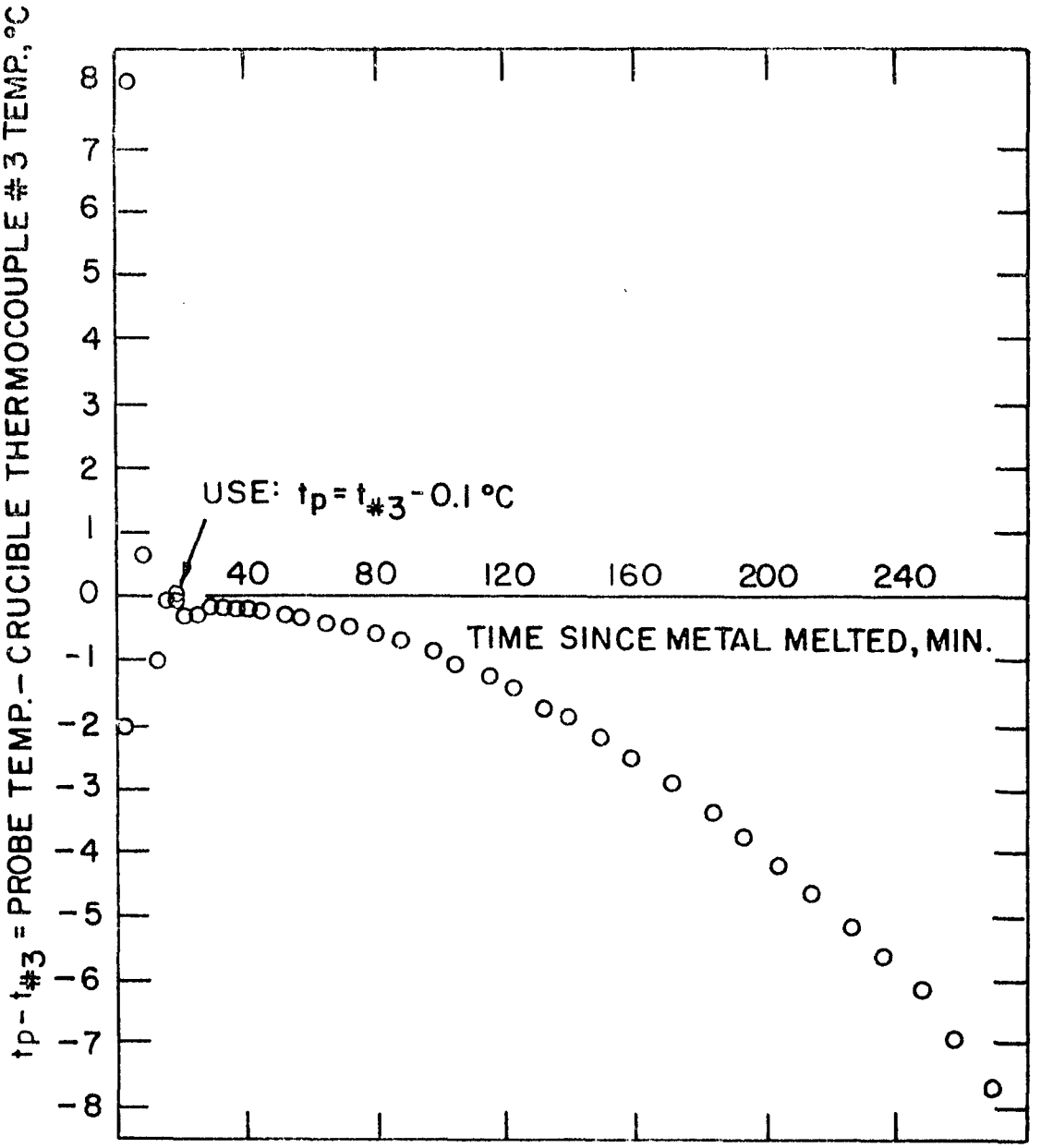
$t_p - t_{\#3}$ = PROBE TEMP. – CRUCIBLE THERMOCOUPLE #3 TEMP., °C
8
7
6
5
4
3
2
1
0
-1
-2
-3
-4
-5
-6
-7
-8
USE: $t_p = t_{\#3} - 0.1$ °C
40
80
120
160
200
240
TIME SINCE METAL MELTED, MIN.

indicated probe temperature. The probe and crucible thermocouples are actually at the same radial position as the outer vaporization holes, as can be seen in Figures 8 and 11. Calibrations of the temperature difference between the probe in hole #2 and the other probes are always done with the same indium-lead alloy composition as is used in the run.

After the run is finished and the crucible cooled, the caps are removed and weighed, since small amounts of condensed metal adhere to them. The crucible is then replaced in the vacuum system upside down on top of a catch crucible. Figure 11 shows the three tiny holes on the perimeter of the outer crucible top which hold pins to align the run crucible and catch crucible. The unvaporized metal is melted into six holes in the catch crucible. Small amounts of metal adhere to the walls and remain in the passages of the run crucible and must be carefully removed by hand. These small bits, together with the slugs from the catch crucible and the condensate on the screw caps, compose the total unvaporized metal. Knowledge of the crucible dimensions, weight of metal vaporized, metal surface temperature, and time of the run enable computation of the vapor pressure of each sample from Equation 5.

A schematic diagram of all the apparatus required for the vaporization is shown in Figure 12. Figure 13 shows a frontal view of the equipment. The author is inserting the inner crucible containing the samples into the outer crucible prior

Figure 11. Picture of inner crucible, with thredded cap removed to reveal sample in hole #6, and outer crucible with thermocouple probe in hole #2

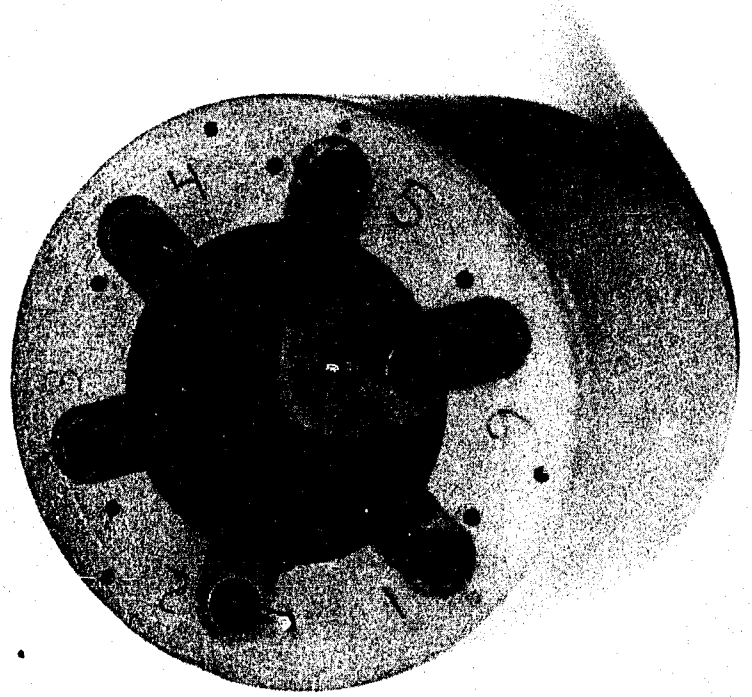

Figure 12. Schematic diagram of experimental equipment

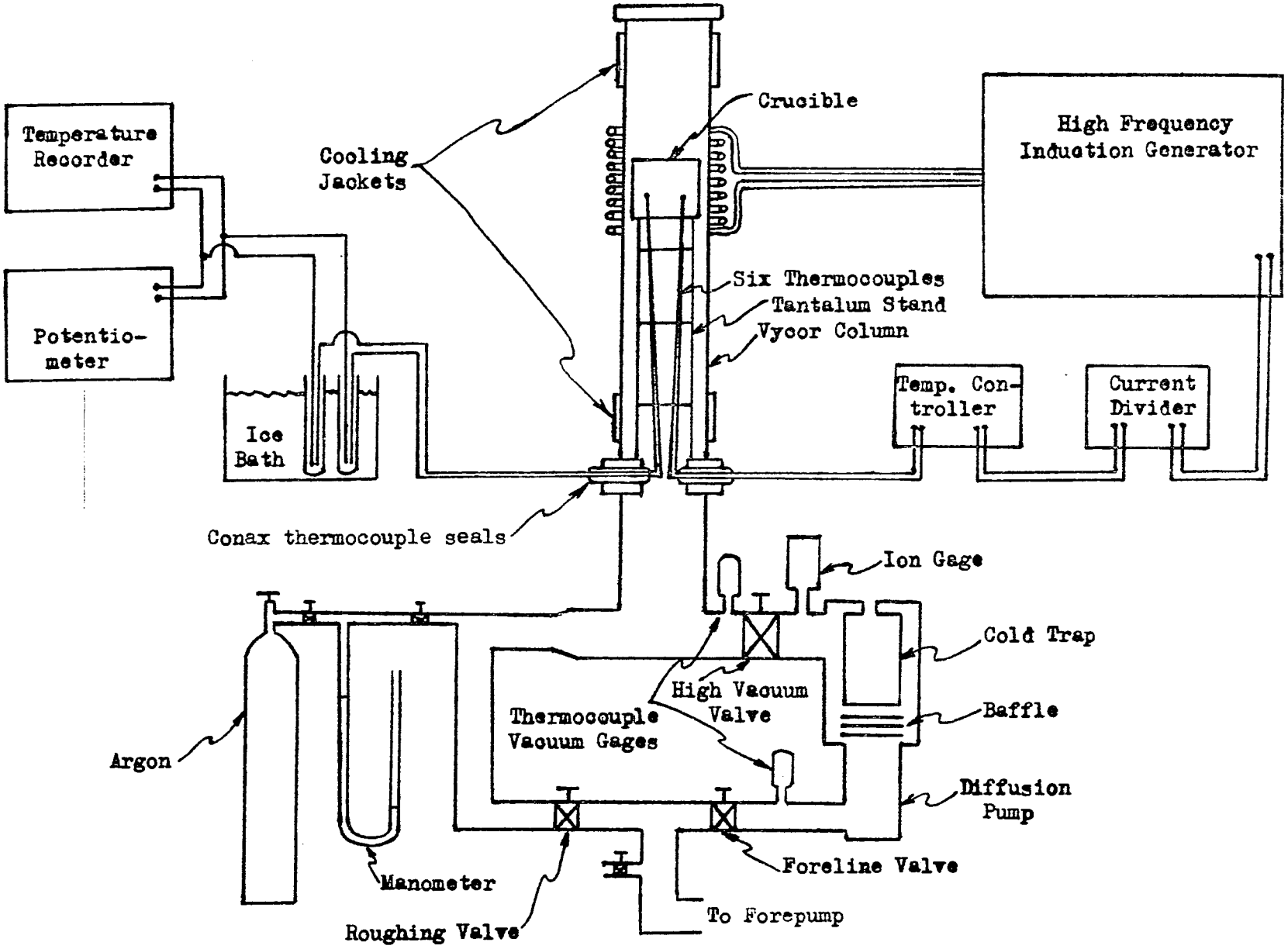
Temperature Recorder
Potentio-meter
Cooling Jackets
Crucible
High Frequency Induction Generator
Six Thermocouples
Tantalum Stand
Vycor Column
Temp. Con-troller
Current Divider
Ice Bath
Conax thermocouple seals
Ion Gage
Cold Trap
High Vacuum Valve
Thermocouple Vacuum Gages
Baffle
Argon
Diffusion Pump
Manometer
Foreline Valve
Roughing Valve
To Forepump

Figure 13. Frontal picture of equipment with author inserting inner crucible containing samples prior to start of run

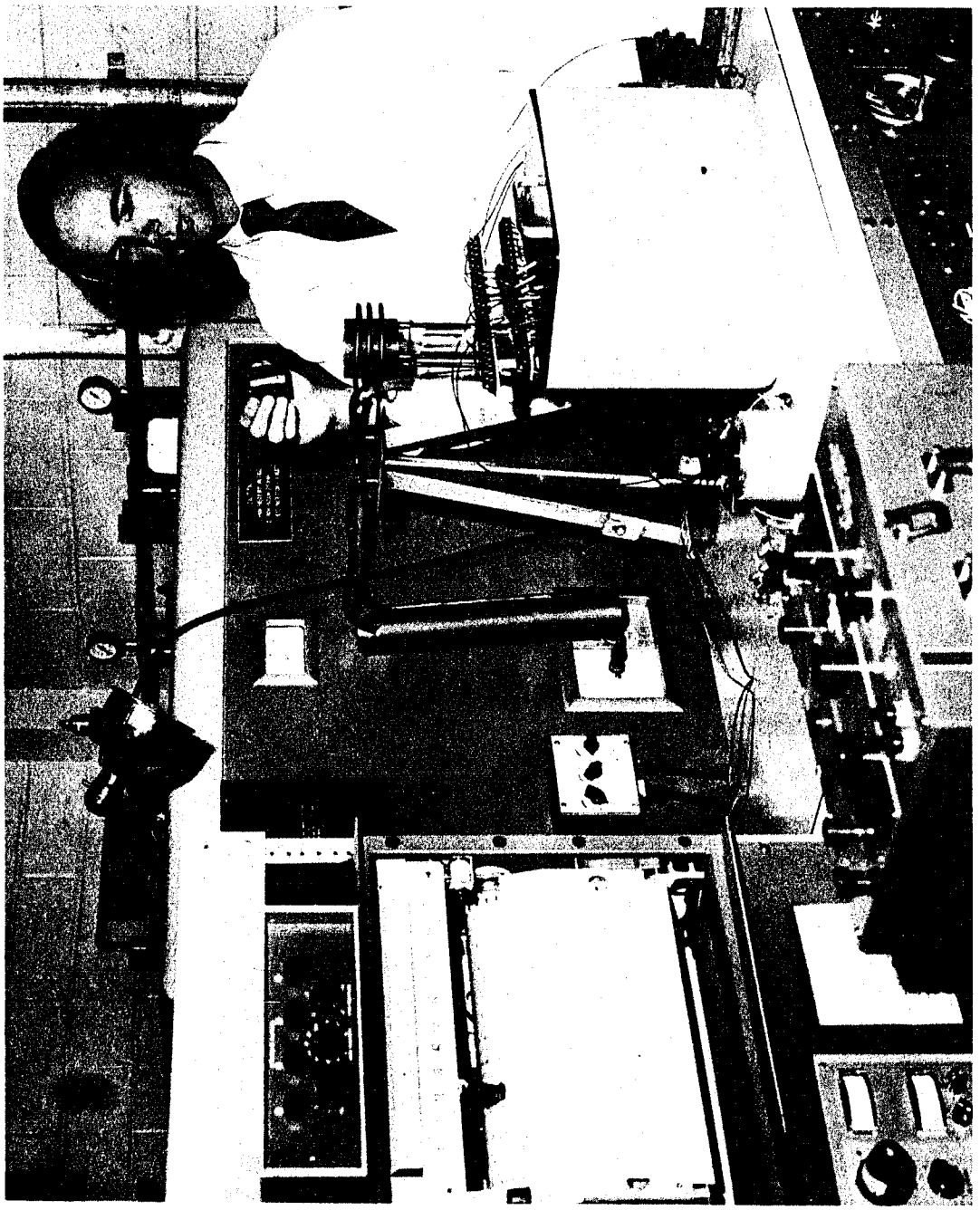

to a run. Figure 14 shows a side view of the equipment after the column has been put into place and pumped down.

The crucible is 2-1/2 inches high and 2-7/8 inches in diameter. It is insulated electrically and thermally from the tantalum support stand by vycor supports. The vycor column enclosing the crucible is 30 inches long, 1/4 inch thick and 3-1/4 inches in diameter inside, and is cooled at the top and bottom with water-cooled copper jackets. The top of the column has a large pyrex window for viewing initial surface conditions, but is clouded by condensed metal as vaporization proceeds. The top and bottom of the column are sealed by lightly greased rubber gaskets.

The heating power is supplied by a 20 kilowatt high-frequency induction generator. It supplies current to a water-cooled 1/4 inch copper load coil of either three turns or nine turns. The latter causes a minimum steady-state temperature of about 590°C in the crucible, and the former 490°C. When tuned to the crucible and load coil, the generator frequency is about 350 kilocycles per second.

The six chromel-alumel thermocouples have alundum insulators. Their #22 gauge wires are lead into the vacuum system through six Conax fittings mounted in the baseplate. The ends of one of these thermocouples, the crucible thermocouple, are joined to a potentiometer or recorder via mercury pools in an ice bath reference junction during a run. Four

Figure 14. Side view of equipment after vycor column has been replaced and pumped down

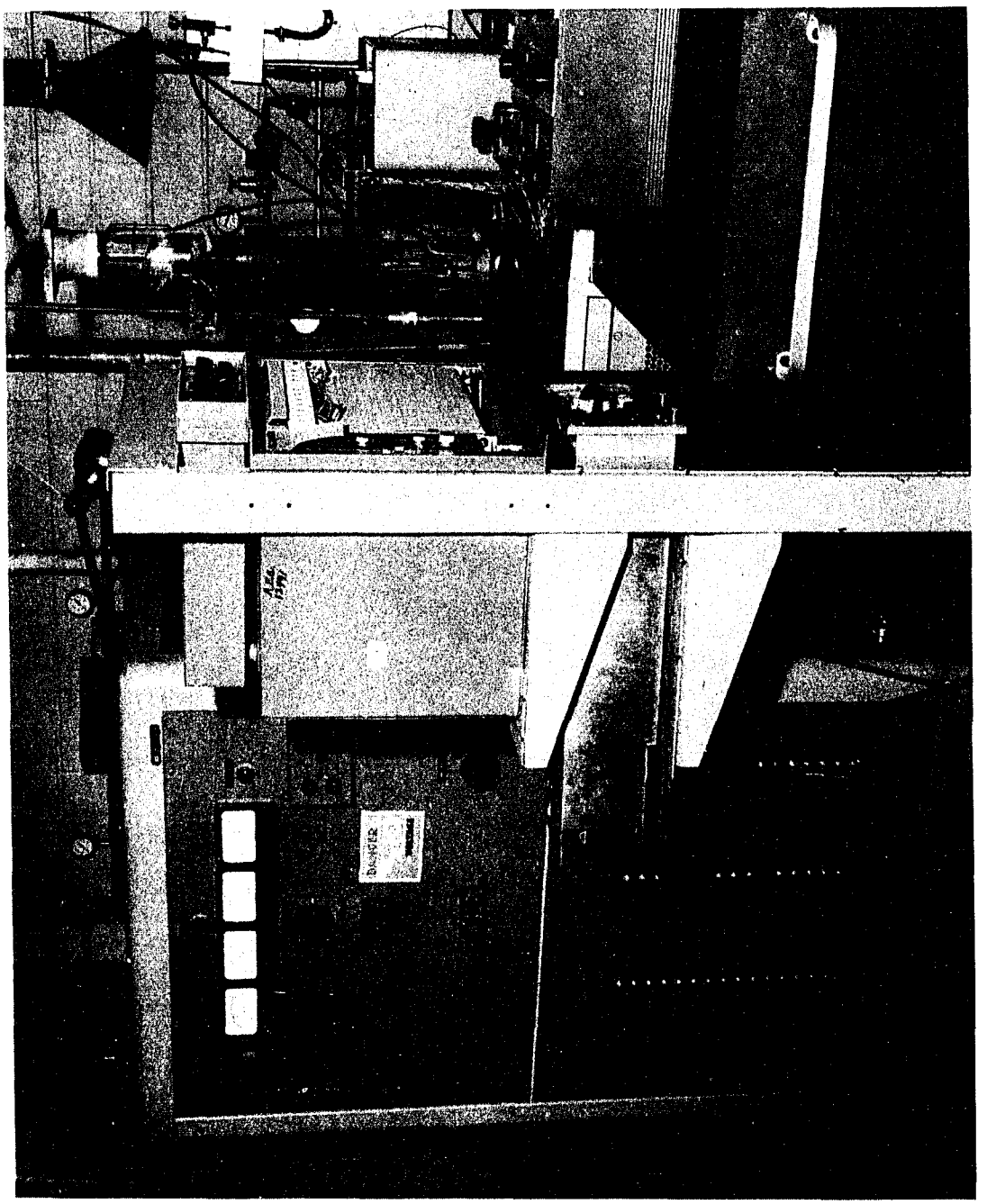

are not used, except for calibration of probe temperature differences.

The other thermocouple supplies its EMF to a reference-junction-compensated temperature controller. This controller has proportional, rate and reset modes which allow a rapid approach to the set point temperature with less than 3°C overshoot and stabilization at the run temperature after less than four minutes. The set point can be set and maintained within 1/4°C. The controller is a current adjusting type with zero to 5 milliamp output. Since this full output causes wide temperature oscillations, a current divider is installed to feed a variable fraction (about 33%) of this current to the induction unit power controller, which consists of a magnetic amplifier and saturable core reactor.

The vacuum system pumps continuously during a vaporization run, and maintains the residual gas pressure at 2×10^{-6} mm Hg or less after two or three hours from the start of the run. Initial heating causes outgassing from the crucible which may raise the pressure to 1×10^{-5} mm Hg. It should be mentioned that at these residual pressures, the rate of collision of oxygen and water molecules with the metal surface is sufficient to cause some oxidation. However it has been shown thermodynamically and will be shown experimentally in the Results section that graphite acts to reduce lead oxides. Vaporization tends to eliminate both lead and indium oxides.

The vacuum system consists of a 15 cfm mechanical forepump, a 400 l/sec silicone oil diffusion pump, a water-cooled baffle to reduce oil backstreaming into the column, and a liquid nitrogen cold trap. The entire system on the column side of the diffusion pump is made of stainless steel for easy cleaning, except for the nickel-plated baffle and copper cooling coil. Low pressures are monitored with an ion gauge, and micron range pressures with thermocouple gauges. Provision is made to allow backfilling the column with gas cylinders to any desired pressure. Hydrogen and phosgene were used in early attempts to reduce oxides, and argon is always used as a backfill gas before admitting atmospheric gases in order to reduce subsequent outgassing time.

After a run is completed, the column is covered with a film of condensed lead. Since this film does not appear to be liquid except adjacent to the crucible, the lead is condensing as a solid and the column cannot be much hotter than 327°C. The lead condensate can be removed by using the column as a reflux condenser over a boiling pot of 50% concentrated nitric acid and 50% water, by volume.

Standard operating procedure calls for outgassing the crucible and screw-in caps for at least two hours at 1000°C after completing a run and before spot welding the thermocouple probes for the next run. During this outgassing, additional air cooling is supplied to the top pyrex plate and

to the column just above the induction coil. After spot welding the new probe all is ready for sample loading for the next run.

The preliminary vaporization trials were all made with crucibles machined from AGSX grade graphite. A much purer UF-4S grade with higher density and smaller grain size has been used to make another run crucible, another catch crucible, and an alloy mixing apparatus. These were used in the final runs with pure lead and the indium-lead alloys.

The mixing and casting apparatus is shown in Figure 15. It is constructed entirely of graphite. The mold halves, chamber and paddle are UF-4S grade, and all other parts are AGSX grade. All samples used in the final runs were prepared with this apparatus, whereas preliminary run samples were prepared in a cruder version lacking a mixing chamber.

The desired weights of indium and lead (e.g., approximately 25 and 45 grams, respectively for a 50 atom % alloy) after being etched with 50% nitric acid are put into the mixing chamber. The vycor column is put on the apparatus evacuated for at least two hours. The ball-tip of the stirring paddle covers the capillary hole. The metals are melted and held at about 350°C, well above the liquidus temperature but well below vaporization temperature. The melt is stirred vigorously for a minimum of five minutes using manual power applied external to the vacuum system. The drive shaft is

Figure 15. Graphite mixing and casting apparatus used for vacuum fabrication of sample rods

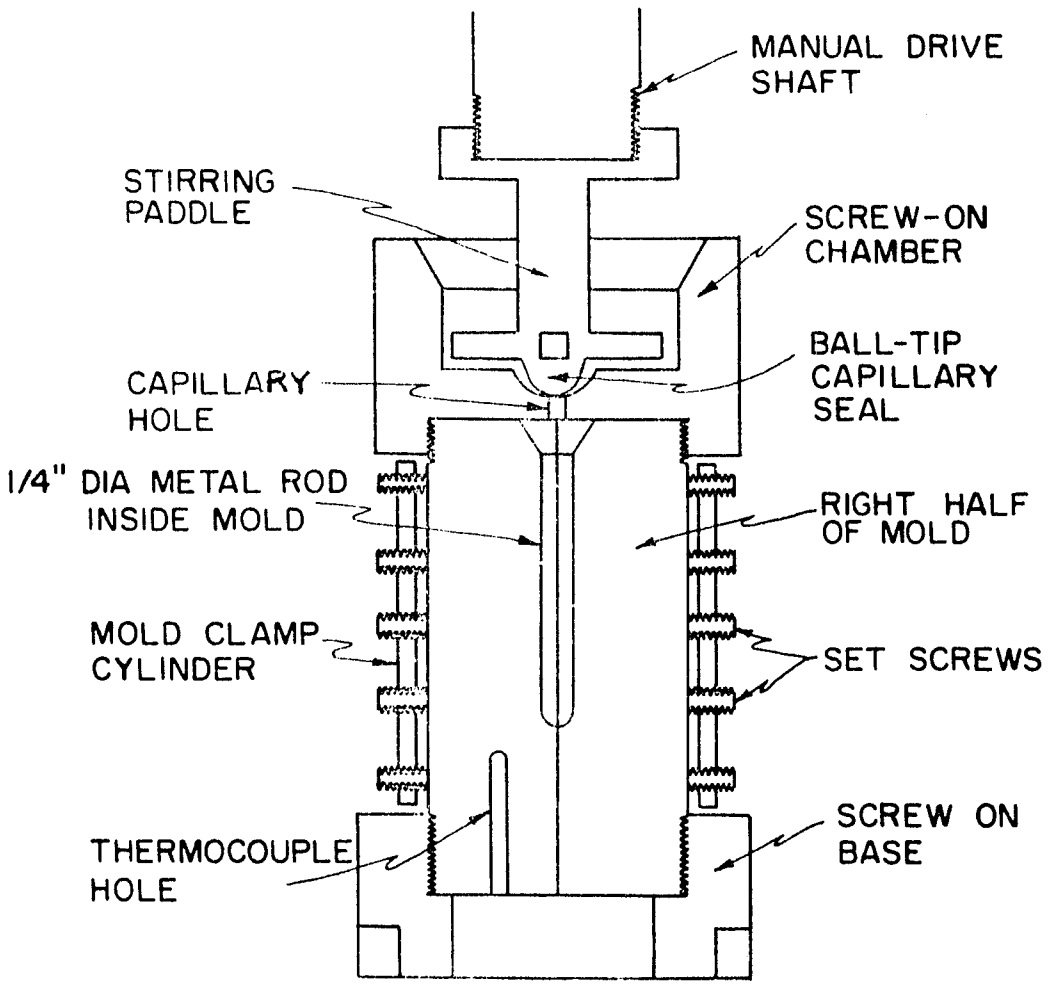

MIXING AND CASTING APPARATUS

then raised, allowing the homogeneous alloy to flow into the mold, and the power is turned off.

The capillary hole had to be enlarged from 1/16-inch diameter for pure lead to 11/64-inch for indium and indium-lead alloys in order that the majority of metal would pass through. About five grams remain in the mixing chamber. This contains surface oxide as well as some graphite worn off by the mixing operation. The 1/4-inch sample rods produced are uniform in composition and usually free of void spaces, although occasionally a small void is present. The bottom of the rod usually contains a small amount of graphite on the surface, but this part is not used for samples.

Figure 16 shows the assembled mixing and casting apparatus resting on its ceramic base attached to the vacuum system baseplate. The 22-turn induction heater load coil is actually outside the evacuated vycor column when in use. Also shown in a rod produced in the apparatus, accidentally bent by the photographer. Figure 17 shows a top view of the stirring paddle and mixing chamber.

The 1/4-inch diameter rods produced can easily be sliced with a razor blade into samples of desired weight. These samples are etched again in 50% nitric acid, weighed on an analytical balance, and are ready to slide into the melting chamber of the run crucible. Crucible hole diameters were measured with a feeler gauge and micrometer.

Figure 16. Picture of stirring paddle and mixing chamber of mixing and casting apparatus

Figure 17. Picture of mixing and casting apparatus mounted on vacuum system baseplate inside 22-turn induction heater load coil, and a fabricated rod

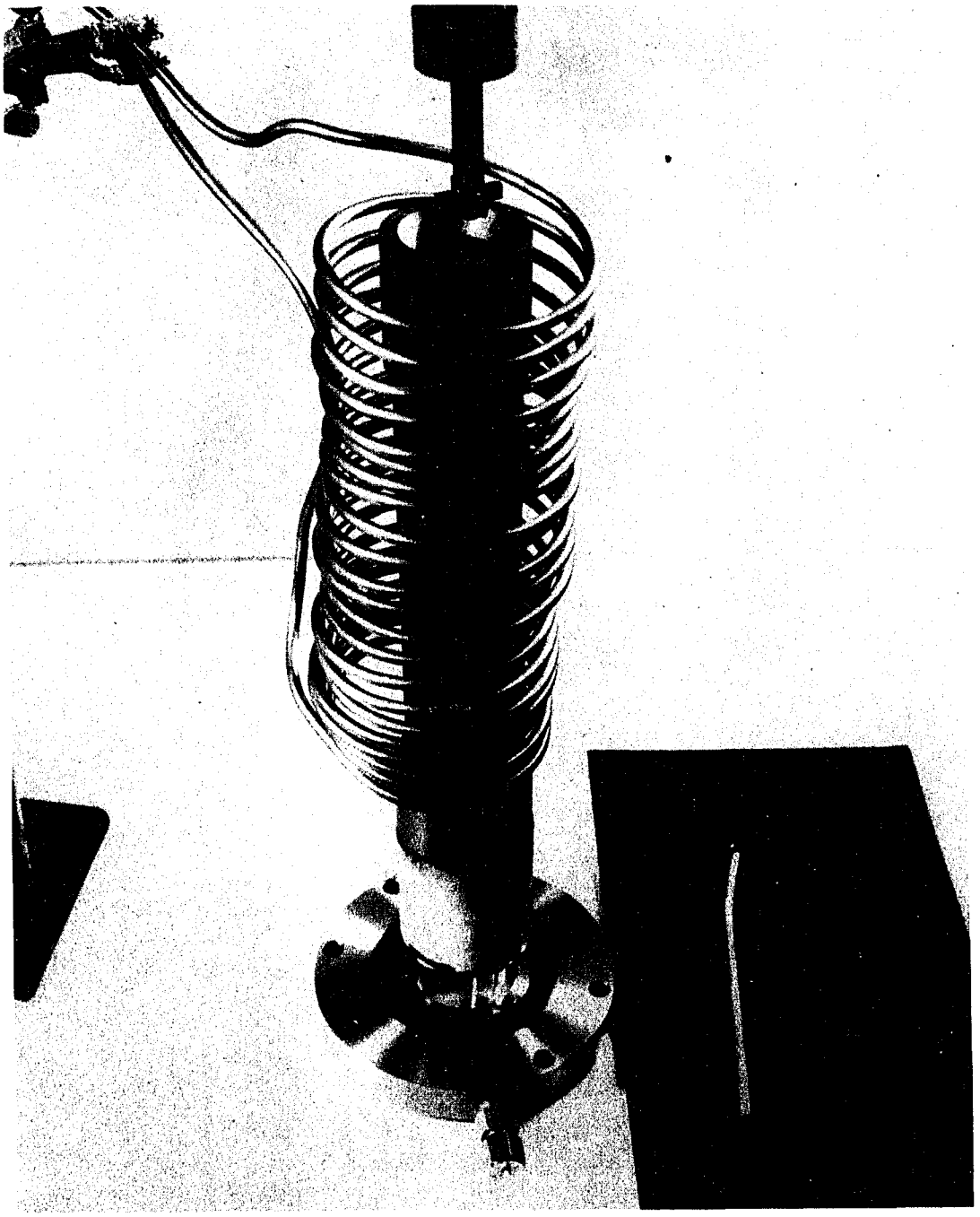

CALCULATION PROCEDURE

This section will briefly describe how the raw data is processed, although not all the details are given. A Fortran computer program is used because of the repetitive nature of the calculations and in order to insure accuracy. The most complicated calculation is a linear least squares fit.

The sample surface temperature determination is rather long. Periodically during the run, usually at least once every half hour for short runs and every four hours for long runs, the crucible thermocouple is read. These EMF readings are converted to temperatures from standard temperature versus EMF tables for chromel-alumel thermocouples. The average of these values for the entire run is computed. Using the temperature difference measured between the probe in hole #2 and the crucible thermocouple (as discussed in association with Figure 10), the average hole #2 temperature is computed. Using the calibrations of the temperature difference between the other five holes and hole #2 (to be presented in the Results section), the average hole temperature for the five useful vaporization holes is computed. Using the method of Wolkoff et al. (126) these hole temperatures can be corrected to give the surface temperature T. This method requires data shown in the Results section, but these corrections are always less than 0.2°C.

The starting time of the run is taken as the time when the temperature first attains the set point temperature. The ending time t is taken as the time the power is turned off. Transient time is negligible because of rapid heating and cooling, and great dependence of vapor pressure on temperature. The vaporization surface area s is taken as the cross-sectional area of the cylindrical vaporization hole with its dimensions corrected for thermal expansion. The true vaporization area is larger than this because of the liquid meniscus, but account of this is taken in Sandry and Stevenson's (101) effective Clausing factor.

The molecular weights M of lead and indium monatomic gases are used and the condensation coefficients α is assumed unity.

The initial alloy mole fraction is based on the weights of the ingredients to make the alloy rod. The final mole fraction is found from the weights of vaporized lead (and indium), and the average value is used. The mole fraction is not permitted to change more than 1% during a run with 50% alloys, and not more than 0.4% during a run with 10 atom % lead alloys.

In order to find the effective Clausing factor K, the average vaporization surface temperature is used to find the temperature of the inner sample hole using a calibration curve shown in the Results section. These two temperatures are

used to compute the indium and lead pure component densities from Equations 27 and 28. The actual volume these occupy (based on the average mass in the crucible during a run) is found assuming there is no volume change on mixing. From a knowledge of the liquid densities and thermally corrected dimensions of inner and outer holes, the channel and capillary, the length l between the equator of the assumed hemispherical liquid surface and top of the vaporization hole is computed. From the l/r ratio found next, the effective Clausing factors (accounting for surface area of the sample) of Sandry and Stevenson (101) are calculated from Equations 31 and 32.

$$K = \frac{2}{1+e^{\nu}} \tag{31}$$

$$\nu = 0.3152582 + 0.8440872 \ln(l/r) - 0.1278427 \ln^2(l/r)$$

$$+ 0.06256759 \ln^3(l/r) + 0.006614625 \ln^4(l/r)$$

$$- 0.007730225 \ln^5(l/r) + 0.001074625 \ln^6(l/r) \tag{32}$$

The values of K do not vary significantly from the beginning to end of a run because l/r is near a value of 8.0 where K is not much affected by small changes in l.

The mass loss m of a sample is the initial sample weight minus the weights of slug recovered in the catch crucible, the small pieces removed from the run crucible, and the metal deposited on the screw caps. In the case of a pure lead

sample, this is the net mass vaporized. In the case of an alloy sample, the weight of indium that would vaporize under the run conditions assuming that the solution is ideal is calculated from Equation 5 using Herrick's (43) indium vapor pressure equation. The constants for the equation are given in Table 2. This weight is subtracted from the mass vaporized to get the mass of lead vaporized. The mass of indium vaporized is always less than 2% of the mass of lead vaporized even with 90 atom % indium alloys.

The lead vapor pressures P or partial pressures p are computed from the Langmuir equation, Equation 5 or Equation A1 in Appendix A. A least square fit of Equation 7 is performed for lead. The second law heat and entropy of vaporization, and third law heats of vaporization at 298°K for lead, and the lead activity coefficients for the alloys are all calculated as described at the end of the Theory section, along with their standard deviations. Appendix A1 gives an error analysis, wherein the standard deviations to be expected from known experimental errors are calculated for the vapor pressures and activity coefficients.

RESULTS AND DISCUSSION

As has been mentioned previously, the Langmuir method (and modified Langmuir method) at first appears to be the simplest way to vaporize a substance. To measure low pressures, one need only measure the surface area, surface temperature and rate of weight loss into a vacuum. From other Langmuir vaporizations done in this laboratory, it was expected that the surface contamination might be a problem, but that use of graphite crucibles would probably solve it. Temperature and mass loss measurements were not expected to be problems, and the effective surface area measurement problem was solved by the Monte Carlo calculations of Sandry and Stevenson (101) as discussed earlier.

Probably because these problems were not anticipated, the methods of solution tried were not very elegant or even scientific in attempts to bypass them quickly. Recognition that the surface temperature problem even existed was not immediate. Nevertheless, at least a partial solution to each of these three problems has been obtained and will be outlined in three following parts of this section. The fourth part summarizes lead vapor pressure results and lead activity coefficient determinations.

Surface Contamination

The first "simple-minded" attempts at Langmuir vaporization were carried out in a cylindrical graphite crucible with six vaporization holes and one thermocouple in the crucible to measure the temperature. The vaporization rate of pure lead and of lead in indium alloys was about 10% of what was expected, and examination of the samples revealed large amounts of oxide on top. When a plexiglas top was added to the column, the less oxidized samples could be identified because their surfaces jiggled from forepump vibrations while the others did not.

Despite the fact that thermodynamically lead oxide should be reduced by graphite above room temperature (see Figure 4), the samples were still oxidized under a vacuum. However, oxidized lead in a graphite crucible rapidly became bright and shiny when placed in a 1000°C muffle furnace at atmospheric pressure. Oxide reformed on cooling could be reversibly removed. However when indium was added to the melt, the oxide could not be removed. Since the reduction could not be done under a seven micron vacuum, it appeared that carbon monoxide was the reducing agent. However, if kinetics were not limiting, indium oxide should also have been reduced (see Figure 4). In a run at 100 microns residual pressure at 800°C, lead ranging from 50% to 85% oxide covered yielded 60 to 75%

of expected weight losses. It is probable that lead oxide vapor pressure was being unknowingly measured. Figure 5 shows that lead oxide is less volatile than lead, but approaches its vapor pressure at higher temperatures.

Raising and lowering the temperatures of oxidized lead, indium and alloy specimens also proved interesting. Under vaporization conditions where the residual pressure was less than 10^{-5} mm Hg, cooling from 1100°C to 620°C caused one oxidized alloy to become completely oxide free. In other trials, cycling between about 850°C and 600°C sometimes eliminated oxide films at the higher temperature, sometimes eliminated them at the lower temperature, sometimes formed them at high or low temperatures, and sometimes did nothing. Identical composition samples in the same crucible most often behaved completely different. Surprisingly enough, in one run using six different composition samples from zero to 100% indium, the percentage of clean surface area was directly proportional to the indium concentration.

Hydrogen and phosgene were used in attempts to remove the surface oxides from samples in the crucible prior to vaporization. A 3.2% hydrogen in argon mixture (non-explosive in the atmosphere) was backfilled into the vacuum system, which was then heated to 800°C. After one hour two samples each of oxidized In, Pb and 50% alloy had clean surface areas of 100%, 20%, 30%, 5%, 0%, 0%, respectively. When the gas

mixture was then evacuated, the samples all started bubbling slowly, and the clean ones glazed over with an oxide film again. It was hoped that phosgene would reduce the surface oxides to volatile chlorides. Chlorides billowed from the samples when heated, but left behind a black residue of unknown substance.

Since it appeared that surface oxides could not easily be reduced to metal, it was decided to try to prevent them from forming. The source of oxygen was not certain. It could have been the vacuum atmosphere, gas trapped in the graphite crucible or oxides originally present in the metal. Cleaning the solid samples with hydrochloric acid increased the liquid surface cleanliness and vaporization rates from indium and alloy samples, but not lead samples. Rates were still very low. Another test used old oxidized samples, old oxidized samples with the surface oxide cut off with a razor blade, and freshly cut samples. Cleanliness and vaporization rates were best with fresh samples and worst with the old uncut samples. These tests clearly indicated that some oxygen had been carried in with the samples, that older samples had apparently gained oxygen in the bulk as well as on the surface, and that cleaning the surface of samples in the solid state prior to vaporization was helpful but not the entire answer to getting clean liquid surfaces.

In order to test whether graphite crucibles were a detriment rather than an aid, alumina, thoria, vitreosil (silica), stainless steel #304, and boron nitride were tried. The first three were mounted as cups in a graphite block. Samples in each were more oxidized than those in the graphite and had lower vaporization rates, although the lower rates were largely caused by temperature gradients between the cups and graphite. The thoria crucible reacted with the 50% alloy sample.

Full-size crucibles were made of the stainless steel and boron nitride, except that a graphite susceptor for the induction heating current had to be used with the BN. In a run under similar conditions as one with graphite, the stainless steel crucible provided cleaner and faster vaporizing samples than graphite. However, it contaminated the samples and column with small flakes of manganese which vaporized from the crucible. In addition hot spots developed on the outside edge of the vaporization holes during outgassing which caused partial melting and small dimples were formed. A clear vycor column was broken trying to remove the dimpled #304 stainless steel crucible from the column after the run.

Samples used in the boron nitride crucible were often lightly coated with white boron nitride powder, but usually had oxide conditions and vaporization rates similar to graphite. Also the bluish cast usually present on lead

samples when slightly oxidized was not present on those run in boron nitride, indicating that carbon might be soluble in lead to an undesirable extent. Later, when clean samples were finally obtained, no carbon contamination was noted. The bluish cast is due to oxide. Unfortunately the boron nitride was not stable under 1000°C outgassing temperatures, as it vaporized much material which condensed as white flakes or powder (thought to be B_2O_3) and also bubbled small amounts of a non-volatile liquid substance containing calcium and silicon. Upon cooling, the liquid solidified clogging the sample holes, and sometimes fracturing the graphite susceptor.

In order to test directly whether the graphite crucible would reduce lead or indium oxides, PbO_2, PbO and In_2O_3 were heated under vacuum at 620°C for 33 hours. The PbO_2 was stoichiometrically converted to PbO. Both lead oxides were reduced to metallic lead at all graphite surfaces, although indium oxide was not affected. The weight losses of both lead oxides agreed with the vapor pressures of PbO determined with the Langmuir and flow methods by Nesmeyanov et al. (82,83) and shown in Figure 5. His pressures are much higher than those of Drowart et al. (23). Of course some lead may have been vaporized along with PbO, although not much appeared to be.

Analytical analyses for carbon and oxygen were performed on old Pb, In, and 50% alloy samples cut in half, and also on pieces from unused bars. Two methods were used: standard

combustion and helium fusion analyses, and microprobe analyzer surface tests. Unused bar analyses were Pb: 54 ppm O (0.07 atom %), 61 ppm C (0.105 atom %) and In: 53 ppm O (0.038 atom %), 43 ppm C (0.041 atom %). Two "surface" samples of Pb contained 245 and 680 ppm oxygen. The maximum carbon concentrations were 162 ppm for "top" of In and 122 ppm for a "bottom" of an alloy. These analyses yield four conclusions: 1) alloys contain more oxygen than either pure component, 2) some pure samples also gained oxygen compared to their unused bar, 3) surface oxide concentrations are much higher than bulk, and 4) indium and alloy samples have gained carbon compared to the unused bar, while lead has about the same amount. The microprobe analyses show uneven amounts of O and C spread over surface samples. Local concentrations are as high as 25% C, 20% O; average concentrations are estimated at 1 to 2% C, less than 1% O. It should be noted from Figure 3 that the lead from the unused bar is saturated with oxygen at 600 or 700°C. Data for indium is not available. This could explain part of the reason for appearance and disappearance of oxide films during temperature cycling.

As the temperature is raised, the surface film may go into solution, and be reformed as the temperature is lowered. The kinetics of solution and formation of the film, as well as oxygen supersaturation, would naturally limit these rates. Decomposition of an oxide film on cooling is difficult to

explain. It is possible that a tight surface film could be fractured by thermal stresses.

Since chemical methods for obtaining clean surfaces had little success, physical methods were tried. A tantalum disk with holes coinciding with the vaporization holes was placed on a graphite crucible. Three samples holes were overfilled with Pb, In and a 50% alloy. At 600°C, a screwdriver inserted into the top of the vacuum system turned the disk to sweep over the liquid surfaces, thus scraping the oxide and additional metal into the empty adjacent hole. All samples were visually clean, and vaporized at rates much higher than before. Kubaschewski and Hopkins (64) point out that invisible oxide layers can persist up to several tens of angstroms thickness. After ten hours the lead sample surface was 40% film covered, but the others were clean. Pressures were 6 to 10 x 10^{-7} mm Hg.

Crucibles similar to that in Figure 8 were then made, the operation of which was previously described. At first, screwdriver slots were provided for the inner crucible, which was turned to mate capillary with channel. Binding of the inner crucible and air leaks introduced by turning the screwdriver halted this method. Finally, use of smaller capillaries lead to the melt and flow method now used to give satisfactorily clean surfaces.

Mass Loss Measurement

Early weight loss measurements were simple, since the sample could easily be tapped out of the crucible and weighed, taking care to collect any small fragments. Tantalum cover plates resting on the vaporization holes to impede vaporization during unsteady state temperature changes were successful. They could be removed by twisting the tantalum disk with the screwdriver. A switch from a resistance furnace to an induction heater with fast temperature stabilization eliminated the need for these cover plates.

With the advent of the melt-and-flow crucible, screw caps were used to prevent vaporization from the inner hole for the entire run. Improved and longer threads finally reduced leakage from about 5% to 0.2 $\pm$ 0.055% of that vaporized intentionally. At the same time, indium samples sustained weight losses of 0.0009 to 0.0036 grams which were not due to vaporization. These were either lost in transferring and weighing operations or absorbed into the crucible. It is believed the latter explanation is likely, since the smaller grain size UF-4S graphite crucible reduced this.

In order to aid in condenser design, three runs were made where a single crucible hole vaporized metal onto a thin vycor condenser plate resting on vycor struts on top of the crucible. The plate was not cooled, and therefore condensed

both indium and lead as liquids. For lead, the condenser was 90% efficient at a 5/16 inch height above the vaporization hole, and 93.7% efficient at 1/8 inch. With indium, the condenser was 96.4% effective at 1/8 inch. In each case the condensate was centered on the condenser inside a radius of 3/8 inch.

Surface Temperature

Induction heating contributes in several ways to surface temperature measuring problems. These problems are temperature gradients in both the crucible and measuring thermocouples which are higher gradients existing with resistance heating, and also radio-frequency interference with the temperature recorder. Radial temperature gradients measured with an optical pyrometer at 1150°C ranged from 5 to 30°C/inch, while angular gradients are about 1 to 6°C/inch. These temperature gradients do cause desirable thermal convection currents in the metal, observable at the infrequent times when a mobile oxide film is present. This convection helps eliminate surface depletion effects. The stray electrical radiofrequency radiation (about 350 kc/sec) seems to cause considerable instability in the temperature recorder, but none in the electronic temperature controller or the potentiometer used for accurate temperature measurements.

One of the biggest problems in temperature measurement has been the calibration of thermocouples. Previous to the

time when the probe method for measuring surface temperatures was adopted, it was realized that thermocouple calibrations reliable to within 1°C would be required. Based on the following results it is clear that chromel-alumel calibrations do not meet this criterion.

Figure 18 shows typical calibrations for new Pt-Pt 13% Rh, old chromel-alumel and new chromel-alumel thermocouples. The uncertainty and drift are evident with the chromel-alumel thermocouples despite great pains taken to insure intimate thermal contact between the Bureau of Standards calibrated Pt-Pt 10% Rh standard and the chromel-alumel thermocouples. A large bead was made with six chromel-alumel thermocouples, a hole drilled in the bead, the bead of the standard inserted, and then the large bead was pinched down. The platinum thermocouples were calibrated by forming one large bead with all the couples, and they were also checked for inhomogeneity.

With the probe method of measurement, it is only necessary that the initial heating up of the wire give consistent EMF readings, since a new probe is used for each run. Figure 18 shows that the chromel-alumel thermocouples achieve tabular EMF readings within about 1°C initially. The probe lead wires are out of the high temperature gradient zone and hence do not change calibration. Any change in the crucible thermocouple calibration is not important, since it is checked versus probe #2 at the start of each run.

Figure 18. Comparison of reliability of calibrations of new and used chromel-alumel thermocouples and new platinum-rhodium thermocouple

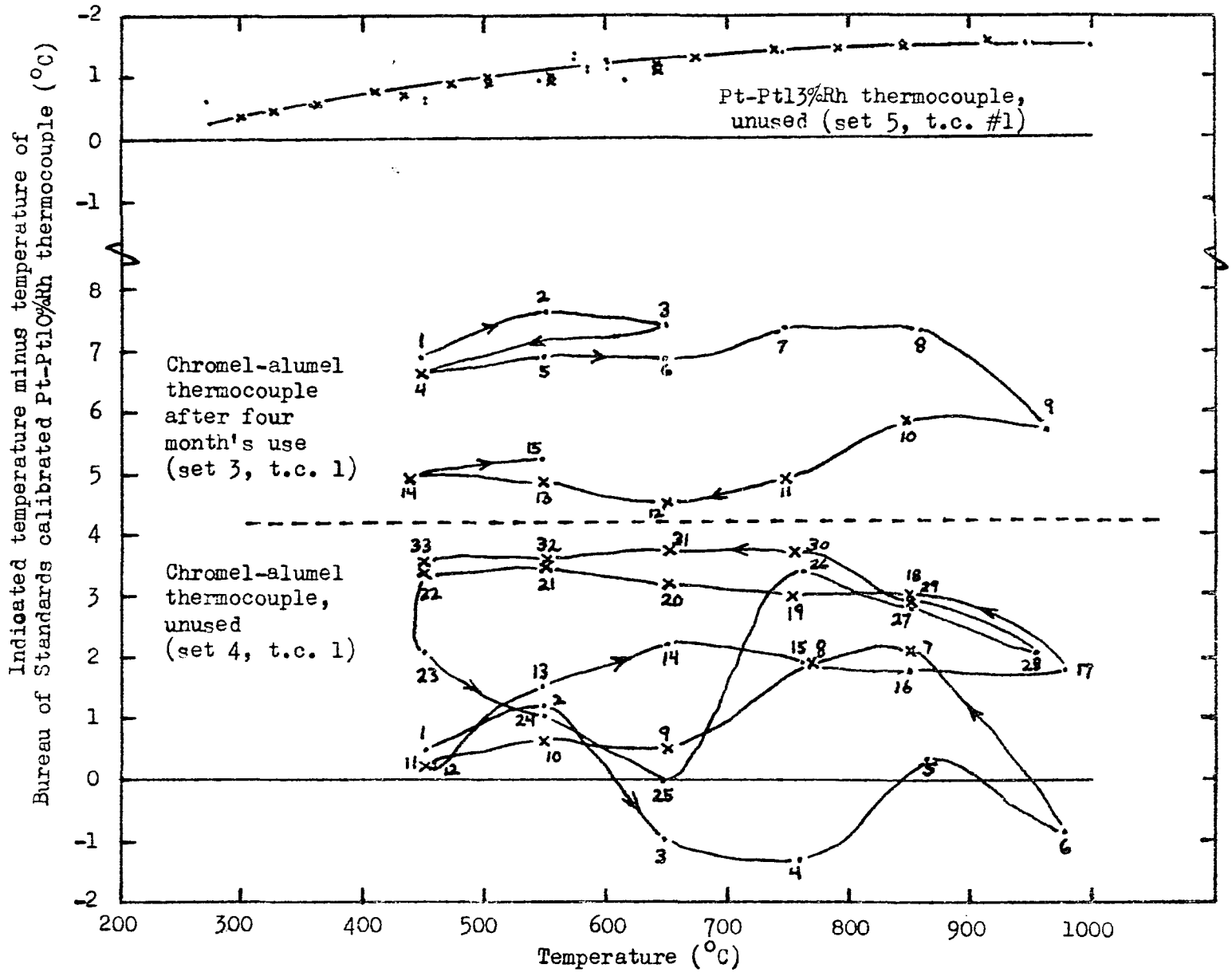
Indicated temperature minus temperature of Bureau of Standards calibrated Pt-Pt10%Rh thermocouple (°C)
Pt-Pt13%Rh thermocouple, unused (set 5, t.c. #1)
Chromel-alumel thermocouple after four month's use (set 3, t.c. 1)
Chromel-alumel thermocouple, unused (set 4, t.c. 1)
Temperature (°C)
-2
-1
0
1
2
3
4
5
6
7
8
200
300
400
500
600
700
800
900
1000

Of prime importance to surface temperature measurements in this work is a paper by Wolkoff, Woodward and Strecok (126) which determines the error in using a thermocouple probe temperature as the surface temperature of a liquid metal. The parameters needed are thermocouple and liquid metal resistivities, liquid metal thermal conductivity, the wire size, and the vertical heat flux at the liquid metal surface. Lyon (69) gives the pure liquid metal properties. Representative values at 600°C are 48.0 and 107.2 micro-ohms/cm cube for the resistivities of indium and lead, respectively, and 0.10 and 0.036 cal/sec-cm-°C for the thermal conductivities. Chromel and alumel resistivities at 600°C are 105.7 and 56.5 micro-ohms/cm cube, respectively.

Estimated surface temperature gradients due to the sum of radiation and latent heat losses are shown in Figure 19. These are based on liquid metal emissivities of 0.28 (that of molten iron), and radiation view factors equal to Clausing factors (equal to 0.22) corresponding to experimental conditions. Sandry and Stevenson (101) show the utility of equating effective Clausing factors and view factors. Figure 20 shows the error in measuring the surface temperature (it is lower than measured) calculated by Wolkoff's (126) method using the gradients from Figure 19. The dashed lines of Figure 20 show the linear fit equations used in the computer calculations. The corrections are actually less than the known temperature

Figure 19. Estimated heat fluxes (radiation, vaporization and total) and vertical temperature gradients at surface of lead and indium melts under experimental run conditions

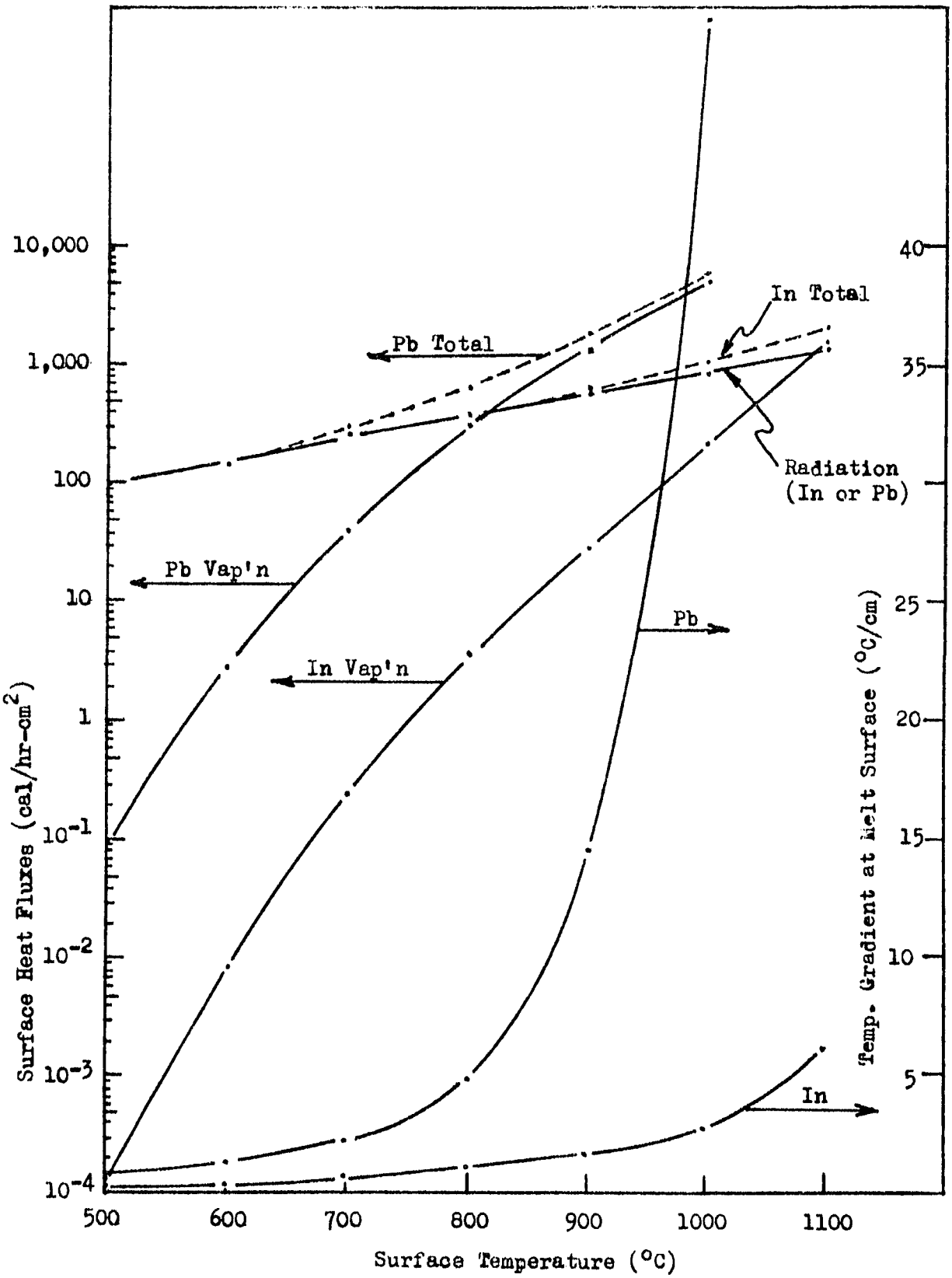
10,000
1,000
100
10
1
10⁻¹
10⁻²
10⁻³
10⁻⁴
Surface Heat Fluxes (cal/hr-cm²)
40
35
25
20
15
10
5
Temp. Gradient at Melt Surface (°C/cm)
500
600
700
800
900
1000
1100
Surface Temperature (°C)
Pb Total
In Total
Radiation
(In or Pb)
Pb Vap'n
In Vap'n
Pb
In

Figure 20. Differences between indicated probe temperature and true surface temperature of lead and indium melts under experimental run conditions calculated by method of Wolkoff et al. (126)

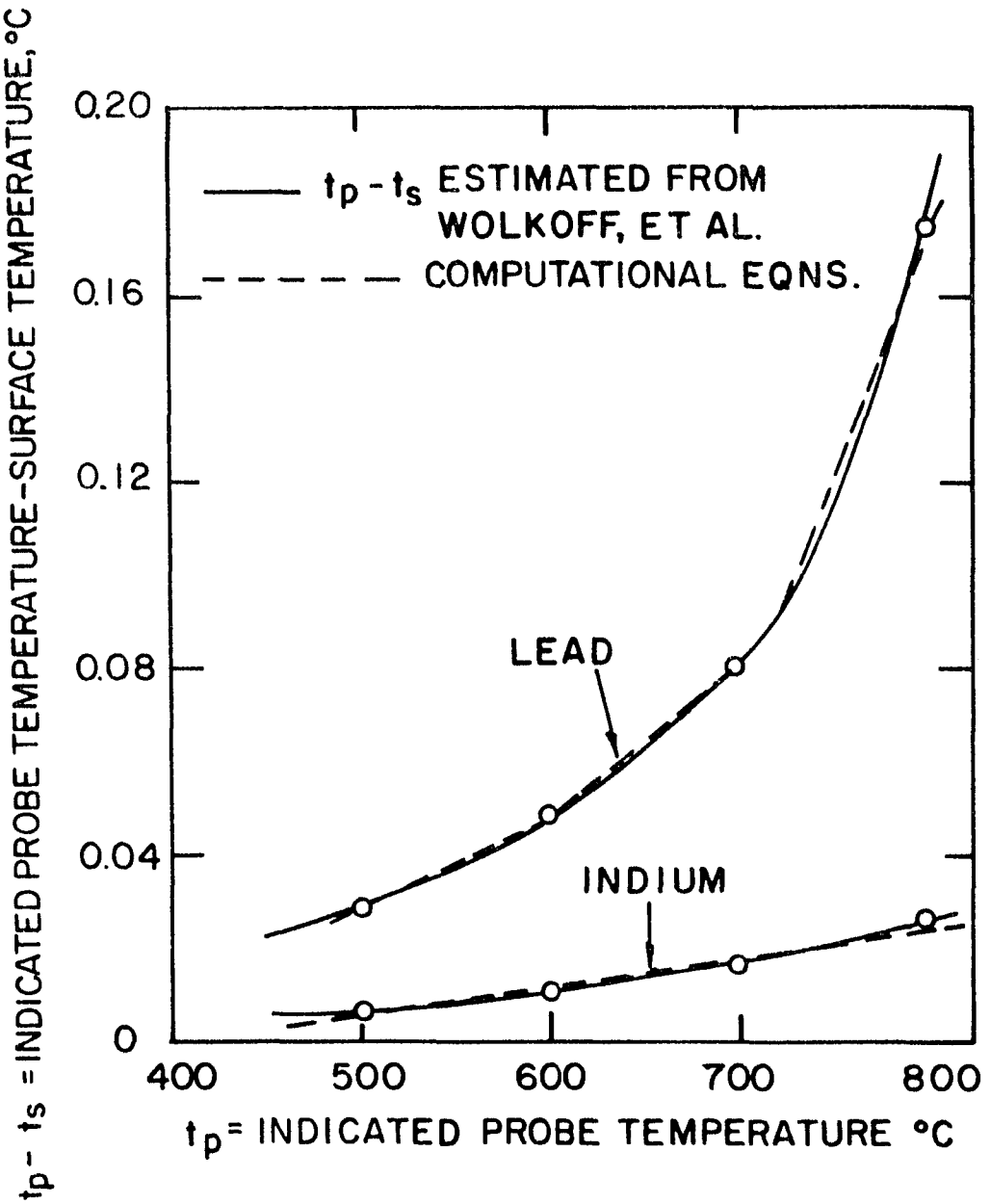
$t_p - t_s$ ESTIMATED FROM WOLKOFF, ET AL.
COMPUTATIONAL EQNS.
LEAD
INDIUM
0.20
0.16
0.12
0.08
0.04
0
400
500
600
700
800
t_p = INDICATED PROBE TEMPERATURE °C
$t_p - t_s$ = INDICATED PROBE TEMPERATURE-SURFACE TEMPERATURE, °C

measuring errors. No probe conduction losses can be tolerated, and this is ensured by preheating the probe wires in the crucible prior to their entry into the melt.

Figures 21 through 24 show the results of calibrating the probe temperature of hole #i (i = 1,3,4,5,6) versus the probe temperature of hole #2 over the temperature range of interest. Figure 21 indicates the reproducibility of the calibrations as long as the relative geometrical position of coil and crucible are maintained constant. This constant geometrical relationship was maintained by bolting the plastic plate attached to the load coil to a metal stand, as can be clearly seen in Figure 13. Figure 21 shows only the representative calibration results for probes #4 and #6 using pure lead. New probe wires were used for each calibration run, as well as new pure lead samples. This necessitated the sequence of crucible removal, melting out the lead into the catch crucible, and run crucible outgassing. Thus, the calibration procedure was identical to a vaporization run procedure. It is apparent that the reliability of the calibrations is about $\pm$ 1°C, which is sufficient precision. The three low points for probe #6 in Run 1 were caused by one of the probe wires contacting the wall of the crucible below the liquid lead surface. This was always prevented in the later calibrations and runs. The linear equations shown represent the dashed lines taken as average values, and are used in the computer calculations.

Figure 21. Examples of reliability of calibrations of the lead melt temperature measured by a probe in hole i (i = 1,3,4,5,6) against the temperature measured by a probe in hole 2

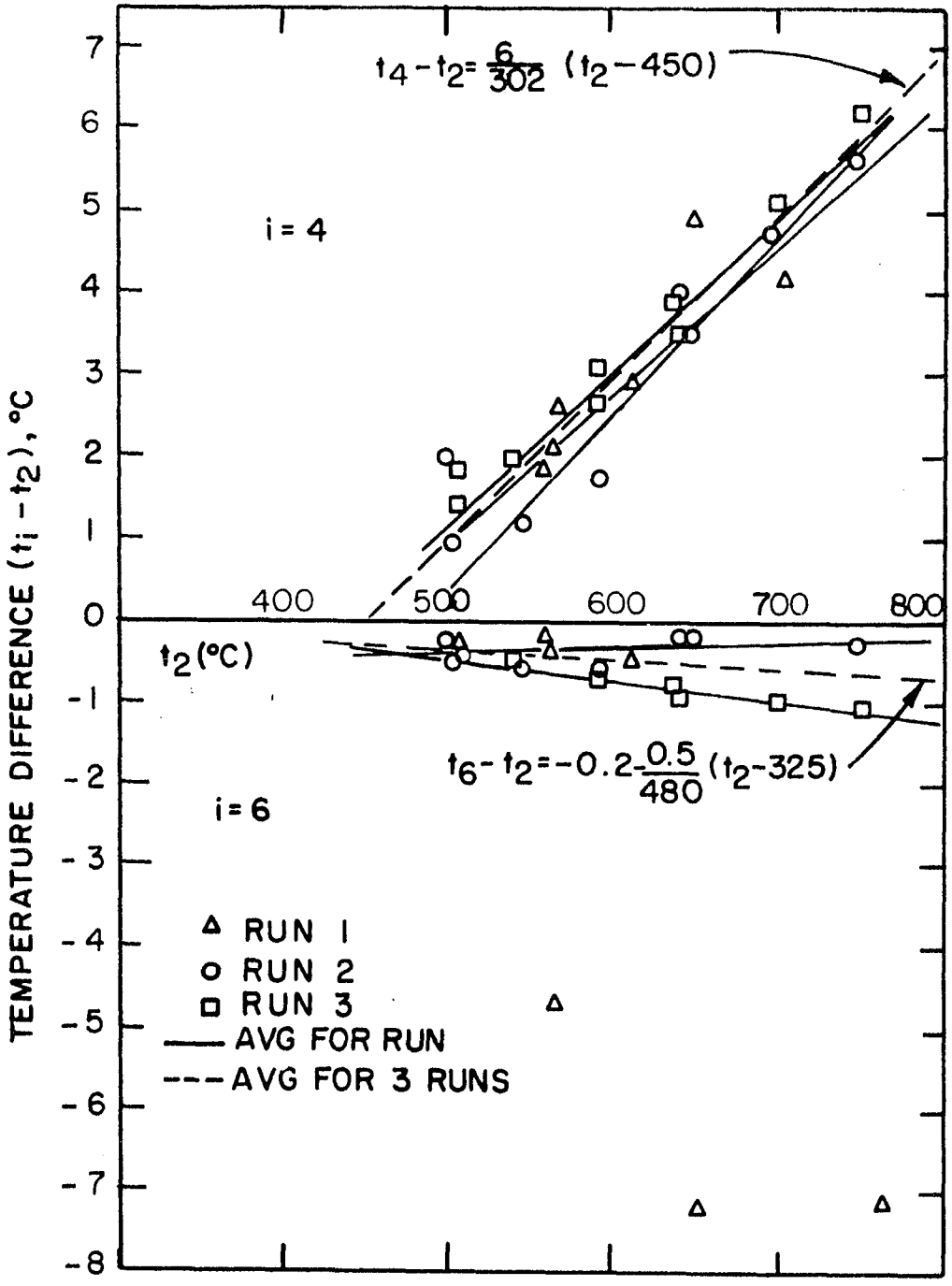
$t_4 - t_2 = \frac{6}{302}(t_2 - 450)$
i = 4
$t_6 - t_2 = -0.2 - \frac{0.5}{480}(t_2 - 325)$
i = 6
t_2(°C)
TEMPERATURE DIFFERENCE ($t_i - t_2$), °C
RUN 1
RUN 2
RUN 3
AVG FOR RUN
AVG FOR 3 RUNS
7
6
5
4
3
2
1
0
-1
-2
-3
-4
-5
-6
-7
-8
400
500
600
700
800

Figure 22 shows the results of the three calibration runs for all five thermocouple probes with pure lead. Individual points are left off for clarity. Probes #4 and #6 are the same as in Figure 21. At 700°C there is a maximum difference of about 10°C between the temperature in holes #1 and #4. During these calibration runs lead melting points measured before the calibration were always within one degree of the accepted lead melting points measured before the calibration were always within one degree of the accepted lead melting point of 327.4°C. After the calibration, the differences were less than 2°C.

Figure 23 shows the calibration results for 50 atom % indium-lead alloys and Figure 24 the results for 90 atom % indium-10 atom % lead alloys. The 3-turn load coil had to be removed between each series of runs in order to use the 22-turn load coil with the mixing and casting apparatus to make new composition samples. Therefore, new coil-crucible geometry existed in each series. The reduced spread between the calibration lines in going from Figure 22 to 23 to 24 is more likely to be due to greater success in centering the coil around the crucible than to the change in alloy composition. These calibrations, the surface temperature corrections of Figure 20, and calibration of probe #2 versus the crucible thermocouple at the start of each vaporization run (as exemplified in Figure 10) are all used in determining the surface temperatures of the samples during a vaporization run

Figure 22. Average of three calibrations of the lead melt temperature measured by a probe in hole i (i = 1,3,4,5,6) against the temperature measured by a probe in hole 2

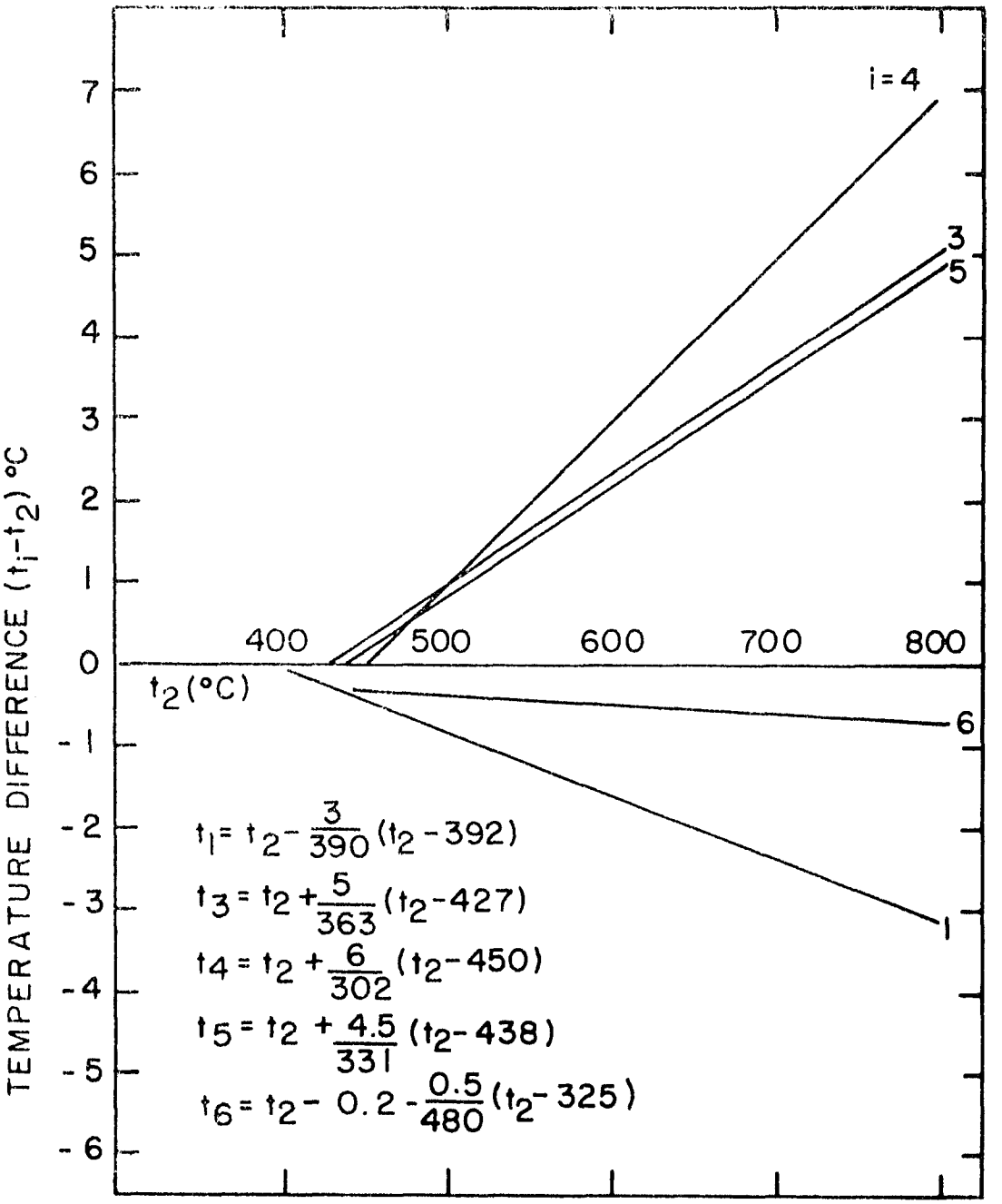
TEMPERATURE DIFFERENCE $(t_i - t_2)$ °C
7
6
5
4
3
2
1
0
-1
-2
-3
-4
-5
-6
400
500
600
700
800
t_2 (°C)
i = 4
3
5
6
1
$t_1 = t_2 - \frac{3}{390}(t_2 - 392)$
$t_3 = t_2 + \frac{5}{363}(t_2 - 427)$
$t_4 = t_2 + \frac{6}{302}(t_2 - 450)$
$t_5 = t_2 + \frac{4.5}{331}(t_2 - 438)$
$t_6 = t_2 - 0.2 - \frac{0.5}{480}(t_2 - 325)$

Figure 23. Calibration of the melt temperature measured by a probe in hole i (i = 1,3,4,5,6) against the temperature measured by a probe in hole 2 for a 50 atom % indium-lead alloy

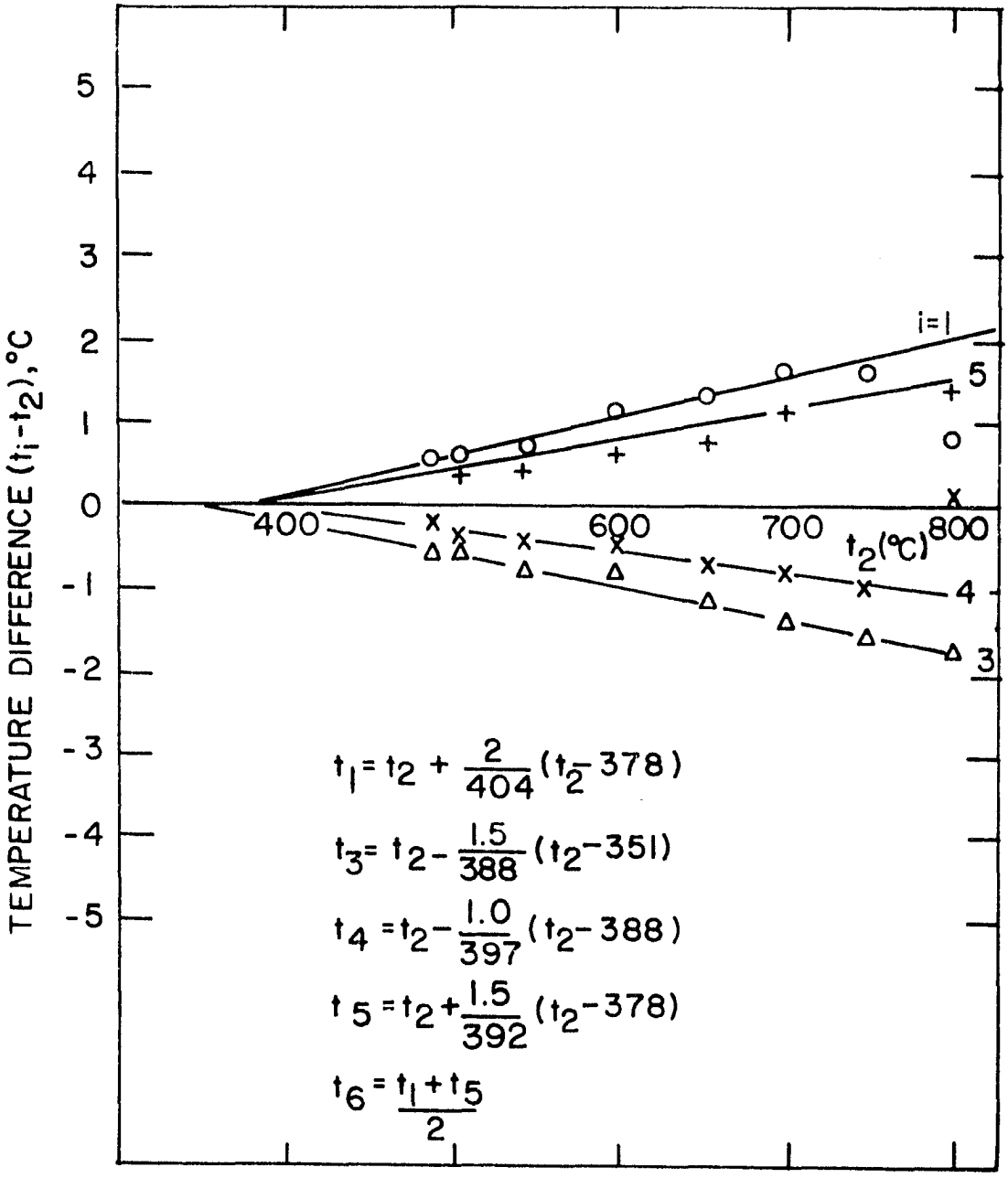
TEMPERATURE DIFFERENCE $(t_i - t_2)$, °C
5
4
3
2
1
0
-1
-2
-3
-4
-5
400
600
700
800
t_2(°C)
i=1
5
4
3
$t_1 = t_2 + \frac{2}{404}(t_2 - 378)$
$t_3 = t_2 - \frac{1.5}{388}(t_2 - 351)$
$t_4 = t_2 - \frac{1.0}{397}(t_2 - 388)$
$t_5 = t_2 + \frac{1.5}{392}(t_2 - 378)$
$t_6 = \frac{t_1 + t_5}{2}$

Figure 24. Calibration of the melt temperature measured by a probe in hole i (i = 1,3,4,5,6) against the temperature measured by a probe in hole 2 for a 90 atom % indium-10 % lead alloy

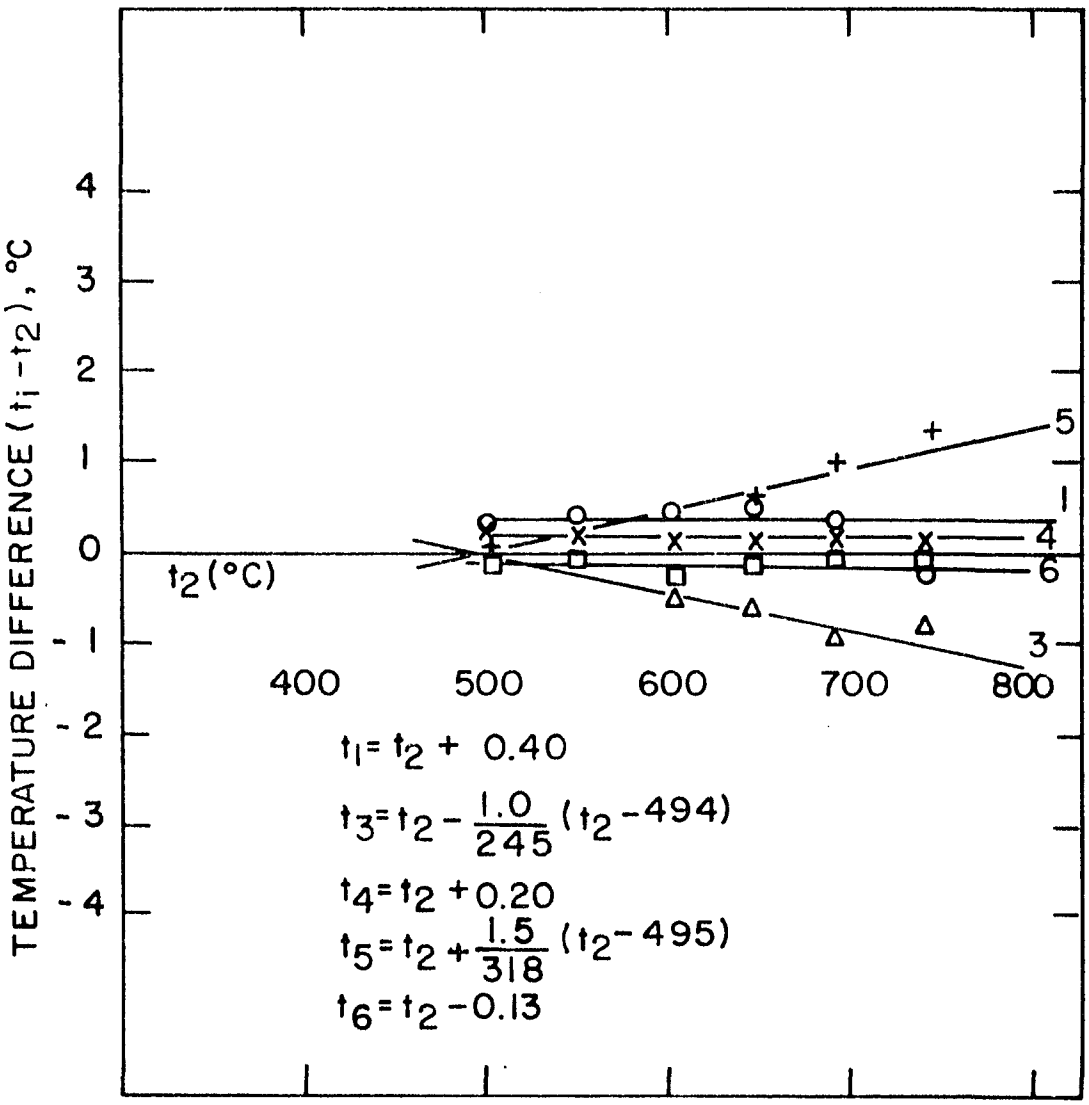
TEMPERATURE DIFFERENCE ($t_i - t_2$), °C
4
3
2
1
0
- 1
- 2
- 3
- 4
t_2 (°C)
400
500
600
700
800
5
1
4
6
3
$t_1 = t_2 + 0.40$
$t_3 = t_2 - \frac{1.0}{245}(t_2 - 494)$
$t_4 = t_2 + 0.20$
$t_5 = t_2 + \frac{1.5}{318}(t_2 - 495)$
$t_6 = t_2 - 0.13$

from the measured crucible thermocouple EMF.

Figure 25 indicates a calibration of the temperature difference between pure lead in a vaporization (outside) hole and a melting (inside) hole as measured by chromel-alumel probes. This difference can be used to determine different densities for the metal in each hole, which in turn will affect calculation of the 1/r ratio and effective Clausing factor. This temperature difference is significant, but its effect on the effective Clausing factor is less than 0.1%.

Vapor Pressures and Partial Pressures of Lead and Indium

The preliminary determinations of lead and indium vapor pressures are summarized in Figure 26 and near the bottom of Tables 1 and 2. These measurements were made using the melt-and-flow technique to provide initially clean vaporization surfaces. However, an AGSX grade graphite crucible was used rather than the much higher purity UF-4S grade graphite crucible used for the final runs. More importantly, the probe technique for measuring surface temperatures had not yet been developed, nor was it realized how large were the deviations of chromel-alumel thermocouples from tabular EMF values.

After these preliminary runs had been completed, attempts were made to calibrate the #22 gauge chromel-alumel thermocouples used in the crucible against a Bureau of Standards calibrated Pt-Pt 10% Rh thermocouple as described earlier.

Figure 25. Calibration of the temperature of the lead melt in an inside (melting) hole against the temperature in the corresponding outside (vaporization) hole using probes

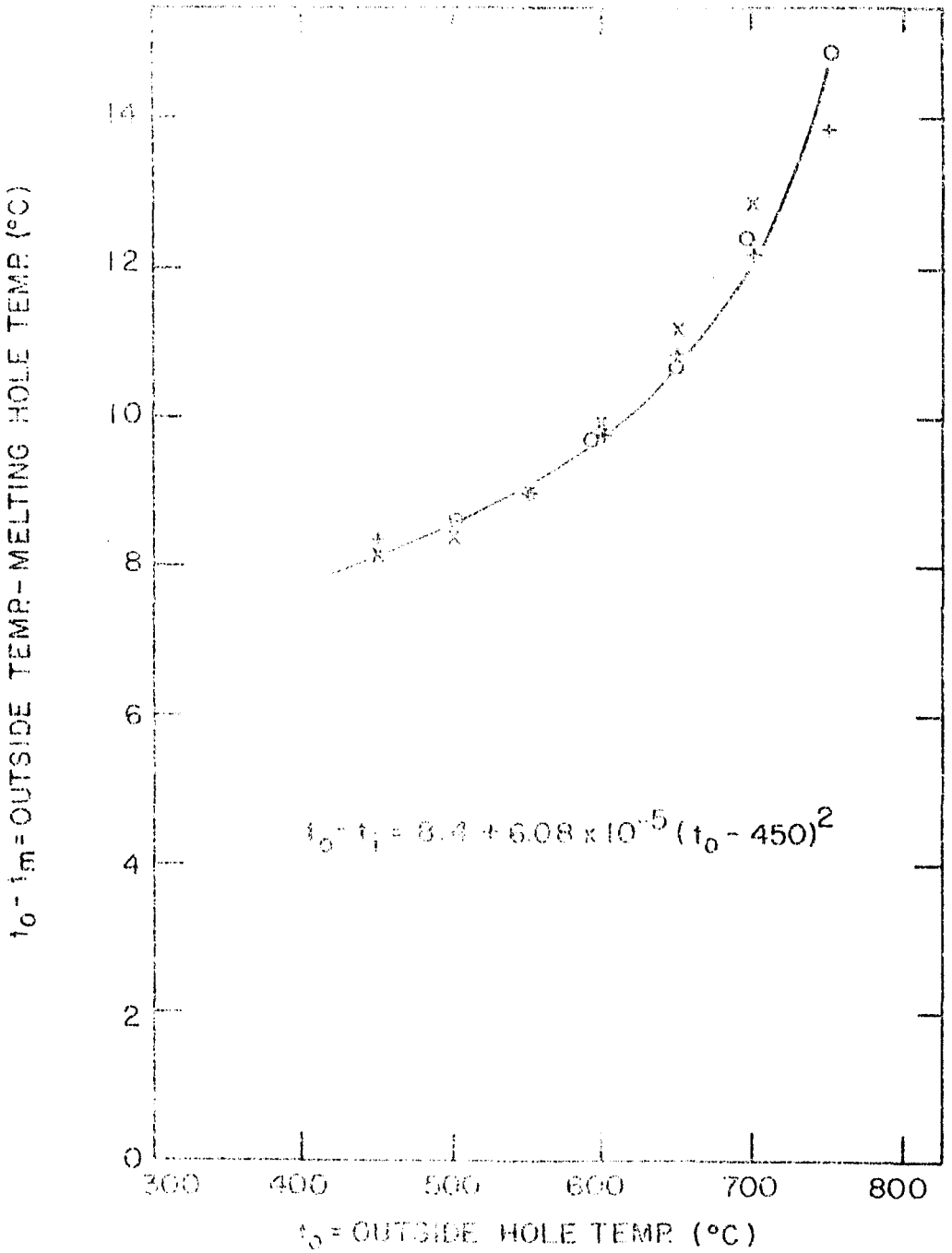
$t_o - t_m$ = OUTSIDE TEMP - MELTING HOLE TEMP (°C)
0
2
4
6
8
10
12
14
300
400
500
600
700
800
t_o = OUTSIDE HOLE TEMP (°C)
$t_o - t_i = 8.4 + 6.08 \times 10^{-5} (t_o - 450)^2$

Figure 26. Clausius-Clapeyron plot of preliminary results for lead vapor pressures and comparison of one preliminary indium run with Herrick's (43) line

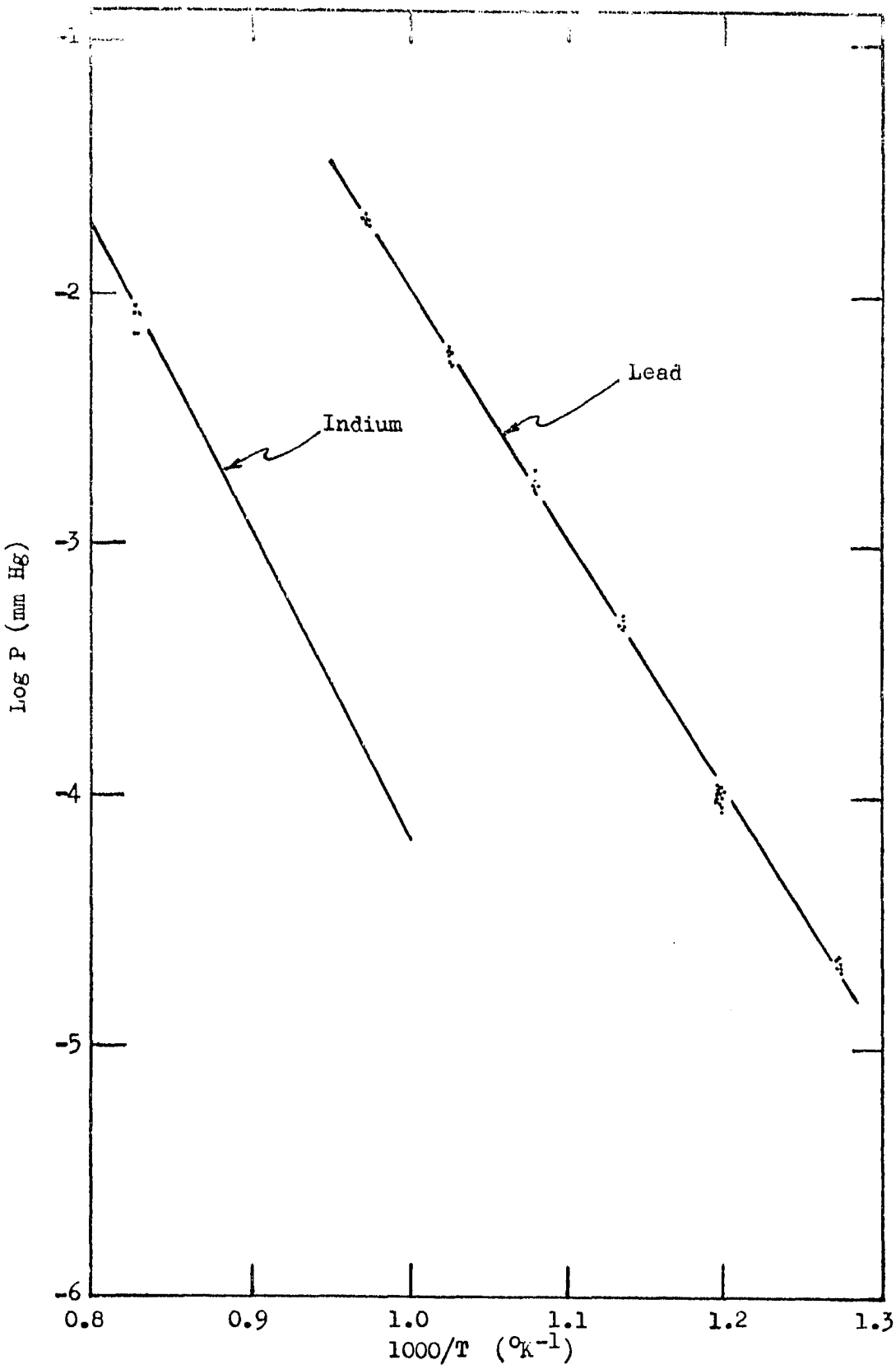
Lead
Indium
Log P (mm Hg)
-1
-2
-3
-4
-5
-6
0.8
0.9
1.0
1.1
1.2
1.3
1000/T (°K-1)

This set of six thermocouples was reading roughly 11°C too high. In addition, the probe measuring technique was employed to find that the hole temperatures ranged from 12 to 23°C higher than indicated by the crucible thermocouples, depending on the hole number. These thermocouples each had a vycor protection tube to prevent graphite contamination of the thermocouple, and were forced into the crucible using small springs to insure a snug fit and hopefully good thermal contact. The vycor protection tube probably accounted for part of the temperature difference. The variation in the temperature difference from one hole to another was probably due in part to coil-crucible geometry and also to the variation in thickness of the tips of the vycor protection tubes.

Both the thermocouple calibrations and probe calibrations were applied to the vaporization rate data "after the fact" to obtain the results shown. The scatter of the lead vapor pressures from the least squares fit line was 11.1% (standard deviation) as shown in Table 1, and the internal standard deviation for the one indium run was 10.1% as shown in Table 2. This scatter is due to temperature uncertainty, and the absolute magnitude of the vapor pressures and third law heat of vaporization are subject to at least a 3 or 4°C temperature uncertainty.

The final values of the lead vapor pressure determined by the far more refined methods described earlier are shown in

Figure 27. The least squares fit equation is

$$\log_{10} P(\text{mm Hg}) = (7.906 \pm 0.049) - \frac{(9795 \pm 43)}{T(°K)} \qquad (33)$$

If atmosphere units are desired instead of millimeters of mercury, replace 7.906 by 5.025. The experimental standard deviation of the data points from this line is 4.7%, as shown in Table 1. This compares very favorably to the expected standard deviation of 3.14% calculated from the theory of propagation of errors in Appendix A. The primary assumptions made in this error analysis are that the temperature error is 1°C and that there is no effect of surface oxide on the results. The near agreement of calculated and experimental standard deviations is a good measure of the validity of these two assumptions.

Table 3 summarizes the experimental data from each of the final six runs with pure lead arranged in order of increasing temperature. The run number gives the chronological order of the runs. Hole #2 always contained the probe thermocouple and yielded no vaporization data. The hole diameters and l/r ratios shown represent thermally expanded values. The remainder of the table is self explanatory.

Figure 28 shows a plot versus temperature of the individual standard third law heats of vaporization of lead obtained from Table 3. It shows a slight decreasing trend with increasing temperature; this indicates a slight temperature

Figure 27. Clausius-Clapeyron plot of final results for lead vapor pressures

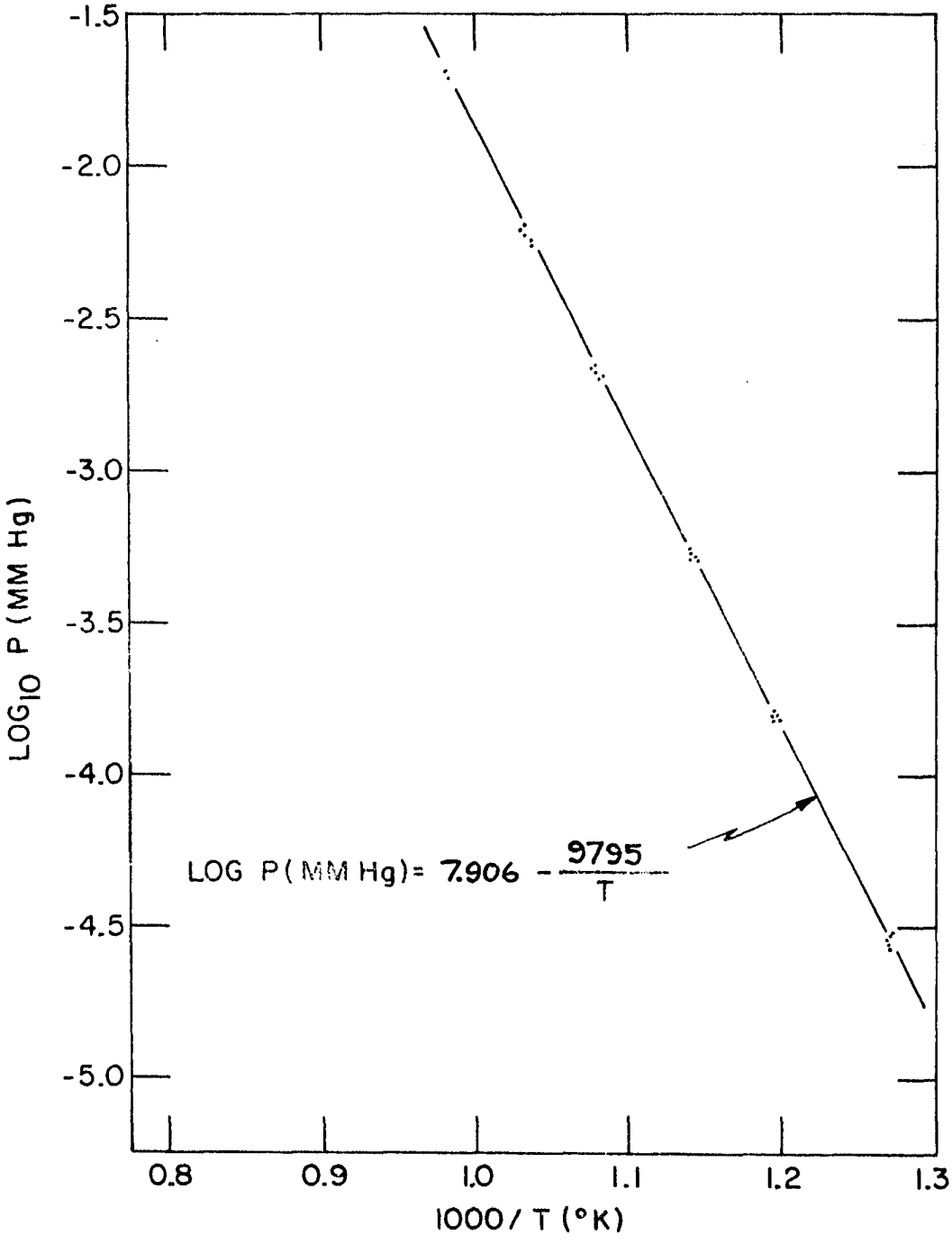
-1.5
-2.0
-2.5
-3.0
-3.5
-4.0
-4.5
-5.0
LOG10 P (MM Hg)
LOG P(MM Hg)= 7.906 - 9795/T
0.8
0.9
1.0
1.1
1.2
1.3
1000/T (°K)

Table 3. Data from lead vaporization runs using melt and flow technique and probe temperature measurement

Run no.	Hole no.	Vaporization hole diameter (cm)	l/r ratio[a]	Modified Clausing factor	Initial weight (g)	Net weight vaporized (g)
5	1	0.627	9.13	0.217	10.2337	0.0306
	3	0.631	9.08	0.217	10.2333	0.0292
	4	0.631	9.03	0.219	10.2355	0.0292
	5	0.631	9.08	0.217	10.2085	0.0297
	6	0.629	9.06	0.218	10.2794	0.0314
6	1	0.627	9.10	0.217	10.2774	0.0766
	3	0.631	9.06	0.218	10.2767	0.0777
	4	0.632	9.01	0.219	10.2596	0.0814
	5	0.631	9.04	0.218	10.2912	0.0868
	6	0.629	9.07	0.218	10.2336	0.0804
3	1	0.627	9.05	0.218	10.3593	0.0555
	3	0.632	9.02	0.219	10.3197	0.0580
	4	0.632	8.97	0.220	10.3088	0.0625
	5	0.632	9.03	0.219	10.2865	0.0613
	6	0.629	9.02	0.219	10.2904	0.0586
4	1	0.628	9.08	0.217	10.2552	0.0988
	3	0.632	9.03	0.218	10.2656	0.1081
	4	0.632	8.96	0.220	10.3025	0.1055
	5	0.632	9.01	0.219	10.3107	0.1042
	6	0.629	9.01	0.219	10.2948	0.0985
2	1	0.628	9.04	0.218	10.3274	0.1269
	3	0.632	9.00	0.219	10.3179	0.1395
	4	0.632	8.95	0.220	10.3263	0.1475
	5	0.632	9.03	0.219	10.2396	0.1486
	6	0.629	9.01	0.219	10.2627	0.1341
1	1[b]	0.628	9.08	0.217	10.2373	0.2403
	3	0.632	9.04	0.218	10.2226	0.2423
	4[b]	0.632	8.99	0.219	10.2307	0.2609
	5[b]	0.632	8.99	0.219	10.3571	0.2737
	6[b]	0.630	9.03	0.219	10.2423	0.2482

[a]Length to radius ratio, where length is distance from top of crucible hole to equator of assumed hemispherical surface of liquid metal.

[b]Samples not used in averages because of surface impurity found after run.

Lead vapor pressure (atm)	Log P vs. 1/T pressure (atm)	Difference in pressures (atm)	Surface temp. (°K)	Third law $\Delta H°_{v,298}$ $\left(\frac{\text{kcal}}{\text{g-atom}}\right)$
3.93×10^{-8}	3.66×10^{-8}	2.76×10^{-9}	785.98	46.53
3.69×10^{-8}	3.95×10^{-8}	-2.57×10^{-9}	788.11	46.75
3.67×10^{-8}	3.96×10^{-8}	-2.90×10^{-9}	788.19	46.76
3.76×10^{-8}	3.93×10^{-8}	-1.71×10^{-9}	787.95	46.71
3.99×10^{-8}	3.73×10^{-8}	2.62×10^{-9}	786.52	46.54
1.99×10^{-7}	1.93×10^{-7}	0.66×10^{-9}	834.31	46.57
1.99×10^{-7}	2.14×10^{-7}	-1.43×10^{-9}	837.49	46.74
2.08×10^{-7}	2.16×10^{-7}	-0.85×10^{-9}	837.86	46.69
2.22×10^{-7}	2.12×10^{-7}	0.99×10^{-9}	837.31	46.54
2.08×10^{-7}	1.98×10^{-7}	0.95×10^{-9}	835.17	46.54
6.65×10^{-7}	6.38×10^{-7}	2.68×10^{-8}	872.99	46.53
6.86×10^{-7}	7.18×10^{-7}	-3.25×10^{-8}	877.00	46.68
7.35×10^{-7}	7.31×10^{-7}	0.40×10^{-8}	877.61	46.59
7.25×10^{-7}	7.15×10^{-7}	1.05×10^{-8}	876.82	46.57
6.98×10^{-7}	6.60×10^{-7}	3.78×10^{-8}	874.11	46.50
2.72×10^{-6}	2.55×10^{-6}	1.68×10^{-7}	922.48	46.45
2.93×10^{-6}	2.92×10^{-6}	0.16×10^{-7}	927.56	46.56
2.85×10^{-6}	2.99×10^{-6}	-1.44×10^{-7}	928.47	46.66
2.82×10^{-6}	2.90×10^{-6}	-0.83×10^{-7}	927.37	46.62
2.69×10^{-6}	2.65×10^{-6}	0.33×10^{-7}	923.93	46.55
7.25×10^{-6}	7.23×10^{-6}	0.22×10^{-7}	963.51	46.53
7.88×10^{-6}	8.35×10^{-6}	-4.85×10^{-7}	969.48	46.65
8.27×10^{-6}	8.59×10^{-6}	-3.15×10^{-7}	970.64	46.61
8.40×10^{-6}	8.31×10^{-6}	0.83×10^{-7}	969.28	46.52
7.61×10^{-6}	7.54×10^{-6}	0.73×10^{-7}	965.24	46.52
2.53×10^{-5}[b]	2.17×10^{-5}	3.66×10^{-6}	1010.93	46.19[b]
2.52×10^{-5}	2.53×10^{-5}	-0.06×10^{-6}	1017.93	46.50
2.70×10^{-5}[b]	2.61×10^{-5}	0.92×10^{-6}	1019.38	46.42[b]
2.83×10^{-5}[b]	2.51×10^{-5}	3.21×10^{-6}	1017.72	46.26[b]
2.59×10^{-5}	2.27×10^{-5}	3.25×10^{-6}	1012.98	46.23[b]

Figure 28. Individual values of standard third law heats of vaporization for lead, showing their slight temperature trend

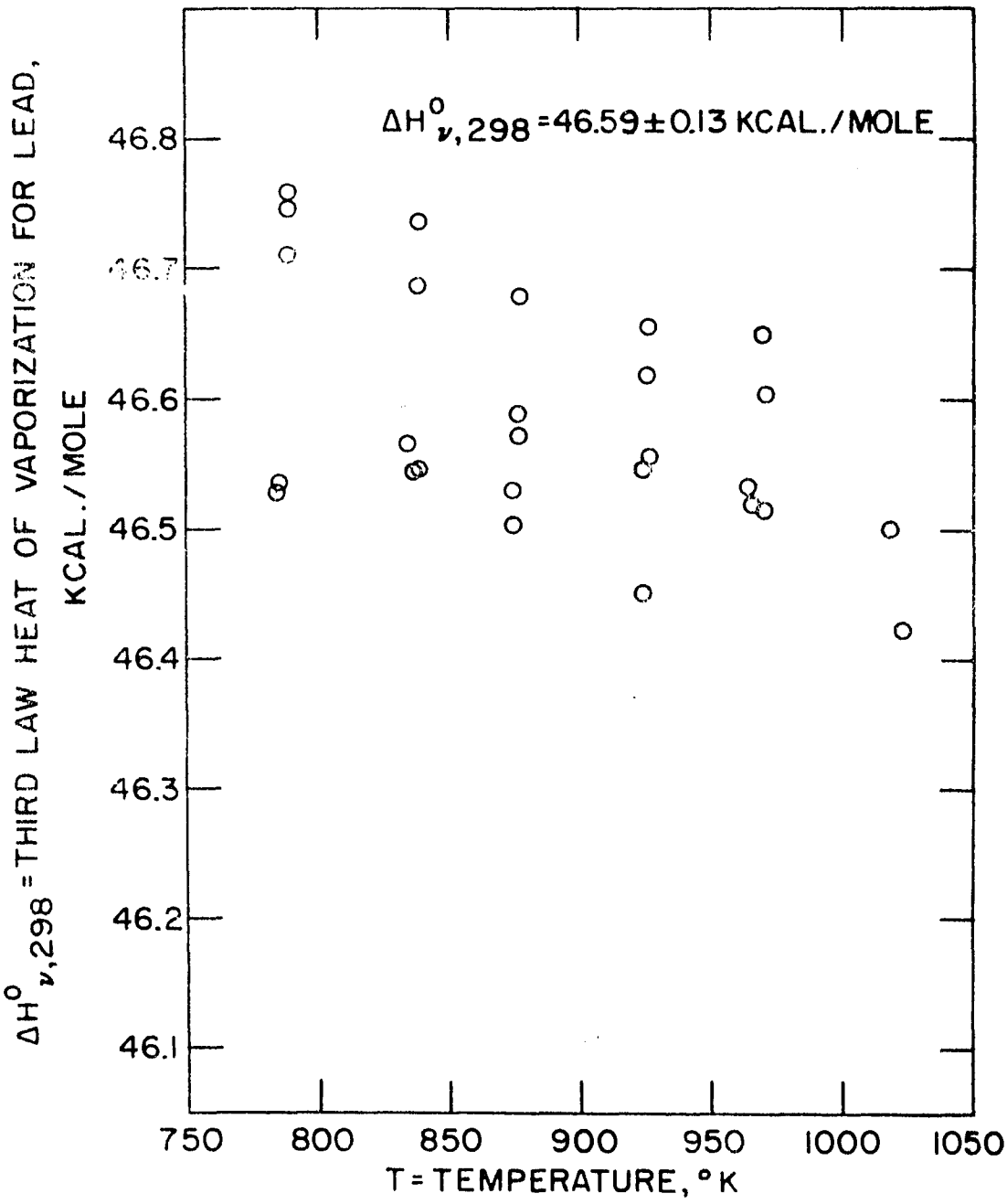
$\Delta H^0_{\nu,298}$ = THIRD LAW HEAT OF VAPORIZATION FOR LEAD, KCAL./MOLE
$\Delta H^0_{\nu,298}$ = 46.59 ± 0.13 KCAL./MOLE
46.8
46.7
46.6
46.5
46.4
46.3
46.2
46.1
750
800
850
900
950
1000
1050
T = TEMPERATURE, °K

dependent error. The same conclusion can be reached because of the slight discrepancy (see Table 1) between the standard second and third law heats of vaporization, and also the deviation of the standard entropy of vaporization from the expected third law value of 26.34 cal/g-mole-°K.

It is believed that this error, corresponding to measuring too low a vapor pressure at the lower temperatures or too high a pressure at the higher temperatures, is due to the presence of an invisible oxide surface film. This film is expected to be thicker at lower vaporization temperatures because of a decreased solubility in the bulk liquid (see Figure 3), because of a lower tendency to be reduced by the graphite crucible (see Figure 4) and lower kinetic reduction rates, and because of its own lower vapor pressure compared to lead (see Figure 5). For the same reasons it would be expected to be thinner at the higher temperatures, and also to possibly make a perceptible contribution to the sample weight loss at the higher temperatures. Nevertheless, these possible errors are very small.

Very nearly perfect agreement is obtained with the results of Kim and Cosgarea (56), and extremely close agreement is obtained with the excellent work of Hawkins and Hultgren (41) and Shiu and Munir (103). The results of this work are also close to the values of Goldfinger and Jeunehomme (32) if an average value for their Clausing factor is selected. This work is in clear disagreement with the work of Aldred and

Pratt (3), and in poor agreement with the early work of Egerton (26).

Unfortunately, the method used in this work could not be applied to high temperature indium vaporizations because the chromel-alumel probes rapidly dissolved in pure indium at the higher temperatures required to obtain measurable indium vaporization rates. No commercial thermocouple can be used as a direct probe in indium because all are soluble.

Lead Partial Pressures Over Indium-Lead Alloys

Table 4 summarizes the experimental data from the four successful vaporization runs of indium-lead alloys. The nominal compositions are 50 atom % lead and 10 atom % lead.

Two runs failed: the seventh because the temperature controller went out of order during the run, and the eighth because too fast a heating rate splashed liquid alloy out of two vaporization holes.

Table 5 is a quick summary of the averages of the data for each of the final ten successful runs. Errors shown are standard deviations. The lead activity coefficients determined, based on the lead vapor pressure from Equation 33, are shown in Figure 29. The error bars represent the standard deviation of the data for the five samples used for each point. These standard deviations are somewhat lower than the 4.7% standard deviations obtained when vaporizing pure lead, and closely

Table 4. Data from indium-lead alloy vaporization runs using melt and flow technique and probe temperature measurement

Run no.	Hole no.	Vaporization hole diameter (cm)	l/r ratio[a]	Modified Clausing factor	Initial weight (g)	Average atom % Pb
9	1	0.628	8.72	0.225	9.3864	49.71
	3	0.632	9.00	0.219	8.6763	49.69
	4	0.632	8.78	0.223	9.0324	49.70
	5	0.632	8.81	0.223	9.0785	49.71
	6	0.629	8.75	0.224	9.2004	49.72
12	1	0.628	8.67	0.226	9.4429	49.63
	3	0.632	8.86	0.222	8.9414	49.62
	4	0.632	8.67	0.226	9.2312	49.64
	5	0.632	8.79	0.223	9.0919	49.59
	6	0.629	8.72	0.225	9.2316	49.63
10	1	0.628	8.51	0.229	8.0705	9.70
	3	0.632	8.52	0.229	7.9812	9.69
	4	0.632	8.36	0.232	8.1770	9.70
	5	0.632	8.33	0.233	8.3165	9.70
	6	0.629	8.44	0.231	8.1113	9.69
11	1	0.628	8.39	0.232	8.2920	9.69
	3	0.632	8.55	0.228	7.9269	9.68
	4	0.632	8.46	0.230	8.0041	9.69
	5	0.632	8.49	0.230	8.0357	9.69
	6	0.629	8.48	0.230	8.0333	9.68

[a]Length to radius ratio, where length is distance from top of crucible hole to equator of assumed hemispherical surface of liquid metal.

[b]Calculated from Equation 5 using Herrick's (43) vapor pressure data.

[c]Calculated from Equation 33 of this work.

Net weight vaporized (g)	Wt. In vaporized as % of Pb[b]	Lead vapor pressure[c] (mm Hg)	Lead partial pressure (mm Hg)	Surface temp. (°K)	Lead activity coefficient
0.1050	0.207	2.26×10^{-3}	2.38×10^{-3}	928.21	1.056
0.0877	0.203	2.11×10^{-3}	2.01×10^{-3}	925.68	0.953
0.0953	0.204	2.14×10^{-3}	2.14×10^{-3}	926.18	1.002
0.0962	0.207	2.24×10^{-3}	2.17×10^{-3}	927.90	0.970
0.0993	0.207	2.25×10^{-3}	2.25×10^{-3}	928.06	1.000
0.1400	0.327	1.08×10^{-2}	1.20×10^{-2}	992.27	1.107
0.1277	0.321	1.01×10^{-2}	1.10×10^{-2}	989.17	1.088
0.1251	0.322	1.02×10^{-2}	1.06×10^{-2}	989.76	1.032
0.1340	0.327	1.07×10^{-2}	1.15×10^{-2}	991.88	1.067
0.1361	0.327	1.08×10^{-2}	1.16×10^{-2}	992.07	1.080
0.0484	1.89	2.18×10^{-3}	2.03×10^{-3}	926.92	0.928
0.0492	1.87	2.12×10^{-3}	2.04×10^{-3}	925.87	0.959
0.0488	1.88	2.17×10^{-3}	1.99×10^{-3}	926.72	0.914
0.0511	1.89	2.20×10^{-3}	2.08×10^{-3}	927.27	0.943
0.0543	1.88	2.15×10^{-3}	2.25×10^{-3}	926.39	1.047
0.0550	1.87	2.09×10^{-3}	2.11×10^{-3}	925.37	1.006
0.0543	1.85	2.04×10^{-3}	2.09×10^{-3}	924.33	1.024
0.0534	1.86	2.08×10^{-3}	2.03×10^{-3}	925.17	0.974
0.0522	1.87	2.11×10^{-3}	1.99×10^{-3}	925.71	0.941
0.0541	1.86	2.07×10^{-3}	2.08×10^{-3}	924.81	1.008

Table 5. Summary of data from runs using melt and flow technique and probe temperature measurement (Errors shown are standard deviations.)

Run no.	Approx. atomic % Pb	Temp. (°C)	Time (hr)	Langmuir percentage[a] for 5 samples	Lead activity coefficient
5	100	514	141.97	99.3±7.4	
6	100	563	72.00	100.5±5.4	
3	100	602	15.92	101.5±3.9	
4	100	652	7.13	100.1±4.4	
2	100	694	3.50	98.6±3.1	
1	100	742	1.95	109.4±7.4[b]	
9	50	654	12.83	99.6±3.9	0.996±0.039
10	10	653	34.35	95.9±5.2	0.958±0.053
11	10	652	37.15	99.1±3.2	0.991±0.033
12	50	718	3.50	107.4±2.8	1.075±0.028

[a]Vaporization weight loss as a percentage of Langmuir weight loss computed from Equation 5 assuming ideal solutions, using lead vapor pressures from Equation 33 and indium vapor pressures from Herrick (43) in Table 2.

[b]Three of these samples were ignored in computations because of surface impurity found after run. Langmuir percentage for other two averaged 101.6%.

Figure 29. Comparison of experimental lead activity coefficients with those of other workers

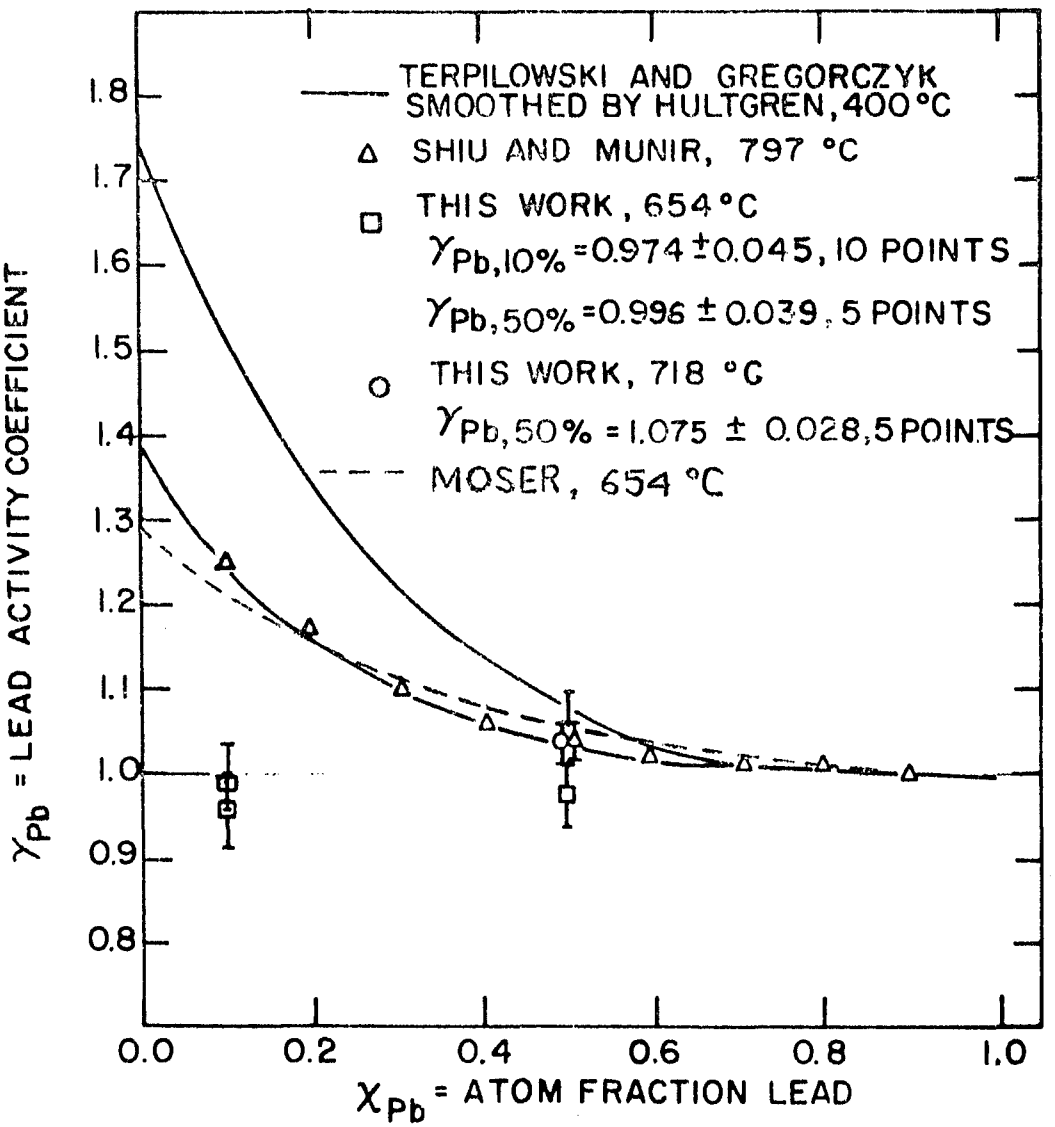
TERPILOWSKI AND GREGORCZYK SMOOTHED BY HULTGREN, 400 °C
SHIU AND MUNIR, 797 °C
THIS WORK, 654 °C
$\gamma_{Pb,10\%}$ = 0.974 ± 0.045, 10 POINTS
$\gamma_{Pb,50\%}$ = 0.996 ± 0.039, 5 POINTS
THIS WORK, 718 °C
$\gamma_{Pb,50\%}$ = 1.075 ± 0.028, 5 POINTS
MOSER, 654 °C
γ_{Pb} = LEAD ACTIVITY COEFFICIENT
X_{Pb} = ATOM FRACTION LEAD
1.8
1.7
1.6
1.5
1.4
1.3
1.2
1.1
1.0
0.9
0.8
0.0
0.2
0.4
0.6
0.8
1.0

approach the 3.14% expected from the error analysis. Part of the reason for this is probably the closer pattern for the temperature probe calibrations in Figures 23 and 24 as compared to Figure 22. The overall error for the activity coefficients is discussed in Appendix A. Table A2 shows that a 3.14% standard deviation is determining both vapor pressures and partial pressures leads to a standard deviation of about 6.43% in the activity coefficient at 50 atom % lead and about 31.5% at 10 atom % lead. Within these wide error bounds, the activity coefficients determined here agree with those of the other authors. Since Shiu and Munir's (103) pure lead vapor pressure data have only slightly more than half the scatter of the data of this work (as is to be expected with torsion effusion work since the same sample and apparatus are used to obtain several data points during one run), their error bounds for activity coefficients should be about half the size for those of this work.

The data of this work appear to indicate that the indium-lead system is ideal, i.e., that the lead activity coefficient is unity. This would be in clear conflict with all the authors mentioned in the Previous Work section who have worked on this system.

It is believed that the discrepancy can be attributed neither to surface oxides nor to errors in surface temperature measurement. An error in the latter of at least 10°C would be needed to cause agreement of this data with that of others at

x_{Pb} = 0.10, whereas it is believed that about 1°C accuracy was attained.

The only feasible explanation is surface depletion of the volatile lead component. Verhoeven (113) shows for a stagnant liquid alloy in a vertical cylindrical container having no horizontal temperature gradients that the critical Rayleigh number is 67.4 for the onset of convective mixing caused by a negative vertical temperature gradient. Using Crawley and Thresh's (19) indium viscosity, and other lead and indium properties from Lyon (69), the Rayleigh numbers at 650°C under experimental vaporization temperature gradient conditions are 28.8 for lead, 1.97 for indium, and an estimated 4.53 for a 50 atom % alloy. Hence, thermal convection would not be expected from the vertical temperature gradients present. Also, since lead is more dense than indium, the alloy's presumed negative vertical density gradient would also stabilize against convection.

However, it is known that a significant horizontal temperature gradient exists across the vaporization hole, and the crucible is being gently vibrated by the vacuum forepump. The spherically shaped meniscus would also be expected to aid convection. Walsh and Burnet (118) found that slight vacuum pump vibrations eliminated surface depletion in their moderate concentration alloys. Contrarily, Bradley and Webster (10) found surface depletion existed in alloys extremely dilute in

the volatile component even under conditions of intense surface agitation. The evidence is conflicting on surface depletion as a cause for lead activity coefficient measurement errors in this work, but surface depletion seems the only possible explanation for the results.

CONCLUSIONS AND RECOMMENDATIONS

As stated in the Introduction, the objectives of this work were 1) development of a theoretically and experimentally sound method for measuring liquid metal vapor pressures in the low pressure region and 2) application of this method to measure lead partial pressures over the indium-lead alloy in order to calculate activity coefficients and other thermodynamic properties. As stated in the Theory section, a modified Langmuir technique was chosen because its theoretical basis is as sound as the more popular effusion techniques and because control of the difficult experimental problems related to surface cleanliness, surface area measurement and surface temperature measurement would be of help in designing industrial molecular distillation equipment. Each of the points mentioned above will now be considered.

The theory of the Langmuir free-surface evaporation method is based on using slow, non-equilibrium vaporization to measure equilibrium vapor pressures. The vaporization rates depend on surface evaporation mechanisms not fully understood at present. It was shown that, under a large portion of the pressure range in which effusion techniques are used, the effusion rates also depend upon the same surface evaporation mechanism. The Langmuir method is dependent on the validity of Langmuir's (65) assumption that at low pressures the vaporization rate

mechanism is independent of the existence of concurrent condensation. Some justification for this assumption was presented in the Theory section on the basis that below one millimeter of mercury vapor pressure, a molecule evaporates from the liquid surface less than one out of every 10^6 times it changes positions with another molecule. Use of the Langmuir method focuses attention directly on the vaporization surface (and on the other wall surfaces involved).

That the method is experimentally sound for pure lead is evidenced by the excellent agreement of the lead vapor pressures determined by this Langmuir method with those pressures determined by effusion methods. The standard heats and entropies of vaporization are in similar accord, as pointed out in the Results section.

Use of this method to determine lead partial pressures in the liquid indium-lead is apparently made impossible because of surface depletion of the volatile lead component. The lead activity coefficients are within the experimental range of precision of others' values, as explained earlier, but this precision is not high. The effusion techniques have a distinct advantage over Langmuir measurements with respect to surface depletion, because a negligible amount of net volatile component vaporization occurs per unit surface area. In industrial molecular distillation equipment, existence of surface depletion would reduce the theoretically high separation

factors possible on the basis of high metal relative volatilities, if high purity and high yields are desired.

The problem of surface cleanliness in the liquid lead and indium-lead systems has been solved by use of a high purity graphite crucible capable of producing a fresh and clean vaporization surface under vacuum by the melt-and-flow technique. This is described in the Equipment and Experimental Procedure section. In the Results section, it is described how the presence of an invisible oxide film might have a very slight influence on the vaporization rates. Provided the residual pressure of industrial equipment is low enough, creation of fresh vaporization surfaces by the use of a feed system similar to the graphite crucible used here would increase vaporization rates by factors of about 2 to 10, based on vaporization rate measurements with oxidized samples in this work. In continuous process equipment, periodical or continuous surface renewal would be helpful. If no effort is made to reduce oxidation, rates about 10% of the theoretical maximum are obtained. If residual pressures less than 10^{-5} mm Hg are used and samples are carefully cleaned prior to use, vaporization rates of 50 to 80% of the theoretical maximum are obtained.

The problem of what is the effective vaporization surface area of the hemispherically shaped samples has been solved by Sandry and Stevenson's (101) Monte Carlo calculations. Since the surface area of a hemisphere is twice that of the

corresponding cylindrical cross section, there is considerable room for error. At the experimental values of 1/r used, the effective Clausing factor computed from Equation 32, is not a strong function of 1/r. Moreover, at these 1/r values Sandry and Stevenson show that whether the vaporization surface is flat or spherical is not too important either. Therefore small deviations from a hemispherical shape do not affect the experimental results.

Surface temperature measurement has been a significant experimental hurdle in this work, since 1°C accuracy is required. The use of induction heating, with its associated disadvantages of large temperature gradients and high frequency electrical noise, has made the surface temperature measurements even more of a problem. Great care must be exercised in eliminating conduction losses in thermocouple measurements and in obtaining good thermal contact of the thermocouples and the substance, the temperature of which is to be measured. The latter is extremely difficult when solid temperatures are to be measured. The liquid metal lends itself to perfect thermal contact when the bare probe method is utilized, but at the expense of metal and thermocouple contamination. The elaborate calibration procedure outlined in the Procedure and Results sections, coupled with the probe error estimation technique of Wolkoff et al. (126), have successfully measured these surface temperatures to about 1°C. There are three sources of

evidence for this: 1) the close agreement of measured lead vapor pressures with others' values, 2) the near agreement of the experimental and error analysis standard deviations for the vapor pressures and 3) the approximate agreement of the standard deviations of vapor pressures from the five samples of each run (see Table 5) with the overall standard deviation from the least squares line. A counter example of this last point is evidenced in the work with indium of Macur et al. (71) as discussed in the Previous Work section.

A few other points should be mentioned. The successful use of this Langmuir method with lead gives credence to the fact that its condensation coefficient, α, is unity. It also gives support for the cosine reflection law being applicable to collisions of lead molecules with graphite walls. The linearity exhibited in the log P versus 1/T plot for lead in Figure 27 above 680°C and extending up to at least 750°C (where from Figure 2 the λ/D ratio is approximately unity) lends support to those who believe Knudsen flow exists down to at least $\lambda/D = 1$ rather than only to $\lambda/D = 10$. This is discussed in the Theory section.

Based on the results and conclusions drawn from this work, the following recommendations for future work in this area are made:

1) A vacuum microbalance would be useful in obtaining immediate measurements of vaporization weight loss rather than

having to use average rates of weight loss over long time periods. This would be especially valuable in measuring vaporization rates from oxidized or partially oxidized surfaces, as exist during industrial applications. Characterization of the amount of oxide present would be necessary. Use of graphite crucibles with a microbalance might not be possible because of the large amount of outgassing occurring.

2) Further study is needed at vaporization rates occurring when the vapor pressures reach the transition regime between Knudsen and viscous flow. This can be done with the present equipment.

3) Large surface areas were not utilized in this study, thus forfeiting this advantage of the Langmuir method enabling measurements of very low pressures. Still, the pressures measured were the lowest by an order of magnitude since 1923. Increasing the surface area significantly would be expected to greatly increase convection effects, as the Rayleigh number varies with D^4 (113), and may eliminate the surface depletion suspected here. It may be, however, that the surface temperature would vary significantly over the surface, and this would have to be checked. This study could also be done with only slight modification of existing equipment.

4) The thermocouple probe method of obtaining surface temperatures of other pure liquid metals, which vaporize below temperatures where radiation pyrometry can be used, should be

reliable provided suitable thermocouple materials can be found. This was the only factor in this work which eliminated accurate indium vapor pressure measurements. These materials need not be completely insoluble, but only slowly soluble. Alternately, a thin coating of insoluble or slowly soluble metal might be coated on the thermocouple probe wires. Figure 6 shows that indium vapor pressure determinations are widely scattered compared to lead, which makes work on indium desirable. Of course, radiation pyrometry requires accurate surface emissivities, which are largely lacking for liquid metals. Hence, a suitable probe would be of use here, also.

5) It is believed that use of ultrahigh vacuum equipment for Langmuir vaporizations is not necessary, as was shown in this work. It would be interesting to check this assumption out for the lead system, however, to ascertain whether or not the slight temperature dependent error noted could be eliminated in vacuums of the order of 10^{-9} mm Hg. Graphite crucibles would probably not be suitable here because of high outgassing.

6) It is suggested that the Langmuir method will never be able to measure the activity coefficient of a volatile component across the entire composition range due to surface depletion at low concentrations of the volatile component. The best vaporization technique to make these measurements is the torsion effusion method. However, it should be realized

that the location, temperature and cleanliness of surfaces inside the cell are important. A preliminary Monte Carlo study of vaporization geometries to be used would be very helpful.

BIBLIOGRAPHY

1. Alcock, C. B., and T. N. Belford. Thermodynamics and solubility of oxygen in liquid metals from e.m.f. measurements involving solid electrolytes. Part 1. Lead. Trans. Faraday Soc. 60: 822-835. 1964.

2. Alcock, C. B., J. B. Cornish, and P. Grieveson. Knudsen effusion studies of compounds of uranium and thorium with elements of groups III b and IV b. Symposium on Thermodynamics with Emphasis on Nuclear Materials and Atomic Transport in Solids Proceedings. Vienna, 1965. Vol. I, paper Sm-66/35. 1966.

3. Aldred, A. T., and J. N. Pratt. Thermodynamic properties of liquid silver-lead alloys. Trans. Faraday Soc. 57: 611-618. 1961.

4. Anderson, J. S. The vapour pressure of metallic indium. J. Chem. Soc. (London) 1943: 141-143.

5. Balson, E. W. Some aspects of molecular effusion. J. Phys. Chem. 65: 1151-1158. 1961.

6. Bandyopadhyay, Gopal K., and Hem Shanker Ray. Kinetics of oxygen dissolution in molten lead. Met. Trans. 2: 3055-3061. 1971.

7. Blakely, J. P., and L. G. Overholser. Outgassing behavior of EGCR moderator graphite. (Oak Ridge National Laboratory, Oak Ridge, Tennessee) U. S. Atomic Energy Commission Report ORNL-3560. 1964.

8. Blocher, John M., and I. E. Campbell. Vapor pressure of titanium. J. Am. Chem. Soc. 71: 4040-4042. 1949.

9. Borg, Richard J., and C. Ernest Birchenall. Activity of Cd in Mg-Cd alloys. Trans. Met. Soc. A. I. M. E. 236: 938-941. 1966.

10. Bradley, R. F., and D. S. Webster. Surface depletion in the vacuum distillation of metals from bismuth. Nuc. Sci. Engr. 35: 159-164. 1969.

11. Brewer, Leo, and James S. Kane. The importance of complex gaseous molecules in high temperature systems. J. Phys. Chem. 59: 105-109. 1955.

12. Brewer, Leo, and Gerd M. Rosenblatt. Thermodynamics of suboxide vaporization. Trans. Met. Soc. A. I. M. E. 224: 1268-1271. 1962.

13. Burns, Richard P. Systematics of the evaporation coefficient of Al_2O_3, Ga_2O_3, In_2O_3. J. Chem. Phys. 44: 3307-3319. 1966.

14. Burns, Richard P., G. DeMaria, J. Drowart, and M. G. Inghram. Mass spectrometric investigation of the vaporization of In_2O_3. J. Chem. Phys. 38: 1035-1036. 1963.

15. Carlson, K. Douglas. The molecular and viscous effusion of saturated vapors. (Argonne National Laboratory, Argonne, Illinois) U. S. Atomic Energy Commission Report ANL-6156. 1960.

16. Carlson, K. Douglas, Paul W. Gilles, and R. J. Thorn. Molecular and hydrodynamical effusion of mercury from Knudsen cells. J. Chem. Phys. 38: 2725-2733. 1963.

17. Clausing, P. Über die Strömung sehr verdunnter Gase durch Röhren von beliebiger Länge. Ann. Physik 12: 961-989. 1932.

18. Cosgarea, A., E. E. Hucke, and D. V. Ragone. Thermodynamic activity measurements using optical absorption in metal vapors. In St. Pierre, George R., ed. Physical chemistry of process metallurgy. Part 1. Pp. 363-371. New York, New York, Interscience Publishers, Inc. 1961.

19. Crawley, A. F., and H. R. Thresh. The viscosities of cadmium and indium. Trans. Met. Soc. A. I. M. E. 245: 424-425. 1969.

20. Cubicciotti, Daniel. A new Σ-plot treatment of equilibrium data and its application to the vaporization of bismuth chloride. J. Phys. Chem. 70: 2410-2413. 1966.

21. DeMarcus, W. C. The problem of Knudsen flow. III. Solutions for one-dimensional systems. (Oak Ridge Gaseous Diffusion Plant, Oak Ridge, Tennessee) U. S. Atomic Energy Commission Report K-1302. 1956.

22. DeMaria, G., J. Drowart, and M. J. Inghram. Thermodynamic study of InSb with a mass spectrometer. J. Chem. Phys. 31: 1076-1081. 1959.

23. Drowart, J., R. Colin, and G. Exsteen. Mass spectrometric study of the vaporization of lead oxide. Trans. Faraday Soc. 61: 1376-1383. 1965.

24. Dutchak, Ya. I., and A. M. Korsunskii. Viscosity and electrical conductivity of indium-lead alloys. (Translated title) Izv. Vyssh. Ucheb. Zaved., Fiz. 12: 121-122. 1969. Original not available; abstracted in Chemical Abstracts 71: 73416r. 1969.

25. Edwards, James W., Herrick L. Johnston, and Walter E. Ditmars. Vapor pressures of inorganic substances. XI. Titanium between 1587 and 1764°K, and copper between 1143 and 1292°K. J. Am. Chem. Soc. 75: 2467-2470. 1953.

26. Egerton, A. C. The vapor pressure of lead. Proc. Roy. Soc. (London) A103: 469-486. 1923.

27. Ellett, A., and H. F. Olson. Reflection of atoms by a crystal. Phys. Rev. 31: 643-647. 1928.

28. Endebrock, R. W., and P. M. Engle. Separation of polonium from bismuth by distillation. (Mound Laboratory, Miamisburg, Ohio) U. S. Atomic Energy Commission Report AECD-4146. 1953.

29. Fajans, K. Über das Schmelzen und die Verdampfungswärme des Graphits. Z. Elektrochem. 31: 63-70. 1925.

30. Freeman, Robert D., and Alan W. Searcy. The effect of channel holes on the force exerted by effusing vapors. J. Chem. Phys. 22: 762-763. 1954.

31. Glassner, Alvin. The thermochemical properties of the oxides, fluorides and chlorides to 2500°K. (Argonne National Laboratory, Argonne, Illinois) U. S. Atomic Energy Commission Report ANL-5750. 1957.

32. Goldfinger, P., and M. Jeunehomme. Mass spectrometric and Knudsen-cell vaporization studies of group 2B-6B compounds. Trans. Faraday Soc. 59: 2851-2867. 1963.

33. Green, S. J., and T. W. Hunt. Accuracy and response of thermocouples for surface and fluid temperature measurements. In Dahl, A. I., and C. M. Herzfeld eds. Temperature - its measurement and control in science and industry. Vol. 3, part 2. New York, New York, Reinhold Publishing Corp. 1962.

34. Greenbank, J. C., and B. B. Argent. Vapor pressure of magnesium, zinc and cadmium. Trans. Faraday Soc. 61: 655-664. 1965.

35. Grieveson, P., G. W. Hooper, and C. B. Alcock. The vapor pressures of the liquid metals copper, silver and gold. In St. Pierre, George R., ed. Physical chemistry of process metallurgy. Part 1. Pp. 341-352. New York, New York, Interscience Publishers, Inc. 1961.

36. Gulbransen, Earl A., and Kenneth F. Andrew. The kinetics of the reactions of beryllium with oxygen and nitrogen and the effect of oxide and nitride films on its vapor pressure. J. Electrochem. Soc. 97: 383-395. 1950.

37. Gulbransen, Earl A., and Kenneth F. Andrew. A preliminary study of the oxidation and the vapor pressure of chromium. J. Electrochem. Soc. 99: 402-406. 1952.

38. Gulbransen, Earl A., and Kenneth F. Andrew. Vapor pressure studies on iron and chromium and several alloys of iron, chromium and aluminum. Trans. Met. Soc. A. I. M. E. 221: 1247-1252. 1961.

39. Hansen, Max, and Kurt Anderko. Constitution of binary alloys. 2nd ed. New York, New York, McGraw-Hill Book Co., Inc. 1958.

40. Harteck, P. Measurements of the vapor pressure of Ag, Au, Cu, Pb, Ga, Sn and calculation of the chemical constants. (Translated title) Z. Phys. Chem. 134: 1-20. 1928.

41. Hawkins, Donald T., and Ralph Hultgren. Vapor pressure of lead and activity measurements on liquid lead-tin alloys by the torsion effusion method. Trans. Met. Soc. A. I. M. E. 239: 1046-1049. 1967.

42. Hendricks, J. W., and D. L. McElroy. High temperature high vacuum thermocouple drift tests. (Oak Ridge National Laboratory, Oak Ridge, Tennessee) U. S. Atomic Energy Commission Report ORNL-P-1069. 1964.

43. Herrick, C. C. Vapor pressure of liquid indium. Trans. Met. Soc. A. I. M. E. 230: 1439-1442. 1964.

44. Heumann, Theo, and Bruno Predel. Thermodynamische Untersuchungen im System Indium-Blei. Z. Metallk. 57: 50-55. 1966.

45. Hirth, J. P., and G. M. Pound. Coefficients of evaporation and condensation. J. Phys. Chem. 64: 619-626. 1960.

46. Honig, Richard E. On the molecular evaporation of group IV B elements. J. Chem. Phys. 21: 573-574. 1953.

47. Hougen, Olaf A., Kenneth M. Watson, and Roland A. Ragatz. Chemical process principles. Part 2. Thermodynamics. 2nd ed. New York, New York, John Wiley & Sons, Inc. 1959.

48. Hultgren, Ralph. Problems and progress in the thermocynamics of metals and alloys. (Univ. of California, Berkeley, California) U. S. Atomic Energy Commission Report UCRL-17467. 1967.

49. Hultgren, Ralph, Raymond L. Orr, Philip D. Anderson, and Kenneth K. Kelley. Selected values of thermodynamic properties of metals and alloys. New York, New York, John Wiley & Sons, Inc. 1963.

50. Hultgren, Ralph, Raymond L. Orr, Philip D. Anderson, and Kenneth K. Kelley. Supplements to selected values of thermodynamic properties of metals and alloys. Loose data sheets; supplement on lead dated 1965.

51. Hume-Rothery, William, R. E. Smallman, and C. W. Haworth. The structure of metals and alloys. Bungay, Suffolk, England, Richard Clay (The Chaucer Press), Ltd. 1969.

52. Johnston, H. L., and A. L. Marshall. Vapor pressures of nickel and of nickel oxide. J. Am. Chem. Soc. 62: 1382-1390. 1940.

53. Kappraff, Jay Marvin. Vaporization of antimony and bismuth alloys. Unpublished M. S. thesis. Ames, Iowa, Library, Iowa State University of Science and Technology. 1960.

54. Kennard, Earle H. Kinetic theory of gases. New York, New York, McGraw-Hill Book Co., Inc. 1938.

55. Kensok, O. J., J. R. Myers, and R. K. Saxer. The chemical activities of cadmium and magnesium in binary Mg-Cd alloys. Trans. Met. Soc. A. I. M. E. 236: 938-941. 1966.

56. Kim, Jang H., and Andrew Cosgarea, Jr. Study of the vapors of liquid lead and bismuth. J. Chem. Phys. 44: 806-809. 1966.

57. Knudsen, M. Die Molekularströmung der Gase durch Offnungen und die Effusion. Ann. Physik 28: 999-1016. 1909.

58. Knudsen, M. Das Cosinusgesetz in der kinetischen Gastheorie. Ann. Physik 48: 1113-1121. 1915.

59. Koch, R. K., and W. E. Anable. Vapor pressures of liquid molybdenum (2,890 to 2,990°K) and liquid zirconium (2,229 to 2,795°K). (Albany Metallurgy Research Center, Albany, Oregon) U. S. Bureau of Mines Report of Investigations 7063. 1968.

60. Koch, R. K., and W. E. Anable, and R. A. Beall. Vapor pressures of liquid columbium (2,740 to 3,140°K) and liquid hafnium (2,500 to 2,810°K). (Albany Metallurgy Research Center, Albany, Oregon) U. S. Bureau of Mines Report of Investigations 7125. 1968.

61. Koch, R. K., and W. E. Anable, E. D. Calvert and R. A. Beall. Vapor pressures of liquid titanium and liquid iron. In Orekoski, M. A., and R. R. Bunshah, eds. Vacuum Metallurgy Conference Transactions. Boston, Massachusetts, American Vacuum Society. 1966.

62. Koike, Yoshiyasu, and John M. Sivertsen. Local atomic arrangement in In-Pb alloys. J. Physical Soc. Japan 29: 1235-1241. 1970.

63. Krupkowski, A., and J. Golonka. Vapour pressures of liquid copper and silver. Bulletin de l'Academie Polonaise des Sciences 12: 69-74. 1964.

64. Kubaschewski, O., and B. E. Hopkins. Oxidation of metals and alloys. 2nd ed. New York, New York, Academic Press, Inc. 1962.

65. Langmuir, Irving. The vapor pressure of metallic tungsten. Phys. Rev. 2: 329-342. 1913.

66. Langmuir, Irving. The evaporation, condensation and reflection of molecules and the mechanism of adsorption. Phys. Rev. 8: 149-176. 1916.

67. Lenz, Terry Gene. Determination of thermodynamic activities for the tin-thallium system by vaporization measurements. Unpublished M. S. thesis. Ames, Iowa, Library, Iowa State University of Science and Technology. 1964.

68. Littlewood, Roy, and Sir Eric Rideal. On the evaporation coefficient. Trans. Faraday Soc. 52: 1598-1608. 1956.

69. Lyon, Richard N., ed. Liquid metals handbook. Washington, D. C., U. S. Government Printing Office. 1952.

70. Lyubimov, A. P., and Yu N. Lyubitov. The measurements of the vapor pressure of indium with the mass spectrograph. (Translated title) Obrabotka Stali i Splavov, Moskov, Inst. Stali im. I. V. Stalina, Sbornik 1957: 191-195. Original not available; abstracted in Chemical Abstracts 52: 17862b. 1958.

71. Macur, G. J., R. K. Edwards, and P. G. Wahlbeck. Multiple Knudsen cell effusion. Enthalpies of vaporization of indium and gallium. J. Phys. Chem. 70: 2956-2965. 1966.

72. Marshall, A. L., R. W. Dornte, and F. J. Norton. The vapor pressure of copper and iron. J. Am. Chem. Soc. 59: 1161-1166. 1937.

73. McGonigal, P. J., J. A. Cahill, and A. D. Kirshenbaum. The liquid range density, observed normal boiling point and estimated critical constants of indium. J. Inorg. Nuc. Chem. 23: 1012-1018. 1962.

74. McKenzie, D. E. The volatilization of plutonium from neutron irradiated uranium. Can. J. Chem. 34: 515-522. 1966.

75. Melville, H. W. A note on evaporation from irregular surfaces. Trans. Faraday Soc. 32: 1017-1020. 1936.

76. Moser, Z. Thermodynamic properties of the Zn-Pb-In ternary system in dilute liquid zinc solutions. Met. Trans. 2: 2175-2183. 1971.

77. Motzfeldt, Ketil. The thermal decomposition of sodium carbonate by the effusion method. J. Phys. Chem. 59: 139-147. 1955.

78. Munir, Zuhair A., and Alan W. Searcy. Torsion effusion study of the vapor pressure and heat of sublimation of gallium. J. Electrochem. Soc. 111: 1170-1173. 1964.

79. Munir, Zuhair A., and Alan W. Searcy. Activation energy for the sublimation of gallium nitride. J. Chem. Phys. 42: 4223-4228. 1965.

80. Murphy, J. E., E. Morrice, and M. M. Wong. Preparation of thorium metal by vacuum distillation of electrodeposited thorium-chromium and thorium-manganese alloys. (Reno Metallurgy Research Center, Reno, Nevada) U. S. Bureau of Mines Report of Investigations 7265. 1969.

81. National Carbon Co. The industrial graphite engineering handbook. Cleveland, Ohio. 1962.

82. Nesmeyanov, An. N., L. P. Firsova, and E. P. Isakova. The vapor pressure of lead oxide. Russ. J. Phys. Chem. 34: 573-575. 1960.

83. Nesmeyanov, An. N., L. P. Firsova, and E. P. Isakova. Measurement of the vapor pressure of lead oxide by the flow method. Russ. J. Phys. Chem. 34: 810-811. 1960.

84. Ohno, R., and T. Ishida. Rate of evaporation of manganese, copper, tin, chromium, and sulphur from molten iron under vacuum. J. Iron and Steel Inst. 206: 904-908. 1968.

85. Paule, Robert C., and John L. Margrave. Free-evaporation and effusion techniques. In Margrave, John L., ed. The characterization of high-temperature vapors. New York, New York, John Wiley & Sons, Inc. 1967.

86. Pokrovskii, N. L., P. P. Pugachevich, and N. A. Golubev. Measurement of the density of indium-bismuth and indium-lead metallic solutions. Russ. J. Phys. Chem. 42: 809-811. 1968.

87. Pratt, J. N., and A. T. Aldred. Torsion-effusion apparatus for the study of vapour pressures of alloys. J. Sci. Instr. 36: 465-468. 1959.

88. Predel, B., and A. Emam. Volume changes during the formation of molten alloys of the Ga-In, Ga-Sn, In-Bi, In-Pb, In-Sn, and In-Tl systems. J. Less Common Metals 18: 385-397. 1969.

89. Predel, B., and Hartmut Sandig. Untersuchungen zum Aufbau flüssiger und fester Legierungen der Systeme Indium-Thallium und Indium-Blei mittels Leitfähigkeitmessungen. Z. Metallk. 61: 387-394. 1970.

90. Priselkov, Yu A., Yu A. Saporhnikov, A. V. Tseplyaeva and, V. V. Karelin. A few problems on the accuracy of the effusion method. Determination of the pressure of indium saturated vapors. (Translated title) Isvest. Vyssh. Ucheb. Zaved., Khim. i Khim. Tekhnol. 3: 447-451. 1960. Original not available; abstracted in Chemical Abstracts 54: 21908e. 1960.

91. Rauh, Everett G., and Robert J. Thorn. Vapor pressure of uranium. J. Chem. Phys. 22: 1414-1420. 1954.

92. Romanova, A. V., and B. A. Mel'nik. Structures of indium and lead in the liquid phase. (Translated title) Ukr. Fiz. Zh. 15: 101-106. 1970. Original not available; abstracted in Chemical Abstracts 72: 126082h. 1970.

93. Rosenblatt, Gerd M. Interpretation of Knudsen vapor pressure measurements on porous solids. J. Electrochem. Soc. 110: 563-569. 1963.

94. Rosenblatt, Gerd M. Effect of restrictions to molecular flow upon measurements of vaporization rate and vapor pressure. J. Phys. Chem. 71: 1327-1333. 1967.

95. Rosenblatt, Gerd M., and Pang-Kai Lee. Rate of vaporization of arsenic single crystals and the vaporization coefficient of arsenic. J. Chem. Phys. 49: 2995-3006. 1968.

96. Rosenblatt, Gerd M., and Pang-Kai Lee. Vaporization kinetics and thermodynamics of antimony and the vaporization coefficient of antimony single crystals. J. Chem. Phys. 52: 1454-1464. 1970.

97. Rosenblatt, Gerd M., Pang-Kai Lee, and Michael B. Dowell. Vaporization of solids. Mechanism of retarded vaporization from a one-component single crystal. J. Chem. Phys. 45: 3454-3455. 1966.

98. Rossmann, M. G., and J. Yarwood. The accuracy of the Knudsen effusion method of measuring vapor pressures. J. Chem. Phys. 21: 1407-1408. 1953.

99. Rossmann, M. G., and J. Yarwood. The use of carbon crucibles in measurements on the rate of evaporation of liquid metals in a vacuum. Brit. J. Appl. Phys. 5: 7-13. 1954.

100. Roy, Prodyot, and Ralph Hultgren. Vapor pressure studies of iron-manganese alloys. Trans. Met. Soc. A. I. M. E. 233: 1811-1815. 1965.

101. Sandry, T. D., and F. Dee Stevenson. Molecular conductance from a curved surface through a cylindrical hole by Monte-Carlo methods. J. Chem. Phys. 53: 151-155. 1970.

102. Scheil, Erich, and Hans Leo Lukas. Bestimmung der Mischungswärme und ihrer Temperaturabhängigkeit in binären metallischen Schmelzen mit einem adiabatischen Hochtemperaturkalorimeter. Z. Metallk. 52: 417-422. 1961.

103. Shiu, Douglas H., and Zuhair A. Munir. The heat of vaporization and vapor pressure of liquid lead. Met. Trans. 2: 2953-2955. 1971.

104. Shiu, Douglas H., and Zuhair A. Munir. The activity and related thermodynamic properties of lead in liquid indium-lead alloys. High Temp. Sci. 3: 381-388. 1971.

105. Speiser, Rudolph, and H. L. Johnston. Methods of determining vapor pressure of metals. Trans. Met. Soc. A. I. M. E. 42: 283-307. 1950.

106. Stachura, Stanley John. Vapor-liquid equilibrium in metal systems. Unpublished Ph. D. thesis. Ames, Iowa, Library, Iowa State University of Science and Technology. 1962.

107. Stevenson, F. D., and V. E. Sater. Local thermodynamic consistency of vapor-liquid equilibrium data for binary and multicomponent systems. Am. Inst. Chem. Engr. J. 12: 586-588. 1966.

108. Strauss, S. W., L. E. Richards, and B. F. Brown. The density of liquid lead and dilute solutions of nickel in lead. Nuc. Sci. Engr. 7: 442-447. 1960.

109. Taylor, John B. The reflection of beams of the alkali metals from crystals. Phys. Rev. 35: 375-380. 1930.

110. Terpilowski, Janusz, and Zofia Gregorczyk. Thermodynamic properties of liquid metallic solutions. VIII. The indium-lead system. Arch. Hutnictwa 6: 197-204. 1961. Original not available; abstracted in Chemical Abstracts 56: 10997b. 1962.

111. Ultra Carbon Corp. Data sheet. Boston, Massachusetts. 1967.

112. Uyeha, Hajimu, and Yutaka Hagihara. Application of film theory to analysis of mass transfer in liquid-phase molecular distillation. (Translated title) Kagaku Kogaku 34: 165-169. 1970. Original not available; abstracted in Chemical Abstracts 72: 91736v. 1970.

113. Verhoeven, J. D. Convection effects in the capillary reservoir technique for measuring liquid metal diffusion coefficients. Trans. Met. Soc. A. I. M. E. 242: 1937-1942. 1968.

114. Volmer, M. Molargewichtsbestimmung im Gaszustand bei sehr nedrigen Drucken nach den Experimentalarbeiten von S. Heller und K. Neumann. Z. Physik. Chem., Bodenstein Festband 1931: 863-873.

115. Volmer, M., and I. Estermann. Über den Verdampfungskoeffizienten von festem und flussigem Quecksilber. Z. Physik 7: 1-12. 1921.

116. Von Lange, K. W., and H. Lindsheid. Untersuchung zur Grenzflächenverarmung bei der Knudsen-Verdampfung. Z. Metallk. 61: 676-679. 1970.

117. Voronin, G. F., and A. M. Evseev. Free vaporization of antimony from alloys. Russ. J. Phys. Chem. 39: 87-88. 1965.

118. Walsh, W. J., and George Burnet. Surface concentration changes during distillation of liquid metals. Nuc. Sci. Engr. 25: 227-235. 1965.

119. Ward, John W. Study of some of the parameters affecting Knudsen effusion. III. The vapor pressure of gold. J. Chem. Phys. 47: 4030-4034. 1967.

120. Ward, John W., and R. N. R. Mulford. Study of some of the parameters affecting Knudsen effusion. I. Experimental tests of the validity of the cosine law as a function of cell and sample geometries and materials. J. Chem. Phys. 47: 1710-1717. 1967.

121. Ward, John W., R. N. R. Mulford, and R. L. Bivins. Study of some of the parameters affecting Knudsen effusion. II. A Monte Carlo computer analysis of parameters deduced from experiment. J. Chem. Phys. 47: 1718-1723. 1967.

122. Whitman, Charles I. On the measurement of vapor pressures by effusion. J. Chem. Phys. 20: 161-164. 1952.

123. Winterbottom, W. L. Vapor-solid interactions and the effusion oven. I. The total effusion current through a cylindrical orifice. J. Chem. Phys. 47: 3546-3556. 1967.

124. Winterbottom, W. L., and J. P. Hirth. Diffusional contribution to the total flow from a Knudsen cell. J. Chem. Phys. 37: 784-793. 1962.

125. Wittig, Franz Eberhard, and Peter Scheidt. Die Mischungswärme in den binären Systemen des Indiums und Thalliums mit Zinn und Blei. Z. Phys. Chem. 28: 120-142. 1961.

126. Wolkoff, J., D. A. Woodward, and A. J. Strecok. A thermocouple for the measurement of the surface temperature of a liquid metal. Chem. Engr. Sci. 21: 895-903. 1966.

ACKNOWLEDGMENTS

The author wishes to thank Dr. F. Dee Stevenson for his technical assistance, helpful discussions, patient understanding and moral support.

The author is especially grateful to Mr. Harvey Jensen for considerable help with equipment construction and maintenance.

He also wishes to thank Mr. John Peterson and Mr. Archie Litchfield, now deceased, who fabricated all the graphite equipment used in this work. The help of many other Ames Laboratory personnel is also appreciated, special thanks being due to research helpers Mr. Nick Wilson and Mr. Dean Roorda.

Very helpful discussions were had with Dr. Renato Bautista, Dr. William Walsh, Dr. Terry Lenz, and Mr. Thomas Sandry, among many others.

Special editorial help from Mr. Richard Seemann is also appreciated.

The friendship of many persons in the Ames community is highly valued, as well as that of students and staff.

APPENDIX A

Error Analysis

The theory of propagation of errors is applied to determining, insofar as possible, what standard deviation would be expected in determining vapor pressures of lead. Based on this result, an estimate for the standard deviation of a lead activity coefficient is obtained and found to be much higher than that for the vapor pressure. Consider first the vaporization of pure lead at 700°C. The vapor pressure is determined from the Langmuir equation, Equation 5 with the condensation coefficient assumed unity,

$$P = \left(\frac{m}{st}\right) \frac{1}{0.0583\ K} \sqrt{\frac{T}{M}} \quad \text{(mm Hg)} \ . \tag{A1}$$

The error in P (neglecting the main temperature error) could be found from the theory of propagation of errors, viz.

$$\sigma'_P = \sqrt{\left(\frac{\partial P}{\partial m}\right)^2 \sigma_m^2 + \left(\frac{\partial P}{\partial s}\right)^2 \sigma_s^2 + \left(\frac{\partial P}{\partial t}\right)^2 \sigma_t^2 + \left(\frac{\partial P}{\partial K}\right)^2 \sigma_K^2 + \left(\frac{\partial P}{\partial T}\right)^2 \sigma_T^2} \tag{A2}$$

$$= \sqrt{\left(\frac{P}{m}\right)^2 \sigma_m^2 + \left(\frac{-P}{s}\right)^2 \sigma_s^2 + \left(\frac{-P}{t}\right)^2 \sigma_t^2 + \left(\frac{P}{K}\right)^2 \sigma_K^2 + \left(\frac{P}{2T}\right)^2 \sigma_T^2} \tag{A3}$$

$$\text{Now } m = m_{\text{INITIAL}} - m_{\text{SLUG}} - m_{\text{SMALL PIECES}} - (m_{\text{LOADED CAPS}} - m_{\text{CAPS}}) \tag{A4}$$

If we assume no error in collecting the pieces, the only error in each of these m's is due to weighing. Assume a weighing

error of σ=0.0002 g. Then, treating Equation A4 like A2,

$$\sigma_m = \sqrt{5(0.0002\ g)^2} = 2.237\ (0.0002\ g) = 0.0004474\ g \qquad (A5)$$

In an analogous manner, we can find σ_s and σ_K, despite the fact that obtaining σ_K is rather involved. The list of basic assumed errors is

$$\begin{aligned}
&\sigma_{\text{WEIGHTS}} = 0.0002\ g \\
&\sigma_{\text{DIMENSIONS}} = 0.002 \text{ inch, except for} \\
&\sigma_{\text{HOLE DEPTH}} = 1/64 \text{ inch} = 0.0156 \text{ inch} \\
&\sigma_{\text{CAPILLARY D}} = 0.00781 \text{ inch} \qquad (A6) \\
&\sigma_{\text{CHANNEL D}} = 0.002 \text{ inch} \\
&\sigma_{\text{CHANNEL, CAP. LENGTHS}} = 1/64 \text{ inch} \\
&\sigma_t = 2 \text{ min.} \\
&\sigma_T = 1°C
\end{aligned}$$

The T in Equation A1 does not depict the main dependence of the vapor pressure on temperature. The temperature has a measurement uncertainty, and the desired dependence relation is approximately (see Table 1, Hawkins and Hultgren (41))

$$\log_{10} P = 7.736 - \frac{9.651 \times 10^3}{T}, \text{ (mm Hg)} \qquad (A7)$$

or

$$\frac{dP}{dT} = 2.22 \times 10^4 \frac{P}{T^2} \qquad (A8)$$

Relation A8 should be combined with A3 to give the total

estimate of

$$\sigma_P = \sqrt{(\sigma_P')^2 + (\frac{\partial P}{\partial T})^2 \sigma_T^2} \qquad \text{(A9)}$$

The quantities used for this analysis are $P=7.0 \times 10^{-3}$ mm Hg, m=0.378 g, s=0.317 cm^2, t=8.13 hr., K=0.2193 and T=973°K, which are data from a typical run. Results are shown in the following table:

Table A1. Results of propagation of error analysis to determine expected lead vapor pressure errors at 700°C

Source	Variance $(mm\ Hg)^2$	% of total variance	% error in vapor pressure
Weighing	8.85×10^{-11}	0.18%	0.01%
Surface area	1.25×10^{-8}	25.8%	0.81%
Time	8.22×10^{-10}	1.69%	0.05%
Clausing factor	8.56×10^{-9}	17.60%	0.55%
Temp. (Eqn. A1)	1.29×10^{-11}	0.03%	-
Temp. (Eqn. A7)	2.66×10^{-8}	54.7%	1.72%
	4.86×10^{-8}	100.00%	3.14%

Notice that a 3.14% standard deviation in measuring the lead vapor pressure is predicted, and that temperature error far outweighs other errors in its effect. A 1°C error is probably a close estimate. Notice also that no accounting

could be made for the effects caused by any oxide films that might be present.

We assume the error in measuring x is negligible, a good assumption. From Equation 16

$$\gamma_{Pb} = p/xP_{av} \tag{A10}$$

where P_{av} is the pressure computed from Equation 33, based on at least five data points, so that

$$\sigma_{\gamma_{Pb}} = \sqrt{\left(\frac{1}{P_{av}x}\right)^2 \sigma_p^2 + \left(\frac{-p}{P_{av}^2 x}\right)^2 \sigma_{P_{av}}^2} \tag{A11}$$

Now

$$\sigma_{P_{av}}^2 = \frac{1}{n} \sigma_P^2 \tag{A12}$$

where n is the number of data points making up P_{av}, so that, assuming $\sigma_p = \sigma_P$, Equation A11 becomes

$$\sigma_{\gamma_{Pb}} = \sqrt{\frac{n + \gamma_{Pb}^2 x^2}{nx^2}} \frac{\sigma_P}{P_{av}} \tag{A13}$$

Hence the following Table for $\sigma_p/P_{av} = 3.14\%$:

Table A2. Results of propagation of error analysis extended to lead activity coefficient errors at 700°C

$x=x_{Pb}$	γ_{Pb} (Moser (76))	$\sqrt{\frac{n+\gamma_{Pb}^2 x^2}{nx^2}}$	$\sigma_{\gamma_{Pb}}$ (estimated)
0.9	1.001	1.198	3.76%
0.5	1.052	2.05	6.43%
0.1	1.190	10.015	31.5 %

This table gives an indication of how a small error in determining vapor pressures is magnified in determining activity coefficients. In reality, since P_{av} is computed from Equation 33, which is based on a least square analysis of 27 data points rather than the five of each run, n should be greater than 5 but less than 27. Increasing n to 27 would not materially change Table A2.

APPENDIX B

Material Analyses

The following analyses on materials as received were done by Ames Laboratory personnel. Metals were done by spectrographic analysis, oxygen by helium fusion analysis, and carbon by Ames Laboratory Analytical Chemistry Group I.

	Pb	In	AGSX graphite
Ag	-	FT	-
Al	FT	FT	-
As	-	-	-
Au	-	-	-
B	-	-	-
Ba	-	-	-
Be	-	-	-
Bi	-	-	-
Ca	T	T	T
Cd	-	-	-
Co	-	-	-
Cr	FTX	FTX	-
Cu	FT	FT	-
Fe	FT-T	-	T-VW
Ga	-	-	-
Ge	-	-	-
Hf	-	-	-
Hg	-	-	-
In	FT	Major	
Ir	-	-	-
Li	-	-	-
Mg	FT	FT	T
Mn	-	-	-
Mo	-	-	-
Nb	-	-	-
Ni	-	-	-
Os	-	-	-
P	-	-	-
Pb	Major	-	-
Pd	-	-	-
Pt	-	-	-
Re	-	-	-
Ru	-	-	-
Sb	-	-	-
Si	FT	FT	T
Sn	-	-	-
Sr	-	-	-
Ta	-	-	-
Te	-	-	-
Th	-	-	-
Ti	-	-	T
Tl	-	-	-
V	-	-	T
W	-	-	
Y	-	-	-
Zn	-	-	-
Zr	-	-	-
Carbon	61 ppm	43 ppm	Major
Oxygen	54 ppm	53 ppm	

SYMBOLS

Major Constituent	Minor Constituent
VS=very strong	M=moderate
S=strong	W=weak

Trace Impurity	Other
VW=very weak	blank=not investigated
T=trace	X=interference
FT=faint trace	-=not detected

APPENDIX C

Equipment Description

A more detailed description of each piece of equipment is given here than in the Equipment and Procedure section, but its use is described there.

A. Vacuum system equipment - basically a Vacuum-Electronics Corporation (Veeco) VS-400 Pumping Station

1) Welch Duo-Seal 15 cfm mechanical forepump, 1 hp motor.
2) Veeco diffusion pump, 400 l/sec, stainless steel, 3 stage fractionating, low backstreaming, 500 watt heater.
3) Veeco water cooled baffle, nickel plated. The cooling coils on this have twice sprung leaks and been replaced with copper coils.
4) Veeco cold trap, stainless steel, 0.8 liter capacity, liquid nitrogen lasts about 5 hrs. when filled.
5) Veeco Bayard-Alpert type ion gauge, non-burnout, type RG-75K, 10×10^{-4} to 1×10^{-8} mm Hg.
6) Veeco matched thermocouple gauges, 0-1000 microns.
7) Veeco viton O-rings are used from the diffusion pump to the vycor column, except for one teflon gasket.
8) Dow Corning silicone diffusion pump oil, DC 704, 200 cc.
9) Dow Corning silicone high vacuum grease is used sparingly on seals.

10) Vycor column, 3-1/4 inch ID, except 3 inch ID at top and bottom, 1/4 inch walls, 30 inches long.

B. Heating equipment - Lepel High Frequency Laboratories, Inc. induction generator, model T-20-3-KC-F-S, 20 kilowatt output power, 460 v., 3 phase, 60 amps, 350 kc/sec in use. Power control is by temperature controller signal to internal magnetic amplifier and primary saturable core reactor. Copper load coils were 1/8 inch diameter; 3-turn and 9-turn coils were used for runs, and a 22-turn coil was used with the mixing and casting apparatus.

C. Temperature measurement and control

1) Chromel-alumel thermocouple probes, #28 gauge wire, 0.0126 inch diameter. Chromel-alumel connecting wires, #22 gauge wire, 0.0253 inch diameter.

2) Thermocouple insulators, for probes very high purity alundum, 1/16 in. OD, two 1/64 inch holes. Insulators for connecting wires, 1/8 in. OD, two 1/32 inch holes. McDanel Refractory Porcelain Co.

3) Conax Corporation compression vacuum fittings, type TG-20-A2.

4) Leeds and Northrup potentiometer, Type K-3, used for measuring thermocouple EMF, reads to 0.001 mv.

5) Leeds and Northrup potentiometer, type K-5, used for calibrating thermocouples, reads to 0.01 microvolt.

6) Leeds and Northrup M-Line temperature controller

a) Deviation amplifier - span of ±3°C was used with chromel-alumel thermocouple.

b) Low level set point unit, automatic reference junction compensation, ±0.01 mv = ±1/4°C for chromel-alumel thermocouple.

c) Current-adjusting-type controller having control modes

1) Proportional (0-300%)

2) Rate (0-8 min.)

3) Reset (0-100 repeats/min.)

4) Approach (not used)

and an output of 0-5 ma through 2500 ohms, insensitive to rf interference.

7) Honeywell Electronik 16 recorder, adjustable chart speed, adjustable span, 2 mv. minimum span with calibrated accuracy of 0.005 mv = 0.13°C for chromel-alumel thermocouple sensitive to rf interference.

D. Balance and graphite

1) Analytical balance, Wm. Ainsworth & Sons, Inc., Right-a-Weigh type SC, 200 g. capacity, weighings read to 0.0001 g. with a standard deviation of 0.00003 g.

2) Graphite - The mean coefficient of thermal expansion for both grades between 30°C and operating temperatures is 6.0×10^{-6}/°C. The UF-4S grade is used for the run crucible, the catch crucible, and all parts of the mixing and casting apparatus which contact the metal. AGSX grade is used for supporting parts of the mixing and casting apparatus.